การออกแบบเครื่องปฏิกรณ์ประเภทโมโนลิทเพื่อผลิตไฮโดรเจนภายในรถยนต์

นายธารา จิวานุรักษ์

วิทยานิพนธ์นี้เป็นส่วนหนึ่งของการศึกษาตามหลักสูตรปริญญาวิศวกรรมศาสตรดุษฎีบัณฑิต
สาขาวิชาวิศวกรรมเคมี ภาควิชาวิศวกรรมเคมี
คณะวิศวกรรมศาสตร์ จุฬาลงกรณ์มหาวิทยาลัย
ปีการศึกษา 2559

DESIGN OF MONOLITH-TYPED REACTOR FOR VEHICULAR HYDROGEN PRODUCTION

Mr. Tara Jiwanuruk

A Dissertation Submitted in Partial Fulfillment of the Requirements
for the Degree of Doctor of Engineering Program in Chemical Engineering
Department of Chemical Engineering
Faculty of Engineering
Chulalongkorn University
Academic Year 2016

Thesis Title	DESIGN OF MONOLITH-TYPED REACTOR FOR VEHICULAR HYDROGEN PRODUCTION
By	Mr. Tara Jiwanuruk
Field of Study	Chemical Engineering
Thesis Advisor	Professor Suttichai Assabumrungrat, Ph.D.
Thesis Co-Advisor	Assistant Professor Sompong Putivisutisak, Ph.D.
	Professor Tomohiko Tagawa, Ph.D.

Accepted by the Faculty of Engineering, Chulalongkorn University in Partial Fulfillment of the Requirements for the Doctoral Degree

.....Dean of the Faculty of Engineering
(Associate Professor Supot Teachavorasinskun, D.Eng.)

THESIS COMMITTEE

.....Chairman
(Associate Professor Anongnat Somwangthanaroj, Ph.D.)

.....Thesis Advisor
(Professor Suttichai Assabumrungrat, Ph.D.)

.....Thesis Co-Advisor
(Assistant Professor Sompong Putivisutisak, Ph.D.)

.....Thesis Co-Advisor
(Professor Tomohiko Tagawa, Ph.D.)

.....Examiner
(Chutimon Satirapipathkul, Ph.D.)

.....Examiner
(Pimporn Ponpesh, Ph.D.)

.....External Examiner
(Assistant Professor Kaokanya Sudaprasert, Ph.D.)

ธารา จิวานุรักษ์ : การออกแบบเครื่องปฏิกรณ์ประเภทโมโนลิทเพื่อผลิตไฮโดรเจนภายในรถยนต์ (DESIGN OF MONOLITH-TYPED REACTOR FOR VEHICULAR HYDROGEN PRODUCTION) อ.ที่ปรึกษาวิทยานิพนธ์หลัก: ศ. ดร.สุทธิชัย อัสสะบำรุงรัตน์, อ.ที่ปรึกษาวิทยานิพนธ์ร่วม: ผศ. ดร.สมพงษ์ พุทธิวิสุทธิศักดิ์, ศ. ดร.โทโมฮิโกะ ทากาวา, 140 หน้า.

งานวิจัยนี้ศึกษาการพัฒนาเครื่องปฏิกรณ์หลายหน้าที่ขนาดเล็กเพื่อผลิตไฮโดรเจนสำหรับเซลล์เชื้อเพลิงภายในรถยนต์ โดยการศึกษาแบ่งออกเป็นสามส่วนดังนี้ 1) การเปรียบเทียบการจัดเรียงกระบวนการของเครื่องปฏิกรณ์ควบคู่ความร้อนระดับไมโคร 2) ผลกระทบของการจัดเรียงกระบวนการต่อสมรรถภาพของเครื่องปฏิกรณ์ไมโครแบบเยื่อแผ่น และ 3) การออกแบบเครื่องปฏิกรณ์แบบเยื่อแผ่นประเภทโมโนลิทควบคู่ความร้อนสำหรับรถยนต์ สำหรับเครื่องปฏิกรณ์ควบคู่ความร้อนระดับไมโครและเครื่องปฏิกรณ์ไมโครแบบเยื่อแผ่น เครื่องปฏิกรณ์ทั้งสองศึกษาโดยการจำลองพลศาสตร์ของไหลในรูปแบบสามมิติด้วยโปรแกรมคอมโซลมัลติฟิสิกส์ การจัดเรียงแบบขนานและการจัดเรียงแบบสลับช่องถูกพิจารณาเป็นการจัดเรียงกระบวนการของเครื่องปฏิกรณ์ การจัดเรียงแบบสลับช่องของเครื่องปฏิกรณ์ควบคู่ความร้อนระดับไมโครช่วยลดความต่างของอุณหภูมิระหว่างจุดร้อนและจุดเย็นได้เนื่องจากมีการถ่ายโอนความร้อนสูง ดังนั้นการจัดเรียงนี้จึงเหมาะสมสำหรับเครื่องปฏิกรณ์ที่มีช่องขนาดใหญ่ และเนื่องจากการจัดเรียงแบบสลับมีพื้นที่สัมผัสระหว่างกระบวนการมากส่งผลให้เยื่อเลือกผ่านทั้งหมดถูกใช้งานในเครื่องปฏิกรณ์ไมโครแบบเยื่อแผ่นโดยสามารถแยกไฮโดรเจนได้เพิ่มขึ้นและช่วยลดการสะสมของไฮโดรเจนภายในผนังของเครื่องปฏิกรณ์ แนวโน้มของตัวแปรต่างๆของเครื่องปฏิกรณ์ทั้งสองถูกรายงานในงานศึกษานี้ เนื่องด้วยประสิทธิภาพที่ดีของการจัดเรียงแบบสลับช่อง การจัดเรียงนี้จึงใช้สำหรับการออกแบบเครื่องปฏิกรณ์แบบเยื่อแผ่นประเภทโมโนลิทควบคู่ความร้อนจากโครงสร้างโมโนลิทเชิงพาณิชย์ การออกแบบเครื่องปฏิกรณ์นี้ใช้การจำลองด้วยโปรแกรมแอสเพนพลัส สภาวะที่มีประสิทธิภาพของเครื่องปฏิกรณ์คือทำปฏิกิริยาปฏิรูปที่ความดัน 4 เท่าของบรรยากาศและอัตราการไหลของมีเทนเท่ากับ 0.30 โมลต่อวินาที สำหรับปฏิกิริยาปฏิรูป และ 0.03 โมลต่อวินาที สำหรับการเผาไหม้ จากการจำลองพบว่าประสิทธิภาพของเครื่องปฏิกรณ์ขึ้นอยู่กับพื้นที่แลกเปลี่ยนของโมโนลิท โดยโครงสร้างที่เหมาะสม (พื้นที่แลกเปลี่ยนเท่ากับ 1.5 ตารางเมตร) คือโมโนลิทที่มีความหนาแน่นของช่องเท่ากับ 200 ช่องต่อตารางนิ้วและมีเส้นผ่านศูนย์กลางและความยาวเท่ากับ 150 มิลลิเมตร ซึ่งสามารถผลิตไฮโดรเจนได้มีกำลังงานสูงเทียบเท่า 129 กิโลวัตต์และมีประสิทธิภาพเท่ากับร้อยละ 43.96 ดังนั้นเครื่องปฏิกรณ์ชนิดนี้ซึ่งมีปริมาตร 2.65 ลิตร เป็นเครื่องปฏิกรณ์ที่มีศักยภาพเหมาะสมสำหรับการผลิตไฮโดรเจนเพื่อเป็นแหล่งพลังงานภายในรถยนต์

ภาควิชา วิศวกรรมเคมี	ลายมือชื่อนิสิต .....
สาขาวิชา วิศวกรรมเคมี	ลายมือชื่อ อ.ที่ปรึกษาหลัก .....
ปีการศึกษา 2559	ลายมือชื่อ อ.ที่ปรึกษาร่วม .....
	ลายมือชื่อ อ.ที่ปรึกษาร่วม .....

5571407321 : MAJOR CHEMICAL ENGINEERING

KEYWORDS: HYDROGEN PRODUCTION / MULTIFUNCTIONAL REACTOR / MONOLITHIC REACTOR / MEMBRANE REACTOR

TARA JIWANURUK: DESIGN OF MONOLITH-TYPED REACTOR FOR VEHICULAR HYDROGEN PRODUCTION. ADVISOR: PROF. SUTTICHAI ASSABUMRUNGRAT, Ph.D., CO-ADVISOR: ASST. PROF. SOMPONG PUTIVISUTISAK, Ph.D., PROF. TOMOHIKO TAGAWA, Ph.D., 140 pp.

This thesis studied the development of a small scale multifunctional reactor for hydrogen production for on-board fuel cell. The study was divided into three parts as follows: i) the comparison between the flow arrangements of the thermally coupled micro reformer (TMR) ii) the effect of the flow arrangement on the micro membrane reformer (MMR) performance and iii) design of thermally coupled monolithic membrane reformer (TMMR) for vehicle. In the case of TMR and MMR, both reformers were examined by three dimensional computational fluid dynamic simulation using COMSOL Multiphysics®. Parallel arrangement and checked arrangement were considered as the flow arrangement of the reformers. The checked arrangement in TMR reduced temperature difference between cold and hot spots due to higher heat transfer. As a result, the checked arrangement is appropriate for large channel width reformer. Since the checked arrangement has larger contact area, total membrane area was utilized in MMR. Higher hydrogen permeation and lower hydrogen accumulation were observed. The parameters' influence in TMR and MMR was reported. According to the higher performance of the checked arrangement, the arrangement was employed in the TMMR design based on a commercial monolith configuration. The TMMR was designed using Gibbs reactor and Plug flow reactor models via Aspen Plus. The efficient condition was at 4 atm and methane of 0.30 mol/s for steam reforming and 0.03 mol/s for combustion. It was found that the energy efficiency of TMMR depended on exchange area of monolith. At optimal configuration (1.5 m^2 of exchange area), 200 cpsi monolith and 150 mm of diameter and length produced hydrogen equivalent to 129 kW with 43.96% efficiency. Therefore, TMMR which has 2.65 liters of volume is a potential reformer for on-board hydrogen production.

Department:	Chemical Engineering	Student's Signature	.....
Field of Study:	Chemical Engineering	Advisor's Signature	.....
Academic Year:	2016	Co-Advisor's Signature	.....
		Co-Advisor's Signature	.....

ACKNOWLEDGEMENTS

The author would like to express my sincere gratitude to my advisors, Prof. Dr. Suttichai Assabumrungrat, Asst. Prof. Dr. Sompong Putivisutisak, Prof. Dr. Tomohiko Tagawa, Asst. Prof. Dr. Hiroshi Yamada and Prof. Dr. Choji Fukuhara for invaluable guidance, support and encouragement through my doctoral research study. Their precious advice and teaching have helped me to accomplish this research.

Prof. Dr. Suttichai Assabumrungrat has given me an opportunity to be a Ph.D. student under his advice. He understands my personality and has a lot of patience with me. He guides me everything covering my research, my daily life, and my future plan. Furthermore, Asst. Prof. Dr. Sompong Putivisutisak is my important and beloved teacher. He taught me countless simulation technique and computational fluid dynamic knowledge. These helped and guided me to achieve my researches.

Prof. Dr. Tomohiko Tagawa and Asst. Prof. Dr. Hiroshi Yamada had taken care me well for a year when I was an exchange research student at Nagoya University. Prof. Dr. Tomohiko Tagawa showed me his kindness and his suggestion improved my studies. Additionally, Asst. Prof. Dr. Hiroshi Yamada stood by me in the laboratory and taught me about the experiments. Moreover, Prof. Dr. Choji Fukuhara welcomed me well when I visited his laboratory in Shizuoka University to study electroless plating technique. I had great experience and happiness under the magnanimity from all advisors while I was in Japan.

I also would like to thank Assoc. Prof. Dr. Anongnat Somwangthanaroj as the chairman, Dr. Chutimon Satirapipathkul, Dr. Pimporn Ponpesh and Asst. Prof. Dr. Kaokanya Sudaprasert as the members of the thesis committee for their comment and suggestion.

I gratefully thank the financial supports from the Royal Golden Jubilee PhD Program from the Thailand Research Fund and Chulalongkorn University, the Thailand Research Fund and PTT Group Research Scholar from PTT Group Frontier Research Center. The JSPS Kaken-hi #B23360346 and the JSPS Kaken-hi #015H04178 (Japan) are gratefully acknowledged.

Finally, I acknowledge with thanks to my parents, my family, and my friends in Center of Excellence in Catalysis and Catalytic Reaction Engineering, Chulalongkorn University, Nagoya University and Shizuoka University for worthy support, encouragement all times, and co-operation throughout my study period.

CONTENTS

Page

Page

Page

Page

LIST OF TABLES

LIST OF FIGURES

NOMENCLATURE

p	Pressure (Pa)
C_p	Specific heat at constant pressure (J kg^{-1} K^{-1})
T	Temperature (K)
k	Conductivity (W m^{-1} K^{-1})
$\Delta\hat{H}^0_{c,}$	Heat of combustion (kJ mol^{-1})
Q_i	Source term of species *i* (mol s^{-1} m^{-2})
r_j	Rate of reaction *j* (mol s^{-1} m^{-2})
A_i	Pre-exponential factor
E_a	Activation energy (kJ/mol)
$D_{i,eff}$	Effective mass diffusion coefficient of species *i* in mixture (m^2 s^{-1})
MW_i	Molar mass of species *i* (kg $kmol^{-1}$)
F_i	Mole flow of species *i* (mol s^{-1})
$\vec{v}$	Velocity (m s^{-1})
d_p	Pore diameter of solid phase (cm)
R	Gas constant
J_{H_2}	Hydrogen flux (mol s^{-1} m^{-2})
ΔP	H_2 partial pressure difference between feed and permeate stream
l	Membrane thickness
G	Molar Gibbs free energy (J mol^{-1})
G_i^0	Gibbs free energy of species *i* at its standard state (J mol^{-1})
y_i	Mole fraction of compound *i* in the gas mixture
f_i^0	Fugacity of species *i* at its standard state (Pa)

Greek symbols

ρ	Density (kg m^{-3})
μ	Dynamic viscosity (Pa s)
ω_i	Mass fraction of species *i*

ε	Porosity
τ	Tortuosity
$\hat{\varphi}$	Fugacity coefficient of species *i* in the gas mixture

Abbreviations

TMMR	Thermally coupled monolithic membrane reactor
TMR	Thermally coupled micro reactor
MMR	Membrane micro reactor
PEMFC	Polymer electrolyte membrane fuel cell
GHSV	Gas hourly space velocity (h^{-1})
CC	Combustion channel
RC	Reforming channel
SC	Sweep gas channel
TR	Traditional reactor
MR	Membrane reactor

CHAPTER I
INTRODUCTION

1.1 Rationale

Nowadays, climate change has been brought to our attention as a major issue, since global surface temperature is significantly changed by the increase of carbon dioxide composition in the atmosphere. Carbon dioxide gas majorly emits from human activity and fossil fuel consumption. To reduce the fossil fuel usage, the alternative energy is proposed. Hydrogen gas is considered as a clean energy carrier which can be used to produce electricity by proton exchange membrane fuel cells (PEMFC). Recently, hydrogen has been applied as a fuel for vehicles. Increasing hydrogen usage results in the significant increase of hydrogen demand. Therefore, green hydrocarbon fuels with hydrogen production system must be developed for vehicular application.

In conventional processes of hydrogen production, steam reforming reaction is employed in a packed bed reactor. The disadvantages of this processes are pressure drop, high heat and mass transfer resistance, large size and heavy weight. Furthermore, hot and cold spots possibly appear inside the packed bed, leading to a difficulty for controlling system (Bravo et al. (2004), Fukuhara and Igarashi (2005)). The product stream from the processes contains high composition of carbon monoxide (CO) which poisons the anode side of PEMFC (Babita et al. (2011), Korotkikh and Farrauto (2000)). Clean-up units including high and low temperature water gas shift units and CO

preferential oxidation (COPROX) reactor are required to decrease CO concentration to lower than 10 ppm (Katiyar et al. (2013), Lukyanov et al. (2009), Montané et al. (2011)). Thus, the conventional processes are not suitable for portable system due to the performance of packed bed reactor, large area requirement for several units and heavy catalyst weight.

According to the limitation of vehicular system, micro-channel reactor has been suggested (Holladay et al. (2004), Kolb (2013), Sanz et al. (2013)). It has a diameter smaller than 1 mm. Monolith having multi-micro-channel structure has been conducted in commercial processes such as catalytic convertor, catalyst support, reactors, etc (Frauhammer et al. (1999), Hong Mei et al. (2007), Kim et al. (2009), Moreno et al. (2010)). Due to its multi-channel structure, monolithic reactor can integrate several processes within a single structure. In the case of hydrogen production, heat supply and hydrogen separator are necessary. Heat supply is used to maintain reaction temperature because steam reforming which is widely employed is endothermic reaction. Furthermore, hydrogen must be separated from the product stream due to the limitation of PEMFC. Heat and membrane integration within micro-channel reactor which is thermally coupled micro reformer (TMR) and micro membrane reformer (MMR) has been studied transport phenomena and reactor performance. The advantages of the micro-channel reactor are low heat and mass transfer resistance, high surface area per unit volume, compact size, fast start-up and lower pressure drop.

The process integration within a monolith contains two or three feed streams which are fed separately into their channels. The arrangement of the feed streams is considered as parallel arrangement and checked arrangement. In several studies, the parallel arrangement which is the simple arrangement is employed generally with a simple structure of flow distributor. This arrangement offers low contact area between each process channel. On the other hand, the checked arrangement presents higher contact area, but the structure is complex and needs the complicated flow distributor.

In the study of heat transfer integrated reactor, fuel combustion is conducted as heat source and coupled with steam reforming inside a reformer. Both reactions occurred inside their channels which are separated by reformer wall. The heat integrated reactor in micro scale is studied by experiment and simulation. The parallel arrangement was employed in several studies (Anzola et al. (2010), Frauhammer et al. (1999), Tadbir and Akbari (2012, (2011), Zanfir and Gavriilidis (2003)). Meanwhile, the experimental study of the checked arrangement was reported by Moreno and Wilhite (2010).

For membrane integration studies, palladium membrane separation is selected for hydrogen separation in micro-channel reactor (Kim et al. (2009), Xuan et al. (2012)). The membrane reactor provides better performance and higher efficiency than the traditional reactor (Gallucci et al. (2008), Gallucci et al. (2004a), Shu et al. (1994)). Moreover, the integration of heat supply and membrane separation within a structure

had been investigated by Patel and Sunol (2007). The study considered three channels consisting of combustion channel, reforming channel and separation channel. The arrangement effect has not been mentioned. Therefore, the effect of the flow arrangement on the reactor performance of TMR and MMR must be studied. To achieve the complete hydrogen production process, thermally coupled monolithic membrane reformer (TMMR) which is monolith reactor integrated with heat supply and membrane is proposed as a compact reformer in vehicle. This reformer must be designed to supply sufficient hydrogen production rate.

As aforementioned, this research determined the suitable design of monolithic reactor which integrates heat supply and membrane separation within a single unit for hydrogen production for vehicles. The study has been divided into three parts, the comparison between the flow arrangements of the thermally coupled micro reformer (TMR), the effect of the flow arrangement on the micro membrane reformer (MMR) performance and the compact design of thermally coupled monolithic membrane reactor (TMMR) for vehicles. The flow arrangement including the parallel arrangement and the checked arrangement are investigated for TMR and MMR. The appropriate flow arrangement is recommended in each case. In the design of TMMR, the TMMR was studied to optimize the design and operating condition. This TMMR design was suggested to be applied inside the vehicular system for hydrogen production.

1.2 Objectives

The goal of this research is to develop a compact multifunctional reactor for hydrogen production for on-board polymer electrolyte membrane fuel cell (PEMFC). The specific objectives to achieve this goal are described as the follows:

1. To compare the reactor performance of thermally coupled micro reactor (TMR) in the parallel arrangement and the checked arrangement at various operating and design parameters.
2. To investigate the effect of feed flow arrangement on reactor performance of micro membrane reactor (MMR) at varied operating and design parameters.
3. To design the thermally coupled monolithic membrane reactor (TMMR) with the suitable operating condition to be a single unit reformer for hydrogen production in vehicular system.

1.3 Scope of works

1. This dissertation considered the studies in only mathematical modelling.
2. In thermally coupled micro reactor and micro membrane reactor, the studies were computed using computational fluid dynamic simulation in three dimension.
3. Methane which is widely used as reforming reactant was selected as model compound for simulation.

4. Feed flow configuration conducted in this studies are the parallel arrangement and the checked arrangement.
5. Influence of operating and design parameters was explored. Operating parameters were inlet temperature, steam to carbon ratio in reforming channel, percentage of fuel in combustion channel and gas hourly space velocity (GHSV) of both channels. The design parameters were channel width, wall thickness and reformer length. Moreover, flow direction including co-current and counter current was also investigated.
6. The thermally coupled monolithic membrane reactor was investigated based on commercial monolith structure using Aspen Plus.
7. For vehicles, energy requirement generally is about 100 kW; hence, hydrogen production target of the TMMR was 100 kW.

1.4 Dissertation overview

This dissertation is organized as the list below

Chapter II shows theories relevant to this study. Hydrogen production and fuel feedstock are described. The kinetic model of these fuels for hydrogen production is explained. Membrane separation technology and micro-channel reactor are mentioned. The theory of computational fluid dynamic simulation is informed.

Chapter III reviews about process integrated micro reactor for hydrogen production including heat and membrane integration and the flow arrangement study.

Chapter IV describes the first study which is comparison between parallel and checked arrangements of micro reformer for H_2 production from methane. Micro reformer configuration is illustrated and described. Equations and models used in this simulation are expressed. Effect of parameters on the reactor performance is summarized and the proper arrangement is recommended.

Chapter V provides the second work which is effect of flow arrangement on micro membrane reforming for H_2 production from methane. Simulation methodology including micro structure and modeling is explained. The reactor performance between both arrangements is concluded with the effect of parameters.

Chapter VI explains the design of thermally coupled monolithic membrane reformer for hydrogen production in vehicular application which is the final part.

Modeling and simulation using Aspen Plus are described. Appropriate operating condition and design including the arrangement are summarized.

Chapter VII presents the conclusion and the recommendations of this dissertation.

CHAPTER II
THEORY

2.1 Hydrogen production

Hydrogen is a chemical widely used in several chemical industries. Furthermore, hydrogen and syngas are more efficient clean fuels which eliminate pollutant emission including greenhouse gases especially carbon dioxide (Liu et al. (2010)). Hydrogen production and utilization pathway which was summarized by Holladay et al. (2009) is shown in Figure 2.1.

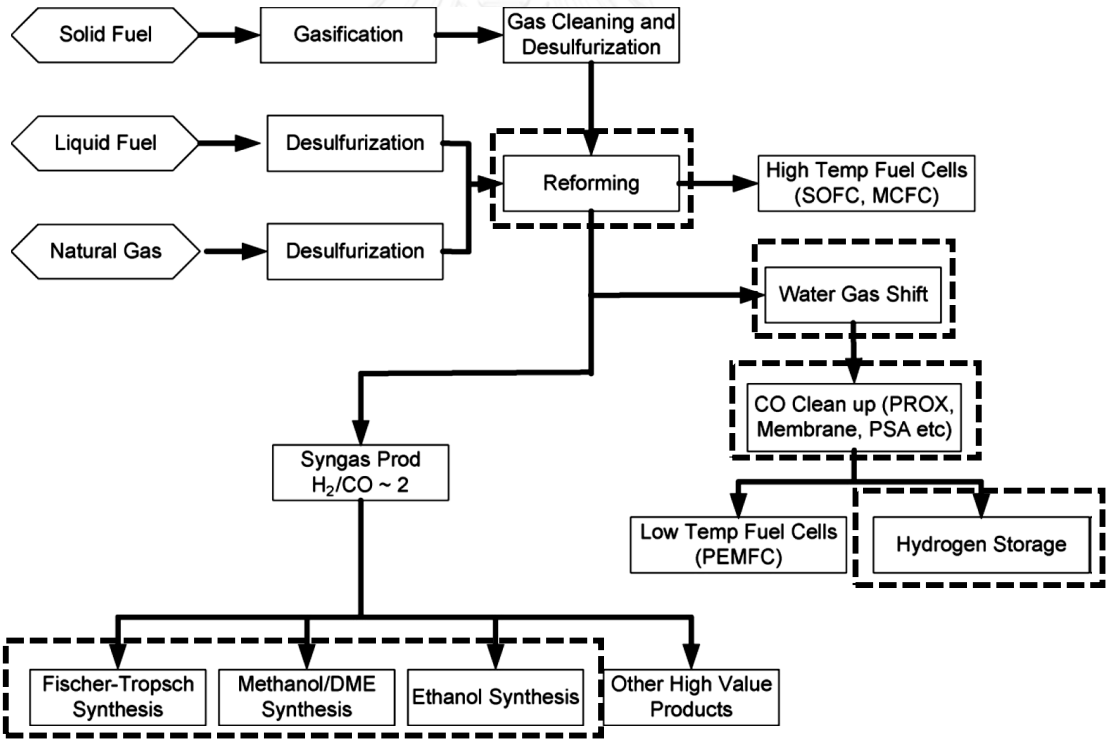

Figure 2.1 Hydrogen production and utilization pathway (Holladay et al. (2009))

To produce hydrogen, the production is classified into two major processes, non-reforming hydrogen production and hydrocarbon reforming process. In the case of the non-reforming hydrogen production, hydrogen is produced from biomass by direct photolysis and fermentation and splits from water by electrolysis and thermal energy. For hydrocarbon reforming process, hydrogen rich stream is produced from hydrocarbon fuels by three main techniques including steam reforming (Eq. 2.1), partial oxidation (Eq. 2.2) and autothermal reforming (or oxidative steam reforming) (Eq. 2.3). Additionally, water in the processes leads to the presence of water gas shift reaction (Eq. 2.4).

Steam reforming reaction:

$$C_nH_mO_p + (n-p)H_2O \rightarrow nCO + \left(n-p+\frac{m}{2}\right)H_2 \qquad (2.1)$$

Partial oxidation reaction:

$$C_nH_mO_p + \frac{(n-p)}{2}(O_2 + 3.76N_2) \rightarrow nCO + \left(\frac{m}{2}\right)H_2 + 3.76\frac{(n-p)}{2}N_2 \qquad (2.2)$$

Autothermal reforming reaction:

$$C_nH_mO_p + x(O_2 + 3.76N_2) + (n-2x-p)H_2O \rightarrow nCO + \left(n-2x-p+\frac{m}{2}\right)H_2 + 3.76xN_2 \qquad (2.3)$$

Water gas shift reaction:

$$CO + H_2O \leftrightarrow CO_2 + H_2 \quad (2.4)$$

Advantages and disadvantages of the three main reactions were summarized in Table 2.1. Steam reforming of hydrocarbon which is endothermic reaction requires an external heat source. The absence of oxygen leads to the lowest operating temperature; consequently, the product contains high H_2/CO ratio which is beneficial. Partial oxidation which is exothermic reaction converts hydrocarbon fuel into hydrogen and syngas by partially combusting. This process does not require a catalyst, but temperature must be controlled to prevent complete combustion. The operation at high temperature provides the lowest H_2/CO ratio and soot formation. Autothermal reforming combines steam reforming and partial oxidation, and an external heat source is not required because of the energy balance from both reactions. However, this process is expensive and complex, and an oxygen separation unit is necessary to feed pure oxygen in order to operate at higher performance. Therefore, the steam reforming of hydrocarbon fuels is the typical preferred process for hydrogen production in industry (Holladay et al. (2009)).

Table 2.1 Comparison of reforming technologies (Holladay et al. (2009))

Technology	Advantages	Disadvantages
Steam reforming	• Most extensive industrial experience • Oxygen not required • The lowest process temperature • The best H_2/CO ratio	• Highest air emissions
Autothermal reforming	• Lower process temperature • Low methane slip	• Limited commercial experience • Requires air or oxygen
Partial oxidation	• Decreased desulfurization requirement • No catalyst required • Low methane slip	• Low H_2/CO ratio • Very high processing temperatures • Soot formation/handling adds process complexity

2.2 Hydrocarbon fuel feedstock for hydrogen production

To produce hydrogen, hydrogen containing fuels such as light hydrocarbons, liquid hydrocarbons, alcohols and biomass are converted into hydrogen rich stream. According to the environmental concern, green hydrocarbon fuels including methane, methanol and ethanol are selected and described in the following sections.

2.2.1 Methane

Methane (CH_4) which is an odorless and colorless naturally presents in natural gas mixed with hydrocarbon and non-hydrocarbon gases. Methane composition in Natural gas is regionally dependent and the composition is summarized in Table 2.2 (Liu et al. (2010)).

Table 2.2 Methane composition in natural gas by region (Liu et al. (2010))

Region	Methane (%)
U.S./California	88.7
Canada/Alberta	91.0
Venezuela	82.0
New Zealand	44.2
Iraq	55.7
Libya	62.0
U.K./Hewett	92.6
U.R.S.S./Urengoy	85.3

Moreover, methane is a main component in biogas which is produced by anaerobic digestion of animal manure and digestible organic wastes. Methane content in biogas producing from various feedstock is reported in Table 2.3 (Al Seadi et al. (2008)). The methane from biogas is a potential renewable energy source and its utilization of untreated animal manure reduces greenhouse gas emissions such as methane and nitrous oxide from storage.

Table 2.3 Biogas production from various feedstocks (Al Seadi et al. (2008))

Feedstock	Biogas yield from fresh feedstock (m^3/ton)	Methane content (%)
Cattle manure	25.0	55
Pig manure	24.0	58
Grass silage	225.0	55
Maize silage	187.0	53
Food waste	179.0	65
Bio-waste (source separated)	145.0	60
Grease trap removal (pre-dewatered)	298.0	61

2.2.2 Methanol

Methanol (CH_3OH) which is the simplest alcohol compound is light, volatile, flammable and poisonous liquid. Methanol is an advantageous fuel as a hydrogen carrier for fuel cell application. Methanol is a liquid at atmosphere and normal temperature, and it has high H/C ratio equivalent to methane. Methanol can be produced from various feedstock by biological and chemical processes.

In biological processes, enzyme is used as biological catalyst for reduction of carbon dioxide (CO_2) to methanol (Obert and Dave (1999)). The enzyme is a reduced nicotinamide adenine dinucleotide (NADH) and it is produced from microbes. This

technologies are not only for recycling of the greenhouse gas, CO_2 but also for an efficient production of alternative fuel, CH_3OH.

Table 2.4 Main liquid product compounds from various biomass pyrolysis at 875 K in wt.% dry basis (Demirbas (2007))

Compound	Beech wood	Spruce wood	Olive husk	Hazelnut shell
Acetic acid	5.3	6.26	5.13	6.46
Methanol	5.82	7.52	7.65	7.26
acetone	1.28	1.36	1.51	1.46

In chemical processes, methanol is a major component of bio-oil which is produced from biomass pyrolysis in biorefinery processes (Garcia et al. (2000), Rioche et al. (2005), Wang et al. (1998)). The composition of bio-oil from various biomasses was reported in Demirbas (2007) and the main components which has high ratios in aqueous phase are summarized in Table 2.4. Moreover, methanol is possibly produced from CO_2 chemical recycling using renewable resources such as solar energy (Centi and Perathoner (2009), Katayama and Tamaura (2005)). Cu-Zn oxides based catalyst is used in the process and the reaction is shown in Eq. 2.5.

$$CO_2 + 3H_2 \leftrightarrow CH_3OH + H_2O \qquad (2.5)$$

Carbon dioxide recycling in the methanol economy is shown in Figure 2.2. Methanol can be used as fuel and chemical reactant, and CO_2 emission is reduced

from recycling. Thus, the methanol producing from CO_2 recycling via photosynthesis can fulfill environmental and economic requirements.

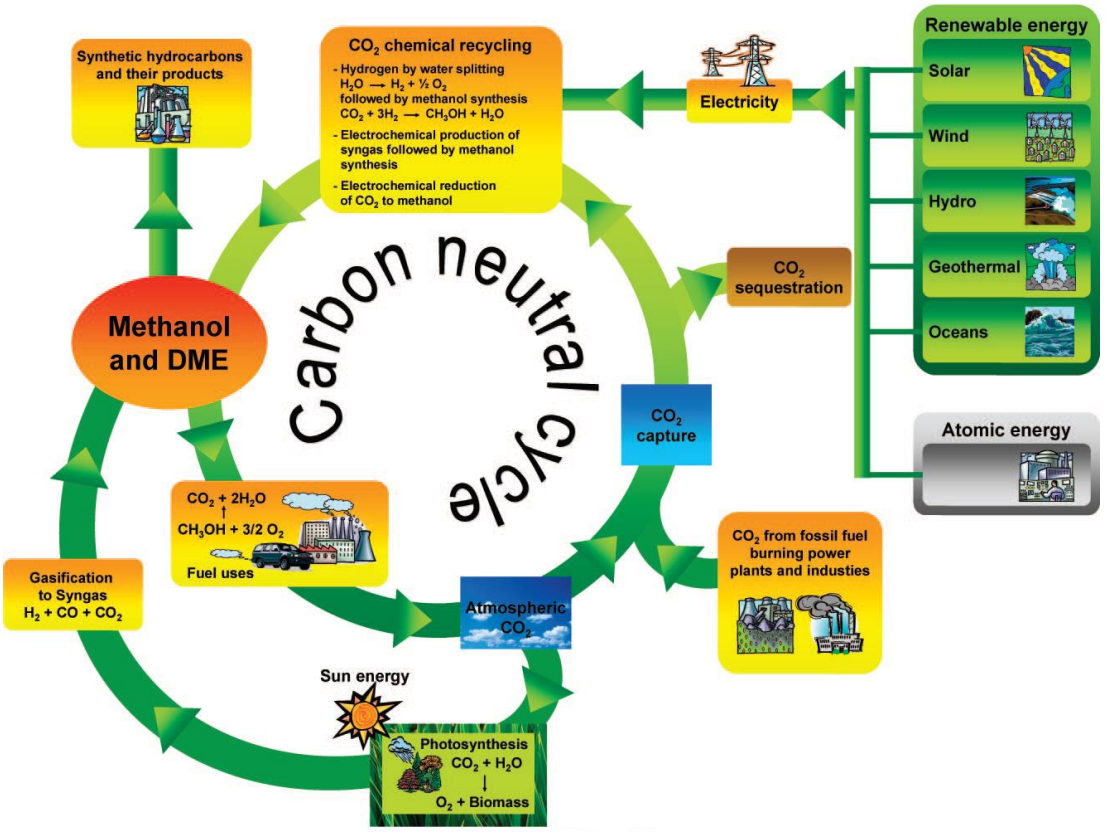

Figure 2.2 Carbon dioxide recycling in the methanol economy (Olah et al. (2008))

2.2.3 Ethanol fuel

Ethanol is an attractive fuel, since it offers relatively high hydrogen content, availability, non-toxicity, and storage and handling safety. Ethanol can be produced by fermentation of biomass such as energy plants, wastes from agro-industry, forestry residue materials, and organic waste (Ni et al. (2007)). Ethanol production from agricultural products such as sugar cane, switchgrass, potatoes, corns, and other starch-

rice is effective and it prospers in the tropical climate country (Hotza and da Costa (2008)). However, the production cost is rather high due to the expensive feedstock. Lignocellulosic materials consisting of cellulose, hemicellulose and lignin are also used for ethanol production (Galbe and Zacchi (2002), Sun and Cheng (2002)). Lignocellulosic material source and its content are shown in Table 2.5. Bio-ethanol production is less complicated than bio-methanol or recycling methane.

Table 2.5 The contents of cellulose, hemicellulose, and lignin in common agricultural residues and wastes (Sun and Cheng (2002))

Lignocellulosic materials	Cellullose (%)	Hemicellulose (%)	Lignin (%)
Hardwoods stems	40–55	24–40	18–25
Softwood stems	45–50	25–35	25–35
Nut shells	25–30	25–30	30–40
Corn cobs	45	35	15
Grasses	25–40	35–50	10–30
Paper	85–99	0	0–15

2.3 Steam reforming kinetic model

Kinetic models of steam reforming depend on catalyst and fuel that are employed in the experiment. The reaction rate constant (k_i) and equilibrium constant (K_i) are generally based on Arrhenius equation as reported in Eqs. 2.6 - 2.7 depending on reaction temperature (T).

$$k_i = A_i \exp\left(\frac{-E_a}{RT}\right) \quad (2.6)$$

$$K_i = A_i \exp\left(\frac{-\Delta H}{RT}\right) \quad (2.7)$$

A_i is pre-exponential factor, E_a is activation energy, ΔH is enthalpy change and R is gas constant. Kinetic models of methane, methanol and ethanol steam reforming are described in this section.

2.3.1 Kinetic model of methane steam reforming

For decades, nickel-based catalyst is commercially used for methane steam reforming processes in the industry (Sutton et al. (2001)). Several literatures presented different kinetic models depending on the catalysts. The most well-known kinetic models of methane steam reforming were given by Xu and Froment (1989). Three significant reactions occurred over Ni/$MgAl_2O_4$ catalyst were proposed as in Eqs. 2.8 – 2.10.

$$CH_4 + H_2O \rightarrow CO + 3H_2 \quad (2.8)$$

$$CO + H_2O \leftrightarrow CO_2 + H_2 \quad (2.9)$$

$$CH_4 + 2H_2O \rightarrow CO_2 + 4H_2 \quad (2.10)$$

2.3.2 Kinetic model of methanol steam reforming

Methanol steam reforming catalyst is divided into two groups, copper-based catalyst and group VIII metal including palladium, platinum and nickel (Sá et al. (2010)). The copper-based catalyst always prefers to operate at low temperature about 573 K because it is deactivated at the higher temperature (Palo et al. (2007)) The kinetic expressions over $Cu/ZnO/Al_2O_3$ are investigated by Peppley et al. (1999a, b). The three overall reactions for methanol steam reforming processes are

$$CH_3OH + H_2O \rightarrow CO_2 + 3H_2 \quad (2.11)$$

$$CO + H_2O \leftrightarrow CO_2 + H_2 \quad (2.12)$$

$$CH_3OH \rightarrow CO + 2H_2 \quad (2.13)$$

2.3.3 Kinetic model of ethanol steam reforming

Ethanol steam reforming is used to increase the hydrogen production due to high hydrogen content of ethanol. Kinetic models based on Langmuir-Hinshelwood's approach are proposed by Sahoo et al. (2007). Three main reactions of ethanol steam reforming are follows:

$$C_2H_5OH + 3H_2O \rightarrow 2CO_2 + 6H_2 \quad (2.14)$$

$$C_2H_5OH \rightarrow CO + H_2 + CH_4 \quad (2.15)$$

$$CO + H_2O \leftrightarrow CO_2 + H_2 \quad (2.16)$$

2.4 Membrane separation technology

In hydrogen separation, common technologies are solvent adsorption, pressure swing adsorption, cryogenic recovery and membrane separation. Comparing between these methods, membrane separation technologies have economic potential in reducing operating costs, minimizing unit operations and lowering energy consumption (Paglieri and Way (2002)).

There are four types of membranes which have been commercialized and developed. The types of membrane are polymeric membranes, porous (ceramic, carbon, metal) membranes, dense metal membranes, and ion-conductive membranes. Comparison of membrane types for hydrogen separation is reported in Table 2.6 (Liu et al. (2010)).

Dense metal membranes have been used for commercial applications because they provide high hydrogen selectivity which is suitable for PEMFC. Palladium which has outstanding ability to transport hydrogen through the metal (Yun and Ted Oyama (2011)) is selected to fabricate as dense metal membranes. Hydrogen is dissolved in bulk metal and then permeated through the metal membrane following a solution – diffusion mechanism which is schematically shown in Figure 2.3 (Liu et al. (2010)).

Table 2.6 Comparison of membrane types for hydrogen separation (Liu et al. (2010))

Parameters	Membrane Type			
	Polymeric	Nano porous	Dense Metal	Ion-Conducting
Typical composition	Polyimide; cellulose acetate	Silica; alumina; zeolites; carbon	Palladium alloys	Water-swollen, strong-acid, cation exchange membranes; dense ceramics (perovskytes)
Diffusion mechanism	Solution–diffusion	Size exclusion	Solution–diffusion	Solution–diffusion
Driving force	Pressure gradient	Pressure gradient	Pressure gradient	Ionic gradient
Operating temperature	≤ 110 ° C	≤ 1000 ° C	150 – 700 ° C	≤ 180 ° C (polymeric); 700 – 1000 ° C (ceramic)
Relative permeability	Moderate - high	Low - moderate	Moderate	Moderate
Typical selectivity	Moderate	Moderate	Very high	Very high
Relative cost	Low	Low	Moderate	Low

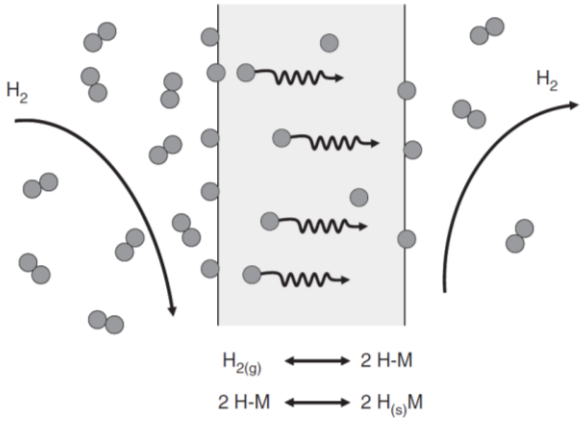

Figure 2.3 Commonly accepted mechanism for the permeation of hydrogen through dense metal membranes (Liu et al. (2010))

Thus, only hydrogen atom that can be dissolved in palladium permeates through the membrane. The expression for hydrogen flux through dense metal membranes is a modified form which is

$$J_{H_2} = P_{H_2}\left(\frac{\Delta P}{l}\right) \tag{2.17}$$

when J_{H_2} is hydrogen flux, ΔP is the partial pressure of gas H_2 in the feed stream minus the partial pressure of gas H_2 in the permeated stream, and l is membrane thickness. The common unit for the permeability (P_{H_2}) is the barrier about 10^{-10} cm^3 (STP) cm / (cm^2·s·cm Hg), and

$$\Delta P = P_{H_2,f}^{n} - P_{H_2,p}^{n} \tag{2.18}$$

where subscript *f* and *p* is at feed side and permeate side, respectively. The exponent (n) is a value between 0.5 and 1.0. Under ideal case (clean membrane surfaces and

no interaction of the membrane surfaces with species other than hydrogen), the value of *n* is 0.5. In case of simulation study, Gallucci et al. (2004a) expressed permeability into

$$P_{H_2} = A_0 e^{\frac{-Ea}{RT}} \quad (2.19)$$

when A_0 is 1.12 x 10^{-5} mol/(m·s·$Pa^{0.5}$), Ea is 29.16 kJ/mol, R is gas constant, and T is temperature.

2.5 Micro-channel reactor

The most common chemical reactors involve with catalyst are fixed bed reactor and it has several limitations. Pressure drop and diffusional limitations depend on particle size of catalyst. To minimize the limitations, large particle size is required for decreasing pressure drop, while the diffusional limitation is minimized at small particle size. To solve these issues, the structured catalyst which forms a thin layer on the wall of the channels is proposed. In the case of hydrogen production, the compact and lightweight systems are also needed in vehicular system, leading to the development of micro-channel reactors (Sanz et al. (2013)).

Micro-channel reactors have been of enormous interest both in the academia and industry. Micro-channel reactors are defined as the devices for chemical reaction whose channels have at least one dimension smaller than 1 mm (Sanz et al. (2013)).

Due to size reduction of the micro-channel reactors, the important advantages are as follows.

1. Decrease in linear dimensions
2. Increase of the surface to volume ratio
3. Volume reduction
4. Fast and inexpensive tests for materials and processes
5. Production flexibility
6. Faster heat and mass transfer
7. Faster start-up
8. Easier scaling up
9. Smaller plant size
10. Lower materials, transport and energy costs
11. Higher flexibility to market demands

The micro-channel reactors have attracted attention in the energy technology field, wherever compact, decentralized solutions are required. Production of fuels and power is the subject of worldwide research efforts in the micro-technology. An overview of the micro-channel reactors application in the field of renewable energy and fuel production is indicated in dot line boxes of Figure 2.1 (Kolb (2013)).

2.6 Computational fluid dynamic simulation

Computational fluid dynamics (CFD) is an analysis method for several systems and the systems involve fluid flow, heat transfer and chemical species phenomena and reaction by using computer-based simulation. This technique has been used in wide range application as follows (Versteeg and Malalasekera (2007)):

- Aerodynamic of aircraft and vehicle
- Hydrodynamics of ships
- Power plant
- Chemical process engineering
- Environmental engineering
- Biomedical engineering

CFD codes are built around the numerical algorithms. All CFD codes consist of three main elements, a pre-processor, a solver and a post-processor. Pre-processor is the input of a problem detail including the geometry, grid generation, the physical and chemical phenomena, fluid properties and specification of boundary conditions. In the solver section, there are four main techniques for numerical solution which are finite difference, finite element, spectral methods and finite volume methods. For the finite element method, the calculation domain is divided into elements by using piecewise function such as linear and quadratic equations. Unknown variables are measured

providing simulation results with residue or error and this error is minimized. The basic steps of the solver are as following:

1. Approximation of unknown variables
2. Discretization into subsequent mathematical manipulations
3. Solution of the algebraic equation

As in post-processor, the results from the solver are displayed in different appropriate visualization tools to analyze the results.

CHAPTER III

LITERATURE REVIEWS

This research mainly focuses on the design of integrated reactor in micro scale for hydrogen production. Literature reviews have been divided into two sections. In the first section, the integrated micro reactors for hydrogen production including thermally coupled reactors and membrane reactors are reported. Secondly, the studies on flow arrangement are reviewed.

3.1 Processes integrated micro reactors for hydrogen production

Process integration in micro reactor for hydrogen production has been studied by experiment and simulation. In thermally coupled reactor studies, combustion is combined with steam reforming to supply heat for a reformer. To purify the hydrogen steam, palladium membrane integration has been investigated. The studies of the thermally coupled reactor and the membrane reactor are summarized in the following sections.

3.1.1 Thermally coupled reactor review

In micro reactor research field, the experiment and simulation are conducted. However, the studies are mostly done by simulation due to the complexity and high expenses of the experimental setup. In the case of the light fuel and diesel micro reformer, the experiment and simulation using computational method were examined

by Grote et al. (2011). The 10 kW steam reforming reactor and a small scale reformer were employed as shown in Figure 3.1a and Figure 3.1b, respectively. Both reactors had superheater in Figure 3.1a or burner in Figure 3.1b for heat generation and reformer for hydrogen production.

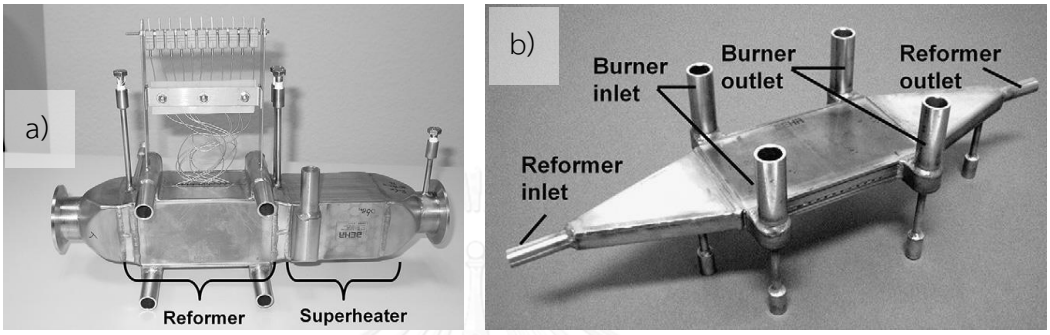

Figure 3.1 The reactors using in the study of Grote et al. (2011): a) The 10 kW steam reforming reactor and b) A small scale reformer

The simulation of this research studied the effect of geometry and flow direction including co-current flow, counter flow and cross flow. The results show that the co-current flow provided fast heating rates and high fuel conversion.

In the simulation-based research, CFD simulation is usually employed by using a commercial program or a developed program. Simulated geometry is considered as a set of square channel in micro scale.

In the case of one dimensional CFD simulation, thermally coupled reactors using methane and ethanol were examined by Frauhammer et al. (1999) and Anzola et al. (2010). Frauhammer et al. (1999) developed a reactor for autothermal operation

of methane steam reforming and methane combustion using simulation and experiment. Both streams were fed in counter flow direction into the monolith reactor with the gas distribution as shown in Figure 3.2a. The gas distribution or reactor head was invented by Von Hippel et al. (1999), and the flow arrangement was parallel arrangement as in Figure 3.2b.

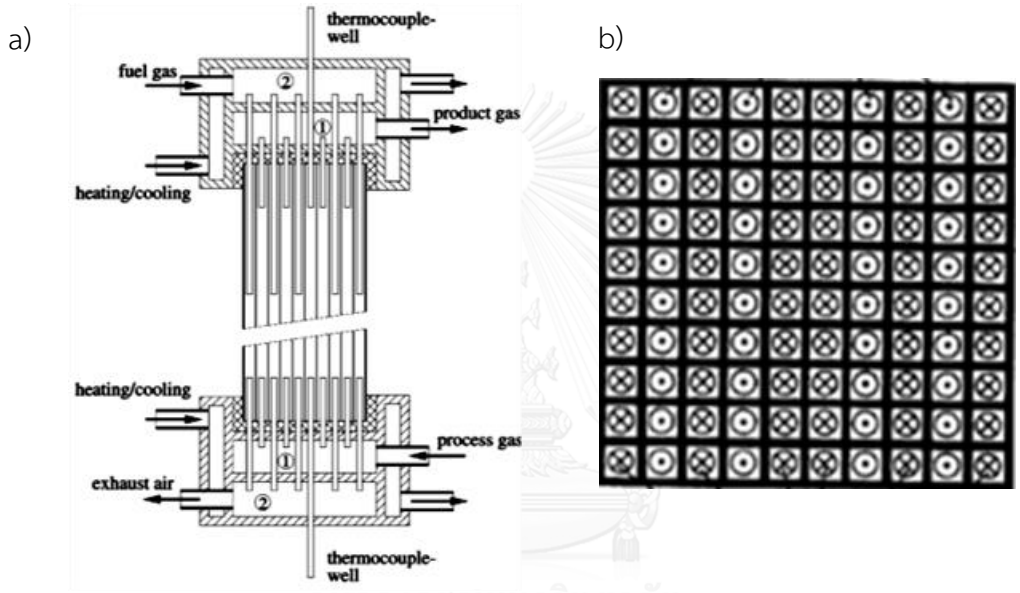

Figure 3.2 Autothermal reactor of Frauhammer et al. (1999): a) Monolith reactor with the gas distribution and b) The flow arrangement when cross and dot channels were combusting and reforming channels, respectively

Anzola et al. (2010) studied a microreformer with heat supply for ethanol steam reformging using a 1D pseudohomogeneous model. The reactor configuration is illustrated in Figure 3.3. Heat duty, channel width, and direction of feed flow

configuration were considered. The higher reactor performance was performed by co-current flow configuration and small channel width.

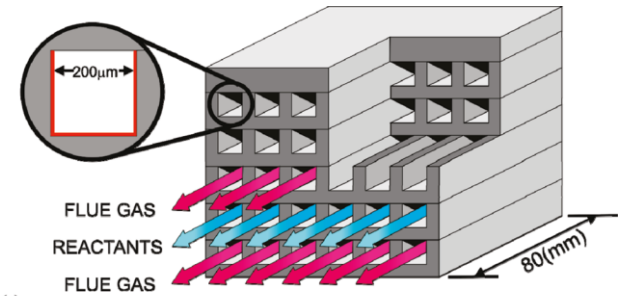

Figure 3.3 Schemes of the ethanol steam reforming microreactor (Anzola et al. (2010))

For two dimensional CFD simulation, methane and methanol steam reforming coupling with combustion were investigated by Zanfir and Gavriilidis (2003) and Tadbir and Akbari (2011), respectively. The configurations which were computed in the studies of Zanfir and Gavriilidis (2003) and Tadbir and Akbari (2011) are shown in Figure 3.4a and Figure 3.4b, respectively.

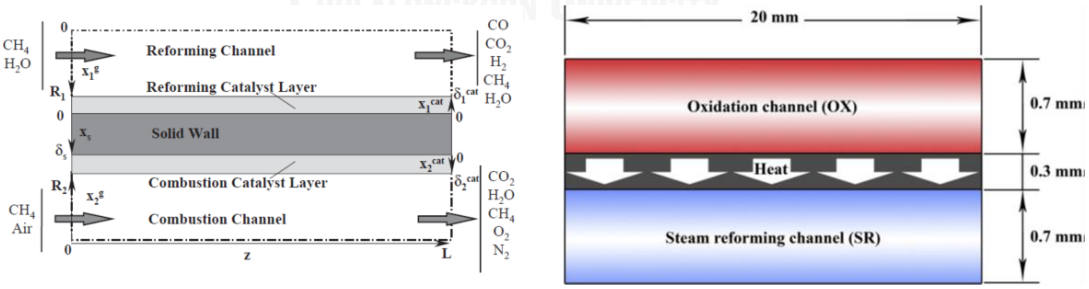

a) b)

Figure 3.4 Two dimensional reactor configuration: a) Zanfir and Gavriilidis (2003) and b) Tadbir and Akbari (2011)

In the study of Zanfir and Gavriilidis (2003), steam reforming and combustion reactions occurred inside catalyst layer of their channels, and the reaction calculation based on catalyst volume depending on diffusivity inside the catalyst layer. This reactor type minimized heat and mass transport resistances, leading to the reduction of temperature gradients between gas phases from 250 K in conventional reformers to 40 K. The increase of distance between plates in the range of 1–4 mm showed no significant difference on reactor performance. The results were similar to the study of Fukuhara and Igarashi (2005). The wall typed reactor which coated catalyst on the reactor wall presented a good exchangeability of thermal energy by conductive heat transfer and the decrease of channel height did not affect the reactor performance. With the respect of the study of Tadbir and Akbari (2011), the catalyst layer was neglected in the calculation. The reaction prediction was based on the surface of catalyst; hence, diffusion through the catalyst layer was eliminated. The effect of operating and design parameters was investigated. Consequently, the optimized gas hourly space velocities suggested at 3000 h^{-1} for reforming channel and 24,000 h^{-1} for combustion channel and thinner wall led to higher conversion of steam reforming. In the difference of reaction based calculation, the comparison between volume and surface based reactions was examined by Irani et al. (2011). Both calculations were compared with the experimental result at the same condition. The surface based reaction exhibited better results in generality and accuracy.

On the assumption of three dimensional CFD simulation, Tadbir and Akbari (2012) studied methanol steam reforming and combustion in micro reformer. The reactor model and the micro reactor cluster are shown in Figure 3.5a and Figure 3.5b, respectively.

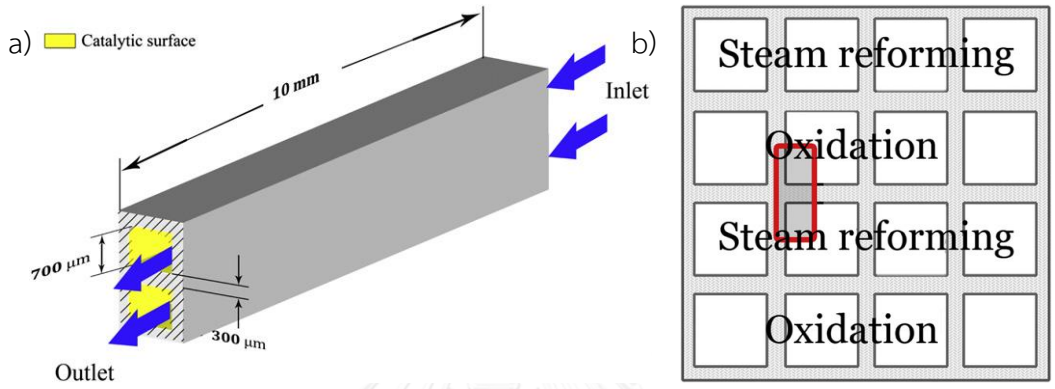

Figure 3.5 The micro reactor model of the study of Tadbir and Akbari (2012): a) The reactor configuration and b) The micro reactor cluster

Calculation domain was specific at the area inside the red boundary in Figure 3.5b, the surface based reaction was employed. Parameters including steam to carbon ratio, methanol mole fraction at the combustion channel, gas hourly space velocities of both channels, catalyst loading in the reforming channel, and the reactor length were investigated the influence on the reactor performance. The reactor performance increased with the increase of steam to carbon ratio, methanol mole fraction for combustion, gas hourly space velocities of combustion channel, catalyst loading and the reactor length. At the recommended condition, a micro reactor consisting of 1540 channels was able to produce enough synthesis gas to run a typical 30 W PEMFC.

In the case of iso-octane steam reforming, micro reformer coupling with methane combustion in square channel reactor as shown in Figure 3.6 was studied by Karakaya and Avci (2011). The flow arrangement was the parallel arrangement. The results from two and three dimensional simulations were compared. Both results were similar; thus, the two dimensional model can be substituted the three dimensional model. It was selected in this further study. Therefore, the two dimensional simulation of the thermally coupled reactor approached the thermally coupled reactor using the parallel arrangement.

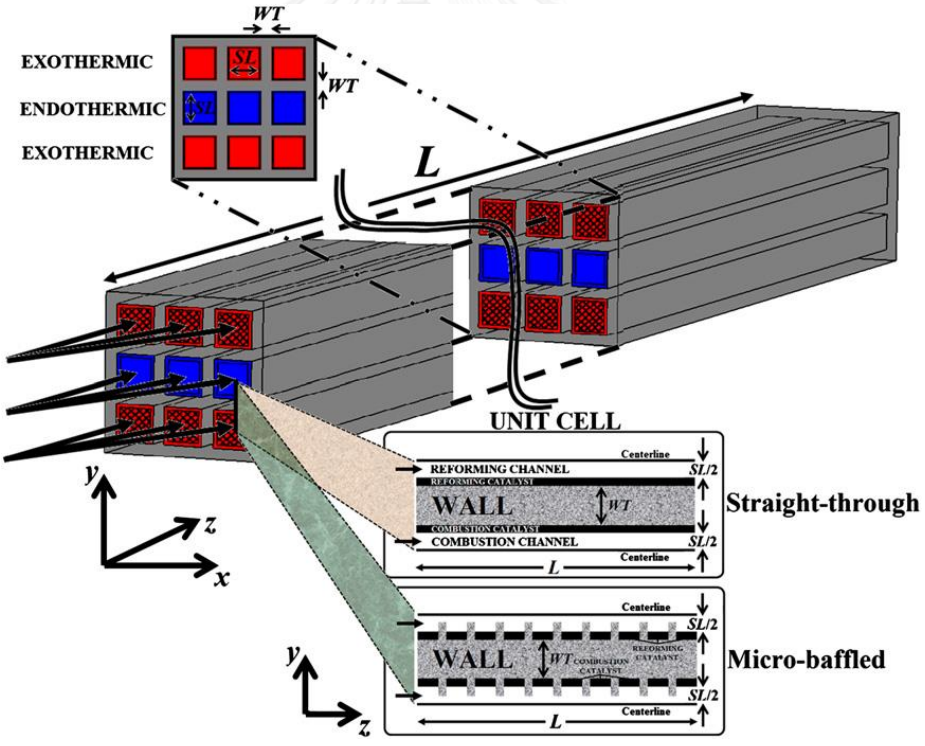

Figure 3.6 Scheme of micro reaction in Karakaya and Avci (2011)

Furthermore, a metallic monolith reactor was also studied by Hong Mei et al. (2007) in three dimensional simulation. The metallic monolith reactor and the

simulation configuration are illustrated in Figure 3.7a and Figure 3.7b, respectively. Methane catalytic combustion occurred in inner area and methane steam reforming performed in annular area. The reactor with the proper structure and catalyst distribution enhanced heat transfer and the methane conversion, resulting in a compact and intensified unit.

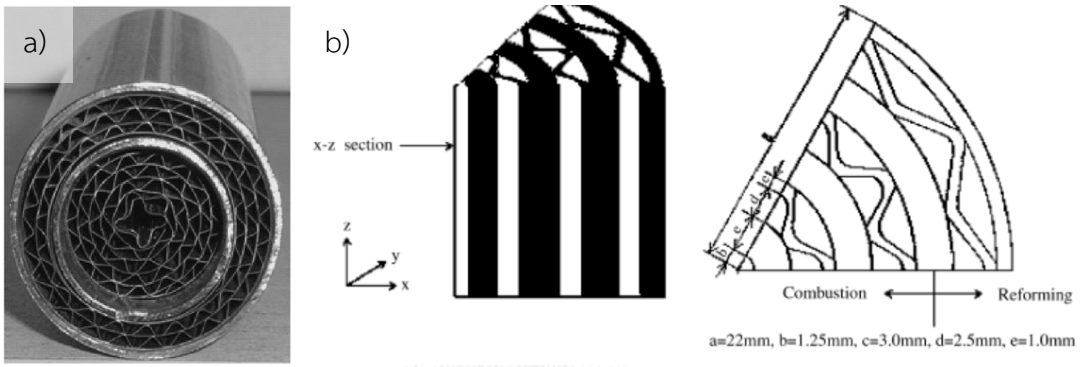

Figure 3.7 Metallic monolith reactor study (Hong Mei et al. (2007)): a) The metallic monolith reactor and b) The simulation configuration

The thermally coupled reactor studies were mostly investigated by simulation. The influence of parameters was examined in these studies and the operating and design parameters were recommended. When comparing with the conventional reformer, the micro reactor exhibited higher reactor performance due to a better heat transfer rate.

3.1.2 Micro membrane reactor

Membrane can be integrated in a micro reactor. Membrane reactor generally produces high selectively produce and improves reactor performance (Lukyanov et al. (2009), Yun and Ted Oyama (2011)). Selective palladium membrane allows only hydrogen to flow through membrane layer. Hydrogen which is separated from reformer channels shifts the reaction equilibrium forward, resulting in the increase of reaction rates. Consequently, the reaction can achieve higher conversion at a lower temperature.

A typical membrane reactor is in tubular configuration consisting of reaction and permeation sections. Inert gas such as nitrogen may be used as a sweep gas for carrying hydrogen product. In the case of micro scale, palladium membrane was considered for fabrication inside cordierite honeycomb structure by Kim et al. (2009). Alumina powder in micro-size and nano-size were coated to cover cracking surface and large pore, resulting in the smooth surface. Palladium was plated on the prepared wall by electroless plating, and Scanning Electron Microscope (SEM) images of palladium films are shown in Figure 3.8. The crystallite size of palladium was about 2 μm with an estimated film thickness of 8 μm. The membrane fabrication was successful and achieved the highest hydrogen flux at 5.5 mmol m^{-2} s^{-1} and the best selectivity at 360 mol H_2 per mol He. Furthermore, Kim et al. (2010) tested the performance of membrane within monolith structure in ethanol reformate stream. Only two channels

were investigated. The hydrogen permeability was 1.73 × 10^{-9} mol m^{-1} s^{-1} $Pa^{-0.5}$ at 350 °C with an activation energy of 7.3 kJ mol^{-1} and the hydrogen/helium selectivity was higher than 1000:1 throughout all exposure tests. Therefore, the membrane fabrication within monolith structure has a possibility to be a micro membrane reformer. These studies support the idea of our research which is the integration of hydrogen production processes within a monolith structure.

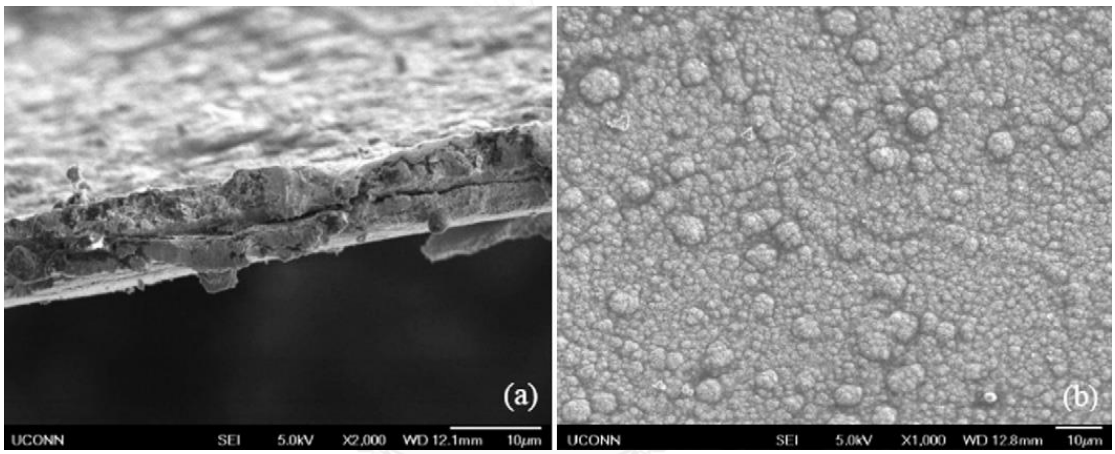

Figure 3.8 SEM images of plated palladium films: a) Film cross-section, 2000×magnification and (b) Film surface, 1000×magnification (Kim et al. (2009))

Autothermal reformer integrated with membrane was investigated by Michelsen et al. (2013) and Xuan et al. (2012). Both researches studied methane steam reforming using two dimensional CFD simulation. In the study of Michelsen et al. (2013), the configuration of membrane reactor is shown in Figure 3.9. The checked arrangement (Figure 3.9a) was employed. In Figure 3.9b, hydrogen which was separated through membrane combusted with oxygen in sweep gas, air and generated heat to

the system. The steam to carbon and steam to oxygen ratios were optimized in steady state analysis, achieving 92% of methane conversion. Furthermore, the dynamic analysis reported that non-linear control schemes may be necessary for satisfactory control performance.

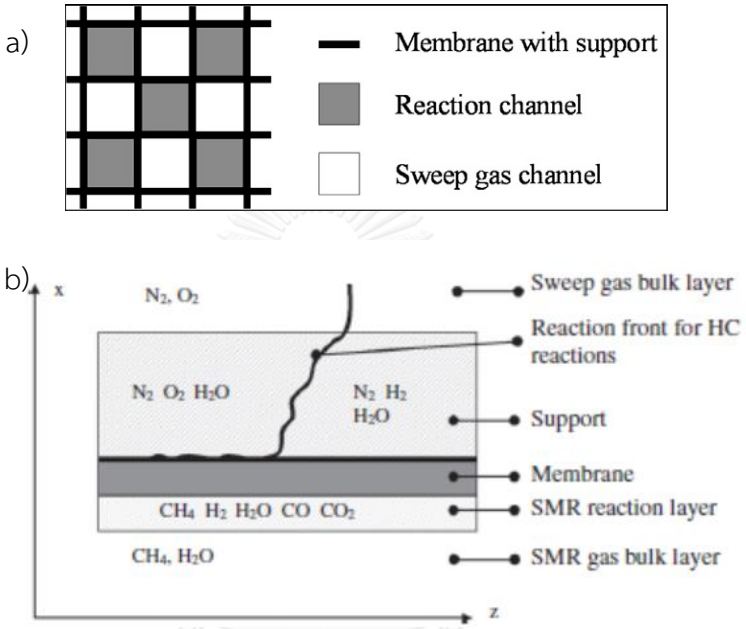

Figure 3.9 The membrane monolith reactor of Michelsen et al. (2013): a) Flow pattern and b) Reactor concept

The relevant physicochemical phenomena during the fuel processing were discussed by Xuan et al. (2012). The reactor shown in Figure 3.10a was simulated in two dimensions. Methane, oxygen and water were fed to the reforming channel, and nitrogen was used as sweep gas. In Figure 3.10b, temperature strongly increased to 1100 K at the contact point between the reactants and the catalyst layer. Hydrogen was produced and separated to permeated channel as shown in Figure 3.10c.

Moreover, the gaseous hourly space velocity was optimized and the optimum was approximately at 18,000 h^{-1}.

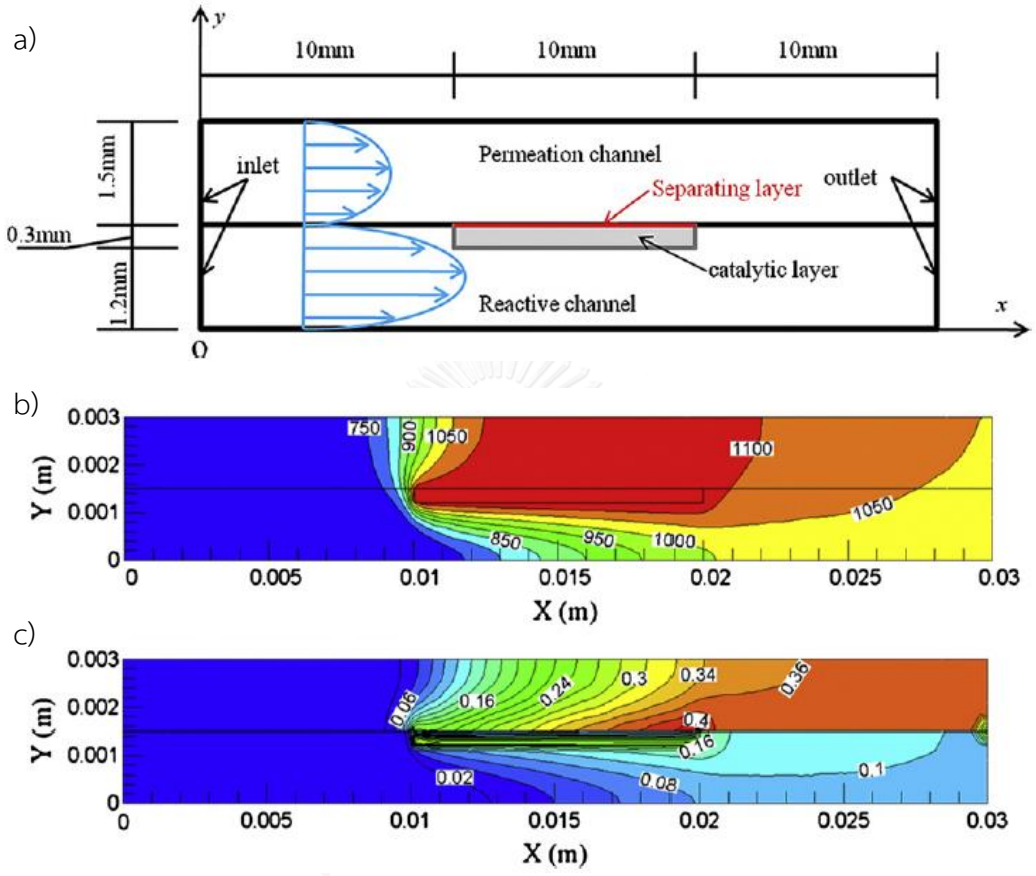

Figure 3.10 Transport phenomena occurring in Xuan et al. (2012) when a) Reactor configuration, b) Temperature profile (in K) and c) Hydrogen mole fraction profile

Membrane reactor simulation was also investigated by using Aspen plus. Ethanol fuel processors using membrane purification for applying to PEMFC were analyzed thermodynamically by Montané et al. (2011). Membrane utilization produced efficiencies as similar as the conventional processes, using reformer, water shift and COPROX reactors. The processes based on a membrane reformer which was simpler

offered the best efficiency. Thus, this reforming process using membrane can be effectively developed and marketed. To design a membrane integrated reactor, a sequential modular approach was employed (Jin et al. (2010), Ye et al. (2009)). Ye et al. (2009) studied the fluidized bed membrane reactors as shown in Figure 3.11a. The reactor was considered as a system of sub-rectors and sub-separators in Figure 3.11b.

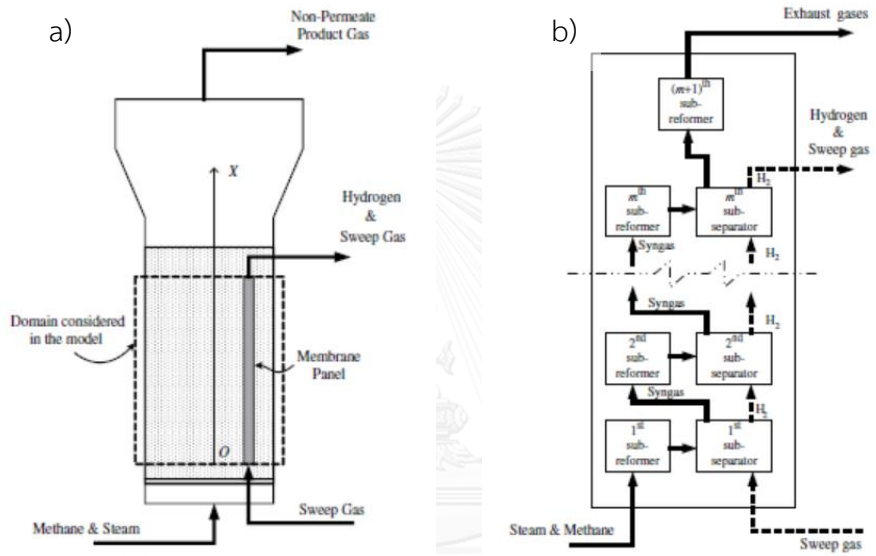

Figure 3.11 Schematic of Ye et al. (2009) simulation: a) A fluidized bed membrane reactor and b) Sequential model of the reactor

Assumption of the model was as follows: 1) One-dimensional plug flow reactor, 2) Uniform temperature, 3) Negligible pressure gradients between both channels, 4) Thermodynamic equilibrium of methane steam reforming reaction and 5) Sieverts' law for hydrogen permeation through the membrane. The influences of reactor pressure, temperature, steam-to-carbon ratio, and permeate side hydrogen partial pressure on reactor performances were explored with the model. It was found that the membrane

integration shifted the equilibrium forward, leading to improving hydrogen yield. In the investigation of Jin et al. (2010), dense oxygen permeation membrane reactor as illustrated in Figure 3.12a was designed to produce hydrogen from oxidative steam reforming of ethanol. Sequential model of this reaction are shown in Figure 3.12b. Sub-separators separated oxygen from air and then oxygen was fed to sub-reactors which was Gibbs reactor. In the simulation result, there was an optimal length of the tubular membrane reactor at an operating temperature and a fixed steam-to-ethanol ratio.

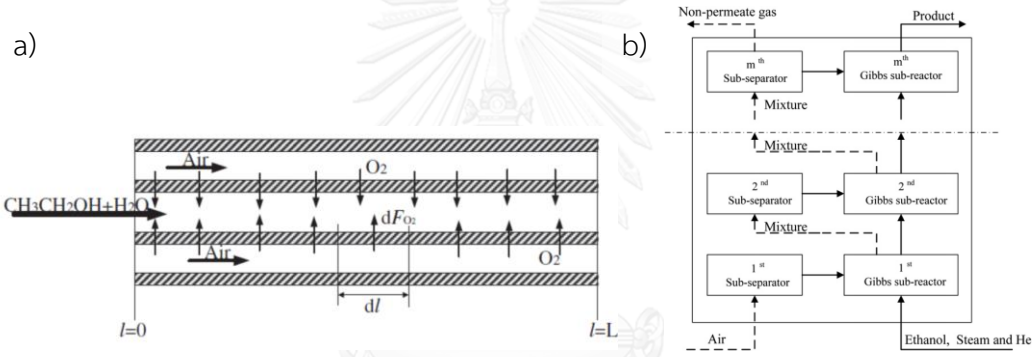

Figure 3.12 Schematic diagram of Jin et al. (2010) simulation: a) A dense oxygen permeation membrane reactor and b) Sequential model

Additionally, thermally coupled membrane micro reactor with heat supply and membrane was studied by Patel and Sunol (2007). The schematic diagram of the reactor is shown in Figure 3.13. The simulation was conducted based on mass and energy balance equations in one dimension using a finite element method. A thermally coupled membrane reactor provided higher reformer performance in terms of methane conversion and hydrogen recovery yield than the conventional reactor

without membrane. The influence of operating parameters and flow direction was also investigated.

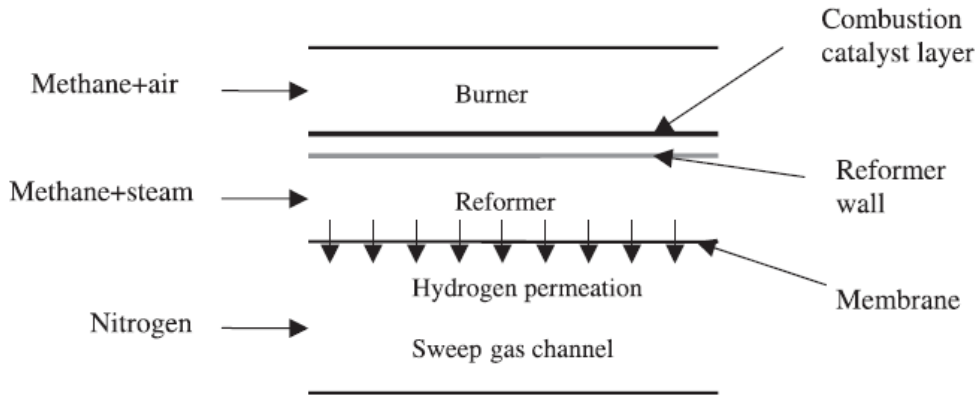

Figure 3.13 The schematic diagram of the Patel and Sunol (2007) reactor

In the research of membrane reaction, the integration of membrane obviously provided better reaction performance with several advantages. Higher conversion can be achieved at lower temperature which is preferable for water gas shift reaction. Consequently, hydrogen yield was higher. Furthermore, the influence of parameters was investigated and reported.

3.2 Flow arrangement studies

Integrated reactors are reviewed and summarized in 3.1 section. However, the feed flow arrangement between two steams of steam reforming and combustion or sweep gas was not considered in the studies. Most studies used the parallel flow arrangement, and two dimensional simulation results were close to the parallel arrangement in three dimensional study (Karakaya and Avci (2011)). The checked

arrangement was conducted only in the study of Michelsen et al. (2013). In the case of experimental study, methanol steam reforming combined with methanol combustion inside a 3x3 square channel monolith (Moreno and Wilhite (2010)). The schematic of the reactor is shown in Figure 3.14. The reactor performance without any external insulation achieved beyond 90% of methanol steam reforming conversion and 70% of hydrogen yields when operated at 673 K.

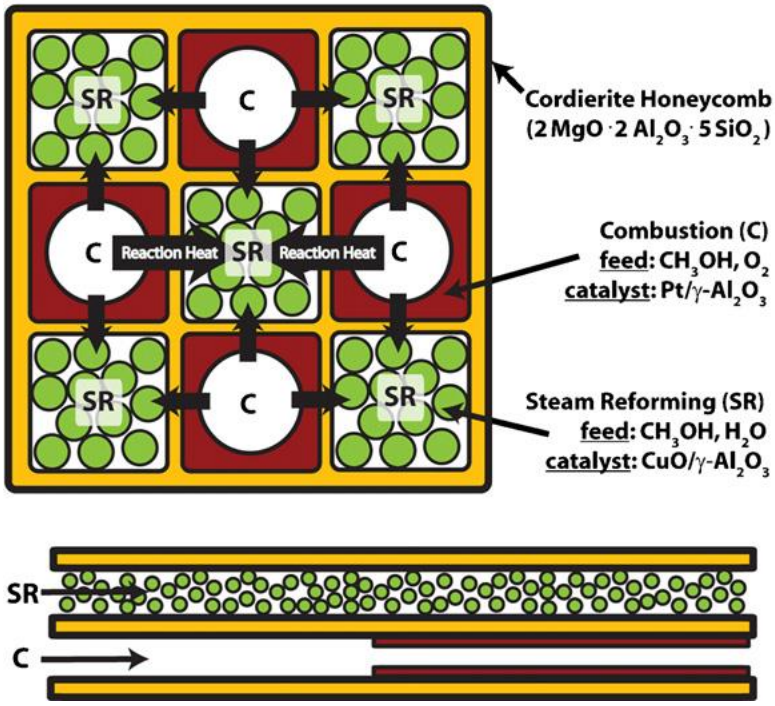

Figure 3.14 The schematic of the reactor of Moreno and Wilhite (2010)

The influence of the flow arrangement was investigated by Moreno et al. (2010). 5x5 square channels of a cordierite monolith with a cell density of 72 cells per square inch (cpsi) was employed as micro channel networks for coupling methanol combustion and steam reforming. Three patterns of the arrangement including the

checked arrangement, the annular arrangement and the annular arrangement with self-insulation were employed as shown in Figure 3.15. The checked arrangement (Figure 3.15a) and the annular arrangement (Figure 3.15b) achieved the highest hydrogen yields when integrating steam reforming with partial oxidation. With integrated steam reforming with combustion, the annular arrangement with self-insulation (Figure 3.15c) achieved highest hydrogen yields. Therefore, the coupled reactors using three patterns are shown insignificantly different reactor performance in their investigation.

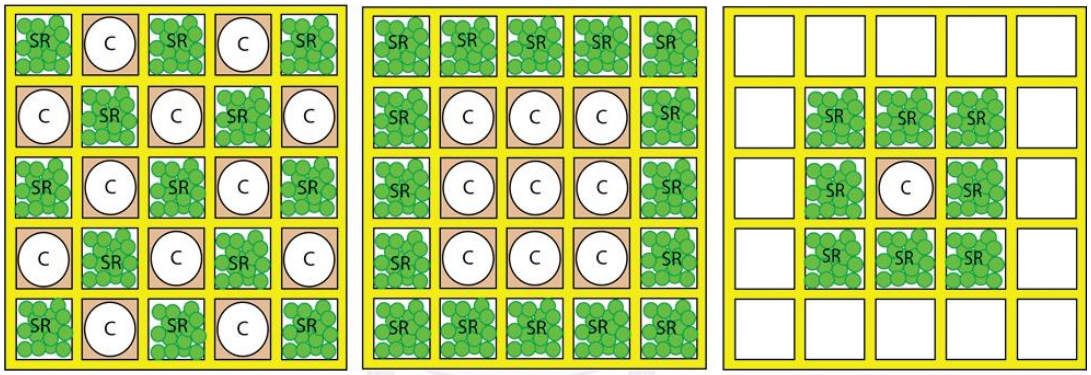

a) b) c)

Figure 3.15 Cross-section illustrations: a) the checked arrangement, b) the annular arrangement and c) the annular arrangement with self-insulation (Moreno et al. (2010))

The comparison between the checked arrangement and the parallel arrangement in integrated micro reactor has not been investigated. The two arrangements have their own advantage - simplicity for the parallel arrangement and higher contact area for the checked arrangement. Thus, the comparison between the arrangements in micro reactor should be studied. In the flow arrangement study, the

three dimensional CFD simulation is necessary to study the reactor performance and the phenomena inside the reactor due to the significant influence of heat and mass transfers in all dimensions.

CHAPTER IV
COMPARISON BETWEEN PARALLEL AND CHECKED ARRANGEMENTS OF MICRO REFORMER FOR H_2 PRODUCTION FROM METHANE

This research studied the reactor performance of parallel and checked arrangements in heat integrated micro-channel reactor. The thermally coupled micro reactor (TMR) was examined by computational fluid dynamic simulation using various operating and design parameter. Simulation methodology and results are described as follows.

4.1 Micro reformer configuration

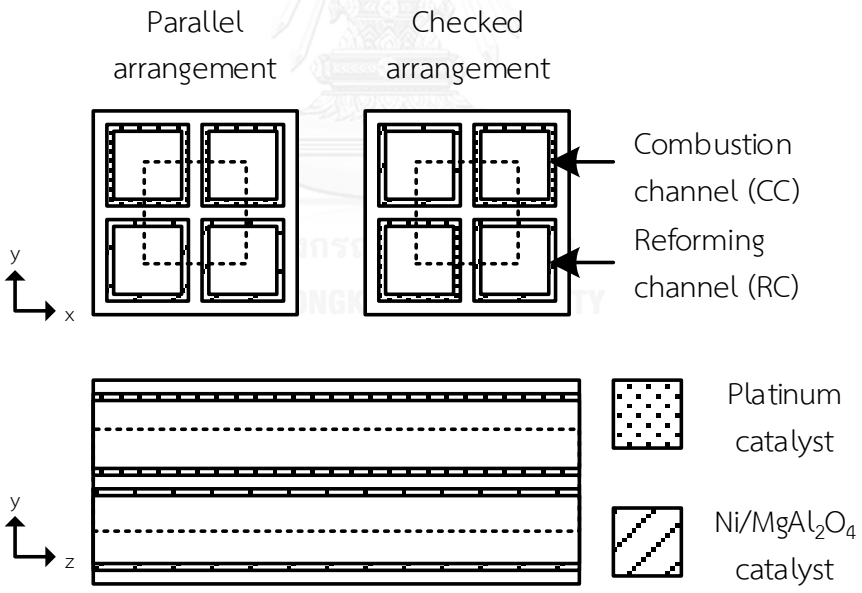

Figure 4.1 Micro reformer configuration of TMR in the parallel arrangement and the checked arrangement

Monolith structure consists of multi-channel inside a single structure. In this study, 2x2 square shape channels inside the alumina structure are considered as micro reformer configuration of TMR as shown in Figure 4.1. Three dimensional calculation domain is the center volume of the configuration due to the symmetry condition. In this calculation, the symmetrical boundary is shown as the dotted line in Figure 4.1.

There are two channel types, reforming channel (RC) and combustion channel (CC). As shown in Figure 4.1, Ni/$MgAl_2O_4$ and Pt catalysts are fixed at 0.04 kg/m^2 and coated on channel walls along the reformer length for RC and CC, respectively. The two channel types are arranged as the parallel arrangement and the checked arrangement.

4.2 Modeling description

4.2.1 Governing equations

For CFD simulation, the steady state governing equations are employed, i.e., continuity, momentum conservation, energy conservation and chemical species conservation equations, which could be written as Eqs. 4.1 - 4.4.

$$\rho(\nabla \cdot \vec{v}) = 0 \tag{4.1}$$

$$\rho(\vec{v} \cdot \nabla \vec{v}) = -\nabla p + \nabla \cdot \left[\mu\left(\nabla \vec{v} + \nabla \vec{v}^{\,T}\right)\right] + \rho \vec{g} \tag{4.2}$$

$$\rho \nabla \cdot \left(C_p \vec{v} T\right) = \nabla \cdot (k \nabla T) + \sum_j \left(\Delta H_j r_j\right) \tag{4.3}$$

$$\rho\nabla\cdot\left(\vec{v}\omega_i\right)=\rho\nabla\cdot\left(D_{i,eff}\nabla\omega_i\right)+\sum_j\left(r_j MW\right)_i \tag{4.4}$$

In this work, the gravity force term in Eq. 4.2 is neglected. The source terms in Eqs. 4.3 and 4.4 which are the last terms of these equations exist specifically on the inner surfaces due to the presence of catalyst. In the investigation by Irani et al. (2011), two approaches for reaction modeling which were surface and volume-base reactions in wash-coated monolith reactors were calculated and compared with the experiment. The results of surface-based reaction was in good agreement with the experiment. For this reason, the catalyst layer thickness is not considered, and therefore the reactions are calculated as surface reactions using the kinetic models.

For RC, the mechanisms and kinetic models reported by Xu and Froment (1989), including methane steam reforming (Eqs. 2.8, 2.10) and water gas shift (Eq. 2.9), are conducted. In the case of CC, methane combustion reaction (Eq. 4.5) is employed and the kinetic model adopted from Zanfir and Gavriilidis (2003) is modeled as Eq. 4.6 where C_{CH_4} is the methane molar concentration.

$$CH_4+2O_2\leftrightarrow CO_2+2H_2O \tag{4.5}$$

$$r_4=4\times10^8\,(1/\mathrm{s})\exp\left(\frac{-90\,(\mathrm{kJ/mol})}{RT}\right)\times C_{CH_4} \tag{4.6}$$

According to the ideal gas law, the gas mixture density is a function of gas composition, temperature and pressure at each point along the reformer. For the gas

properties, viscosity and thermal conductivity are imported from Perry's Chemical Engineers' Handbook (Green and Perry (2008)), while specific heat capacity is adopted from Elementary Principles of Chemical Process (Felder and Rousseau (2005)). Diffusivity is calculated by Fuller correlation and the diffusivity of gas mixture is computed using Stefan and Maxwell theory.

Methane conversion is computed using Eq. 4.7 for RC and CC, and hydrogen selectivity is calculated by Eq. 4.8 for RC.

$$\text{Conversion}_{CH_4} = \left(\frac{F_{CH_4,\text{inlet}} - F_{CH_4,\text{outlet}}}{F_{CH_4,\text{inlet}}} \right) \times 100 \tag{4.7}$$

$$\text{Selectivity}_{H_2} = \left(\frac{F_{H_2,\text{outlet}}}{F_{CO_2,\text{outlet}} + F_{H_2,\text{outlet}} + F_{CO,\text{outlet}}} \right) \times 100 \tag{4.8}$$

4.2.2 Boundary conditions

The boundary conditions for the calculation domain (Figure 4.1) were summarized in Table 4.1. All lateral boundaries are set to symmetry condition. Inlet velocity, temperature and mass fraction are specified at the inlet boundaries. Atmospheric pressure is indicated at the outlet boundaries. No-slip wall condition is applied at the surface of the inner reformer wall. Reactions occur on the inner reformer wall surface and release the heat of reactions which transfers through reactor wall and gas phase.

Table 4.1 List of boundary conditions of TMR study

Boundary	Conditions
Inlet	Prescribed velocity, temperature and mass fraction
Outlet	Atmospheric pressure
Lateral	Symmetry
Inner surface wall	No-slip wall condition, surface based reactions, heat exchange by heat of reactions

4.2.3 Simulation method

The numerical simulation is solved by the finite element method using a well-known commercial program, COMSOL Multiphysics® version 4.4. The simulation procedure is summarized in Figure 4.2. In mesh sensitivity, the structure was meshed into tetrahedral 7.61×10^4, 6.04×10^5 and 1.70×10^6 elements as coarse, fine and finer meshes, respectively. Since the difference between fine and finer meshes did not exceed 1%. Thus, the fine mesh (6.04×10^5 cells) was used in this work.

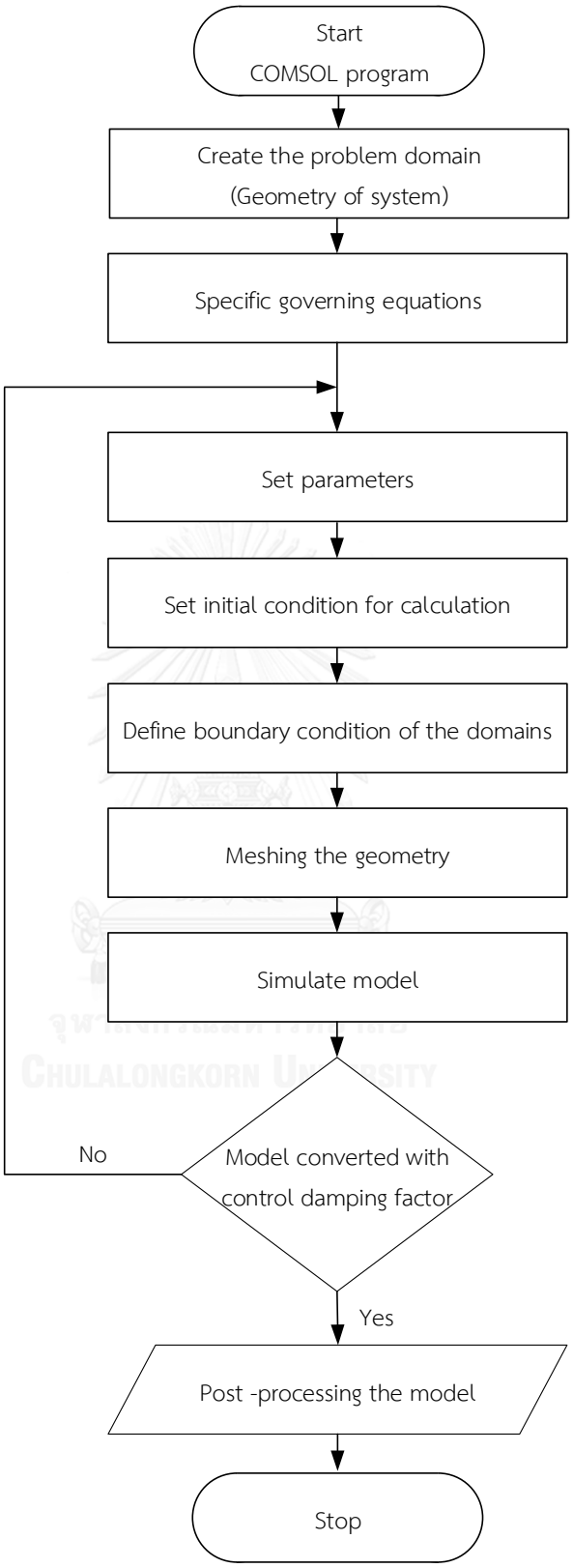

Figure 4.2 Flowchart of simulation procedure for COMSOL Multiphysics®

4.3 Results and discussion

4.3.1 Model validation

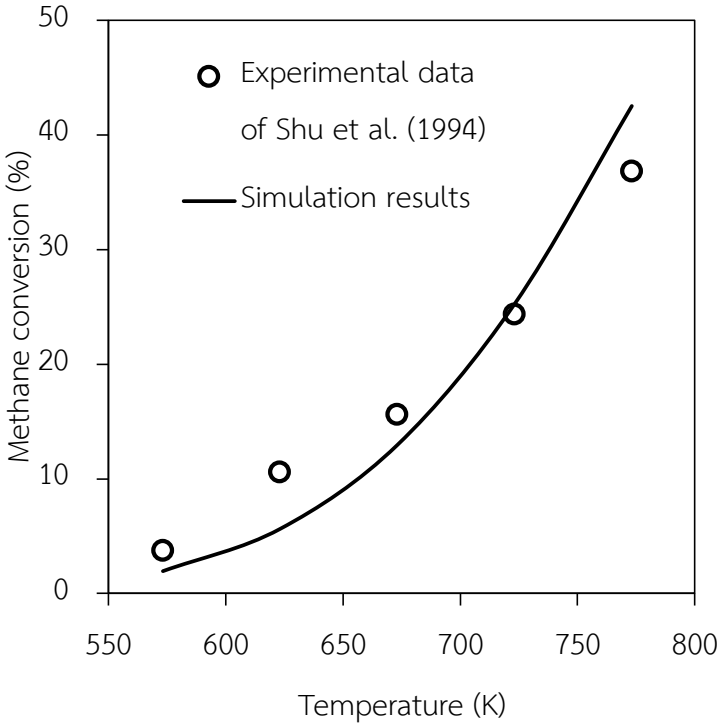

Figure 4.3 Comparison between the simulation results with the experimental data of Shu et al. (1994)

Model validation is necessary to verify the simulation results. The CFD simulation results were compared with the experimental data of Shu et al. (1994). In the experiment, a small tube with 0.95 cm diameter and 3.6 cm length was inserted in another tube with 1.7 cm diameter and 5.1 cm length. Methane steam reforming reaction occurred inside annular volume between both tubes where contained 11 g of nickel based catalyst. The operating condition was set at 3 steam to carbon ratio, 1067 h^{-1} GHSV and 137 kPa. The temperature was varied from 573 to

823 K. The simulation was computed in two dimensional simulation model with axial symmetry. Comparison of simulation results and the experimental data are shown in Figure 4.3. The computed conversions were fitted with the experimental data. Therefore, this model are acceptable and the model accuracy is ensured.

4.3.2 Base case study of TMR

The simulation model was employed to study the reactor performance in the parallel arrangement and the checked arrangement with co-current flow at base case condition as shown in Table 4.2. Simulated velocity and temperature profiles of the parallel arrangement and the checked arrangement are shown in Figure 4.4 and Figure 4.5, respectively.

Table 4.2 Operating and design parameters of base case TMR study

Parameter	Value (unit)
Channel width	1 (mm)
Reformer length	20 (mm)
Catalyst loading in both channels	0.04 (kg/m^2)
Wall thickness	0.3 (mm)
Reforming gas hourly space velocity in RC	6000 (hr^{-1})
Combustion gas hourly space velocity in CC	16000 (hr^{-1})
Outlet pressure	1 (atm)
Inlet temperature	823 (K)
Steam to carbon ratio in RC	2
Methane mole fraction in CC	0.05

For RC and CC, the velocity profiles of both arrangements are similar. Since gas hourly space velocity (GHSV) in the CC is higher than GHSV in the RC, velocity of CC is higher as reported in Figure 4.4. The highest velocity appears at the corners of the model configuration which correspond to the centers of each channel due to fully developed flow. Meanwhile, zero velocity is at the reformer inner wall where the boundary condition is specified as no-slip wall condition and there is no relative motion between the fluids in contact with the reformer wall.

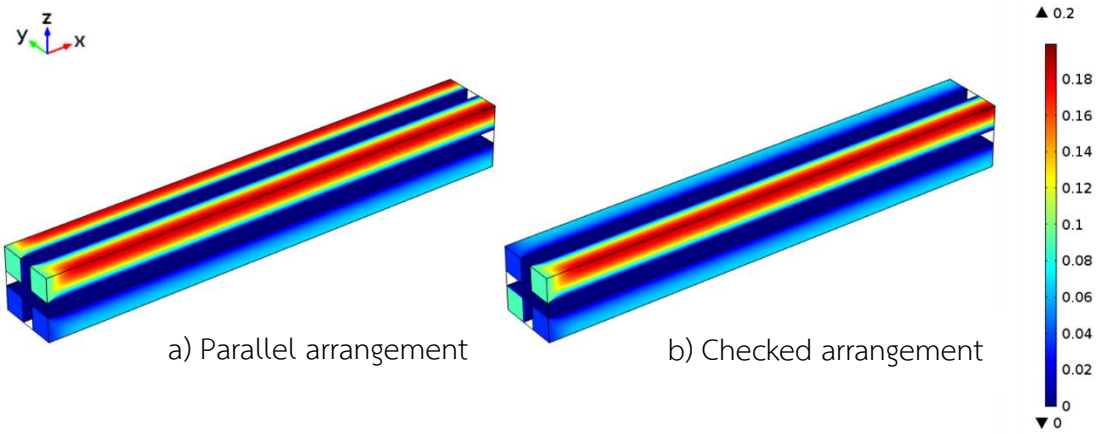

Figure 4.4 Velocity profiles (in m/s) in base case condition for a) The parallel arrangements and b) The checked arrangement

From Figure 4.5, temperatures of both arrangements are lower at the inlets because of the intensive methane steam reforming reaction. After the lowest temperature position, the temperatures are increased along the reactor lengths, since heat is released by the methane combustion. Furthermore, the cold spots appear at

the inlet of the parallel arrangement, while the checked arrangement presents smooth temperature profile along the reformer.

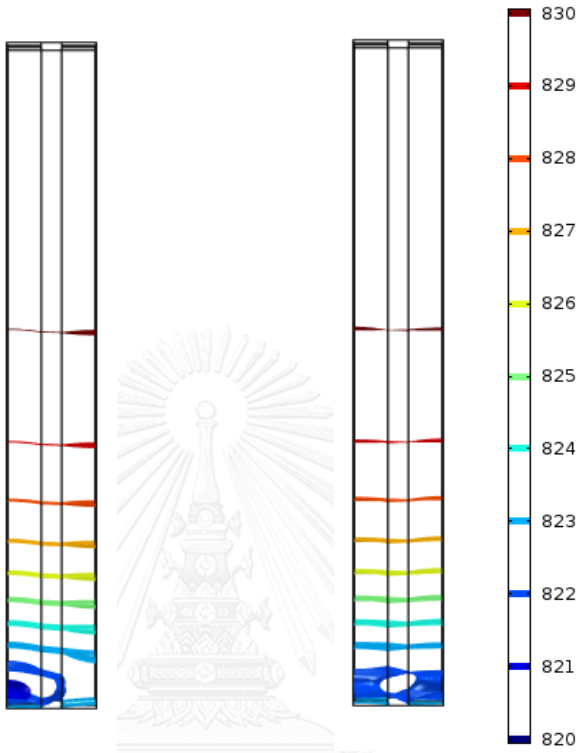

a) Parallel arrangement b) Checked arrangement

Figure 4.5 Temperature profiles (in K) in base case condition for a) The parallel arrangements and b) The checked arrangement

As shown in Figure 4.6, the temperatures of both arrangements for RC and CC are different at first part of the reformer which is especially large in the parallel arrangement, and then the temperatures are nearly the same for both arrangements further along the channel. Thus, the effect of extra exchange area which leads to a

decrease of temperature difference in the checked arrangement appears instantly at the inlet.

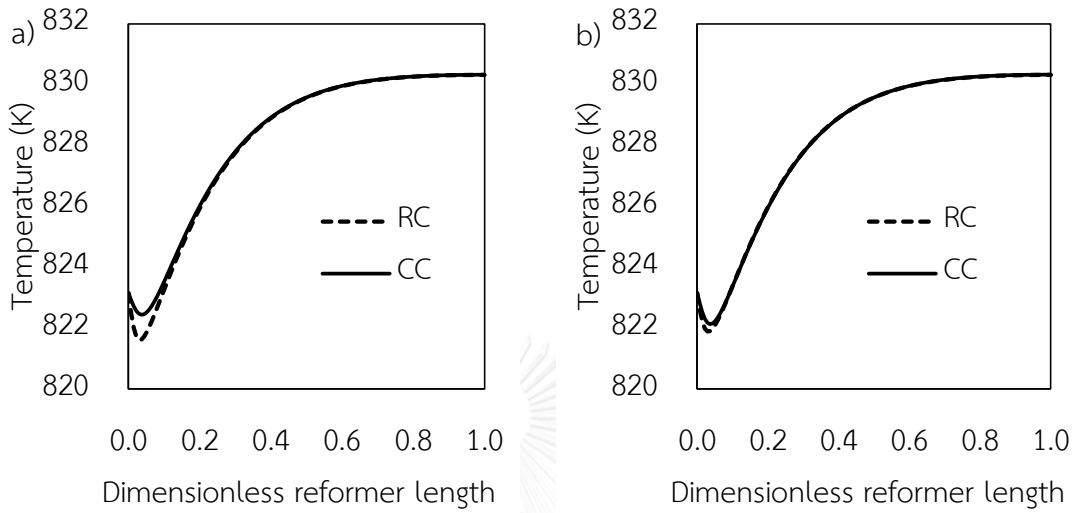

Figure 4.6 Temperature profile at center of both channels in base case condition with co-current flow: a) The parallel arrangements and b) The checked arrangement

Mole fractions along the reformer length in RC of both arrangements are unnoticeable and the results of parallel arrangement are plotted in Figure 4.7. Methane and water are strongly consumed, while hydrogen is intensively produced, in the first 20% of the length. As a result, energy is strongly consumed, decreasing temperature of both channels at the inlet of the reformer. At the outlet, carbon monoxide is about 10% of the gas mixture. In order to use as a fuel cell feed, carbon monoxide in the gas mixture must be reduced to lower than 10 ppm. Thus, purification processes are required for this reformer outlet gas. The outlet methane conversions in RC are about 68.17% for both arrangements, respectively. The methane conversion of both

arrangements is nearly similar which reaches the equilibrium conversions of this condition. The equilibrium terms of steam reforming rates become zero at the half of reactor length in both arrangements. Therefore, temperature which controls the reaction equilibrium is a major factor to limit the reactor performance. The hydrogen selectivity in both arrangements are the same at 57.25 %. In CC, combustion reaction reaches nearly complete reaction for both arrangements.

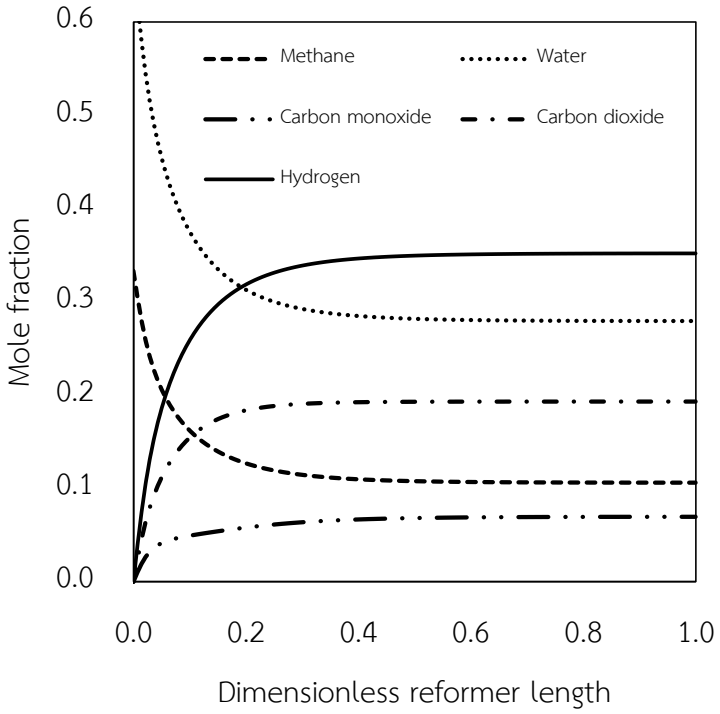

Figure 4.7 Mole fraction profile in RC of base case condition of the parallel arrangement with co-current flow

In the base case study, the results show that the reactor performances of the parallel arrangement and the checked arrangements are not considerably different. The results are supported by the experimental study of Moreno et al. (2010) which

investigated the influence of flow arrangement upon reactor performance in a ceramic micro-channel network for autothermal methanol reformer. Three flow arrangements (checkerboard, annular and self-insulated annular) performed similar hydrogen yields in their investigation. From these results, micro reformers possess a high heat transfer ability for which the heat can be easily transferred through the reformer wall with low heat transfer resistance. Therefore, the additional area of the checked arrangement does not promote the performance of a small scale reformer.

4.3.3 Effect of flow direction

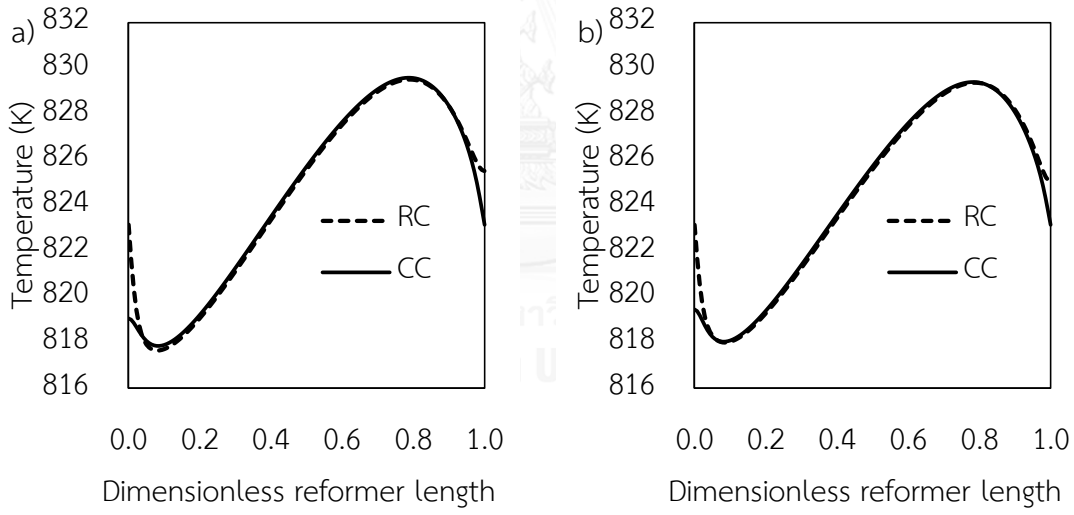

Figure 4.8 Temperature profile at center of both channels in base case condition with counter current flow: a) The parallel arrangements and b) The checked arrangement

Counter current flows were simulated in both arrangements using the base case condition and compared the results with the co-current directions. In RC, methane

conversions of counter current flow are 67.01% and 66.95% for the parallel arrangement and the checked arrangement, respectively.

The temperature profiles at the center of RC and CC in counter current flow are shown in Figure 4.8. The profiles of counter current flow are in the lower temperature range. Steam reforming and combustion reactions intensively perform at inlet of RC and CC; hence, the cold and hot spots are observed at the inlet of both channels in both arrangements. With the counter current flow, the mole fraction profiles of both arrangements are nearly the same as the mole fraction profile of the co-current flow but the reaction is slower than that in the co-current flow because of lower reactor temperature. For these reasons, methane conversion of RC of counter current flow is lower than that in co-current flow in both arrangements. This result is consistent with the study of Grote et al. (2011) and Anzola et al. (2010). The co-current flow is further studied in the next sections.

4.3.4 Effect of operating parameters

Operating parameters, inlet temperature, steam to carbon ratio in RC, methane mole fraction in CC and GHSV of both channels are varied in co-current flow. The reformer performances of the parallel arrangement and the checked arrangement are compared at various conditions. The inlet temperature is varied from 673 to 973 K. The range of stream to carbon ratio and methane mole fraction are from 1.0 to 4.0, and 0.5 to 15.0 %, respectively. The GHSV is varied from 2,000 to 20,000 h^{-1} for RC and

CC. In the simulation ranges, the results of different arrangements are nearly the same for all operating parameters. As shown in Figure 4.9, black lines representing parallel arrangement is overlapped on the gray lines which represents checked arrangement. When varying operating parameters, the temperature profile between two arrangements is similar to the base case study which shows unnoticeable difference between both arrangements.

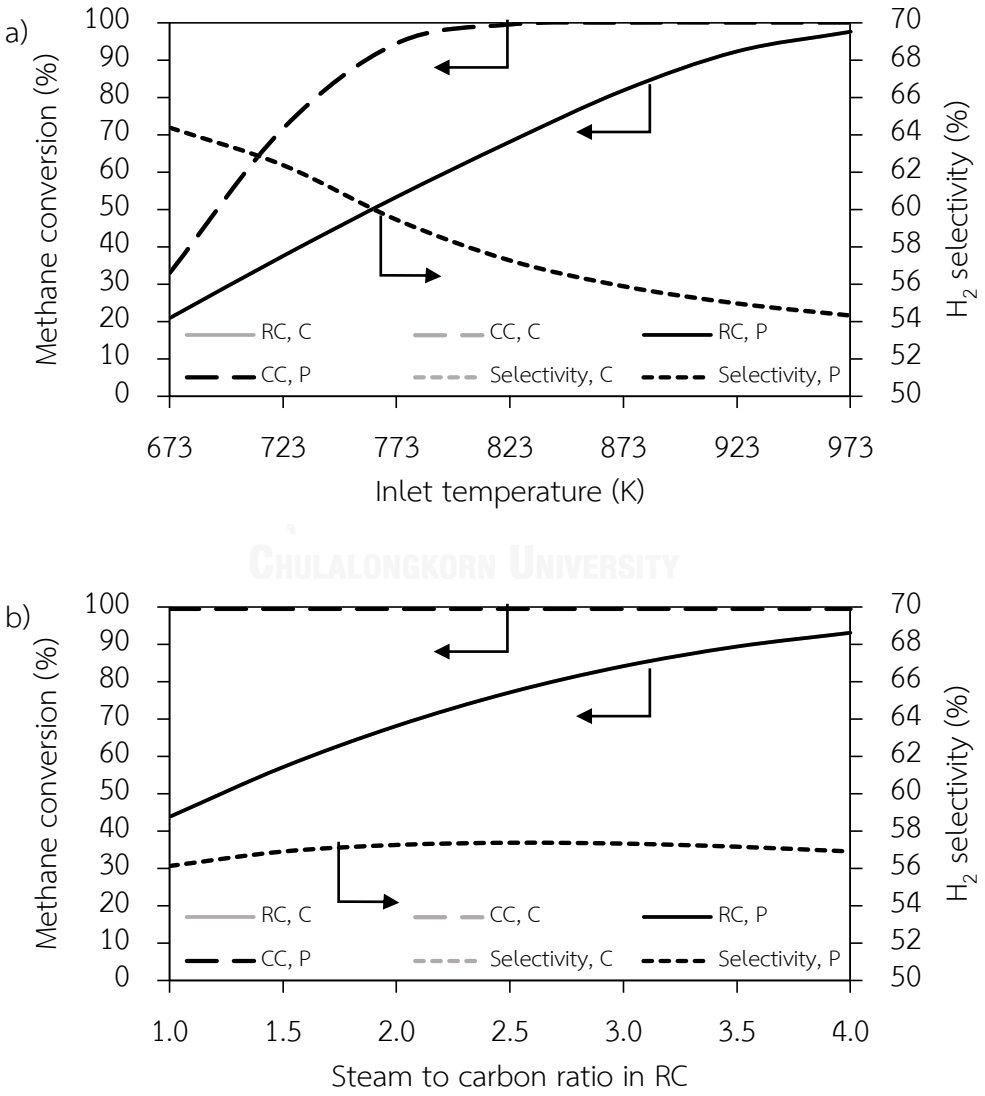

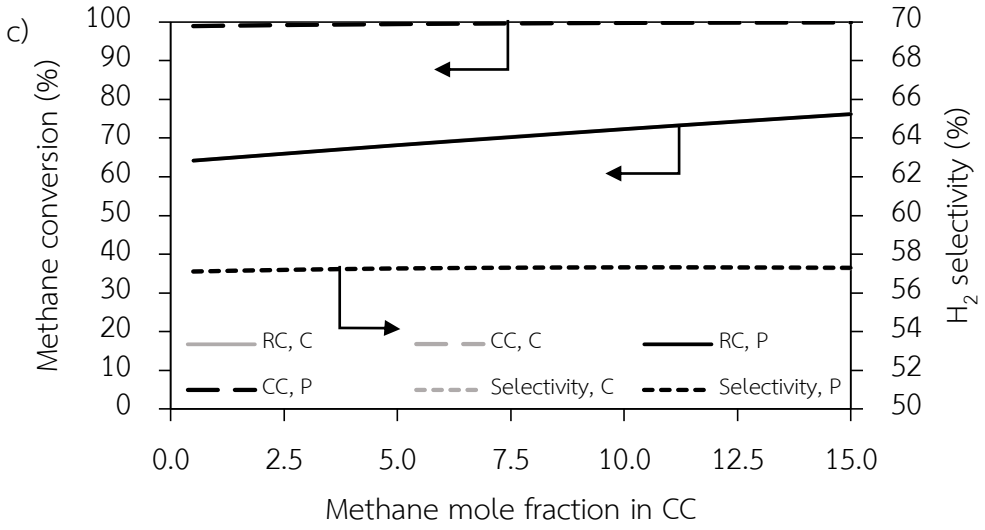
c)
Methane conversion (%)
H_2 selectivity (%)
RC, C
CC, C
RC, P
CC, P
Selectivity, C
Selectivity, P
Methane mole fraction in CC

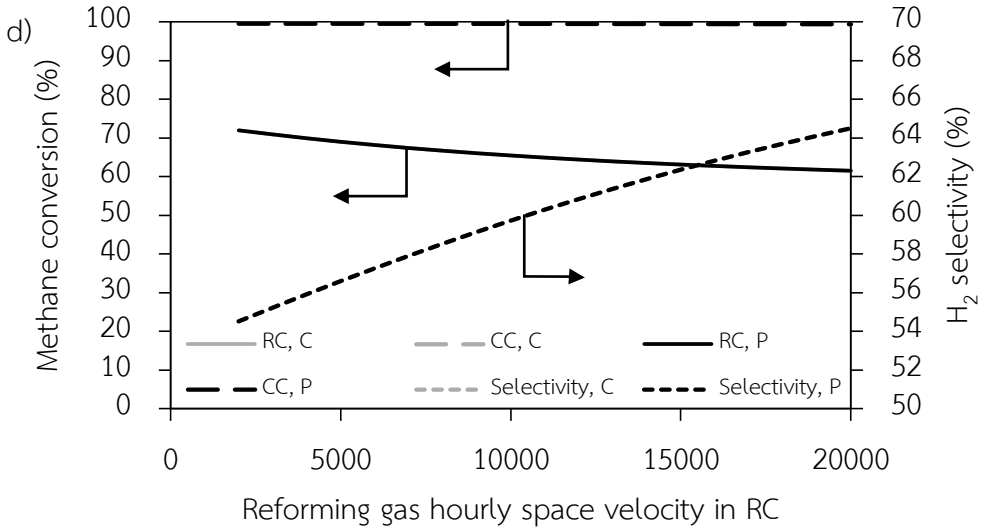
d)
Methane conversion (%)
H_2 selectivity (%)
RC, C
CC, C
RC, P
CC, P
Selectivity, C
Selectivity, P
Reforming gas hourly space velocity in RC

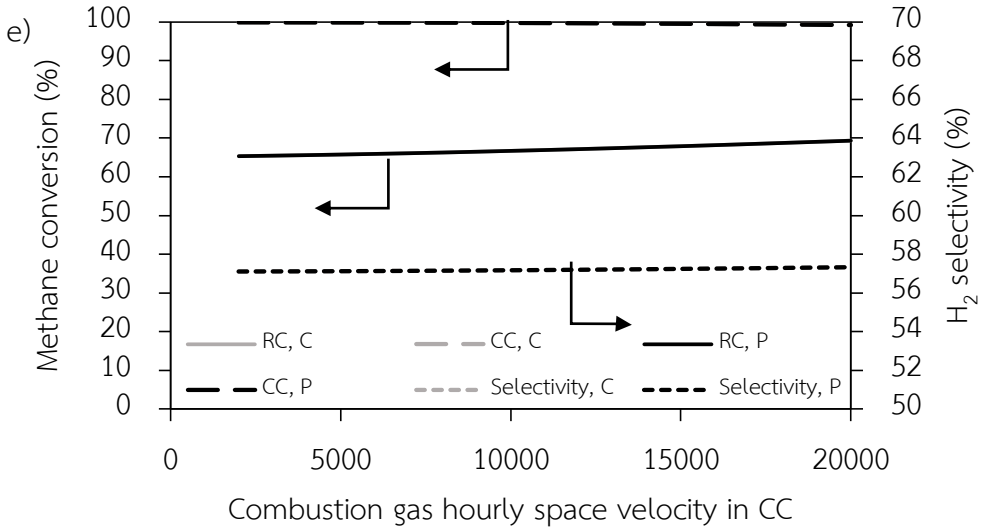

Figure 4.9 Reactor performances of both arrangements at varied operating parameters: a) inlet temperature, b) steam to carbon ration in RC, c) methane fraction in CC, d) GHSV in RC and e) GHSV in CC

The influences of parameters upon the reactor performance depends on the reactor temperature which is affected by adding heat source or heat sink to the reformer. In this study, inlet temperature, methane mole fraction in CC and GHSV in CC (Figure 4.9a, Figure 4.9c and Figure 4.9e, respectively) are considered as the heat sources of the reformer. In CC, increasing of methane mole fraction and GHSV parameters lead to enhanced methane content which is oxidized and releases energy. Therefore the reactor temperature and methane conversion in both channels are higher when increasing these parameters. On the other hand, methane reactant of RC is heat sink of the reformer by steam reforming reaction which is reacted and consumes energy. Steam to carbon ration in RC (Figure 4.9b) is a parameter which affects methane

consisting in RC. Methane composition in RC is reduced, and the energy consumption by reaction also decreases when increasing steam to carbon ration. Moreover, decreasing GHSV in RC (Figure 4.9d) also reduces the reactants, and increases the reactor temperature. Additionally, hydrogen selectivity is controlled by the water gas shift reaction which reduces when increasing temperature. Thus, the methane conversion in RC increases when the inlet temperature, steam to carbon ration in RC, methane mole fraction in CC or GHSV in CC are increased, and decreases when the GHSV in RC is increased.

4.3.5 Effect of design parameters

The design parameters are varied to investigate and to compare the reformer performances between the parallel arrangement and the checked arrangement in co-current flow. The parameters are reformer width, wall thickness and length, and the results of various design parameters are reported in Figure 4.10.

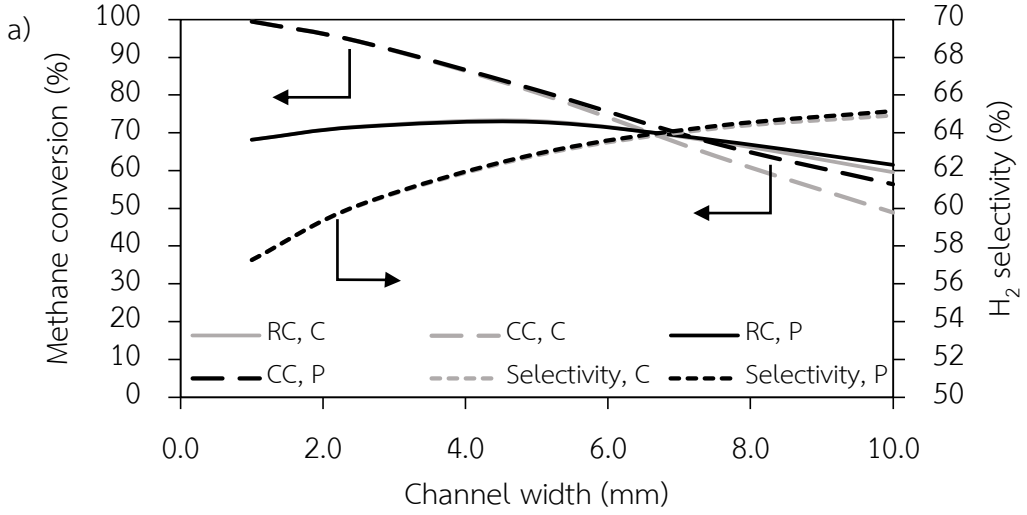

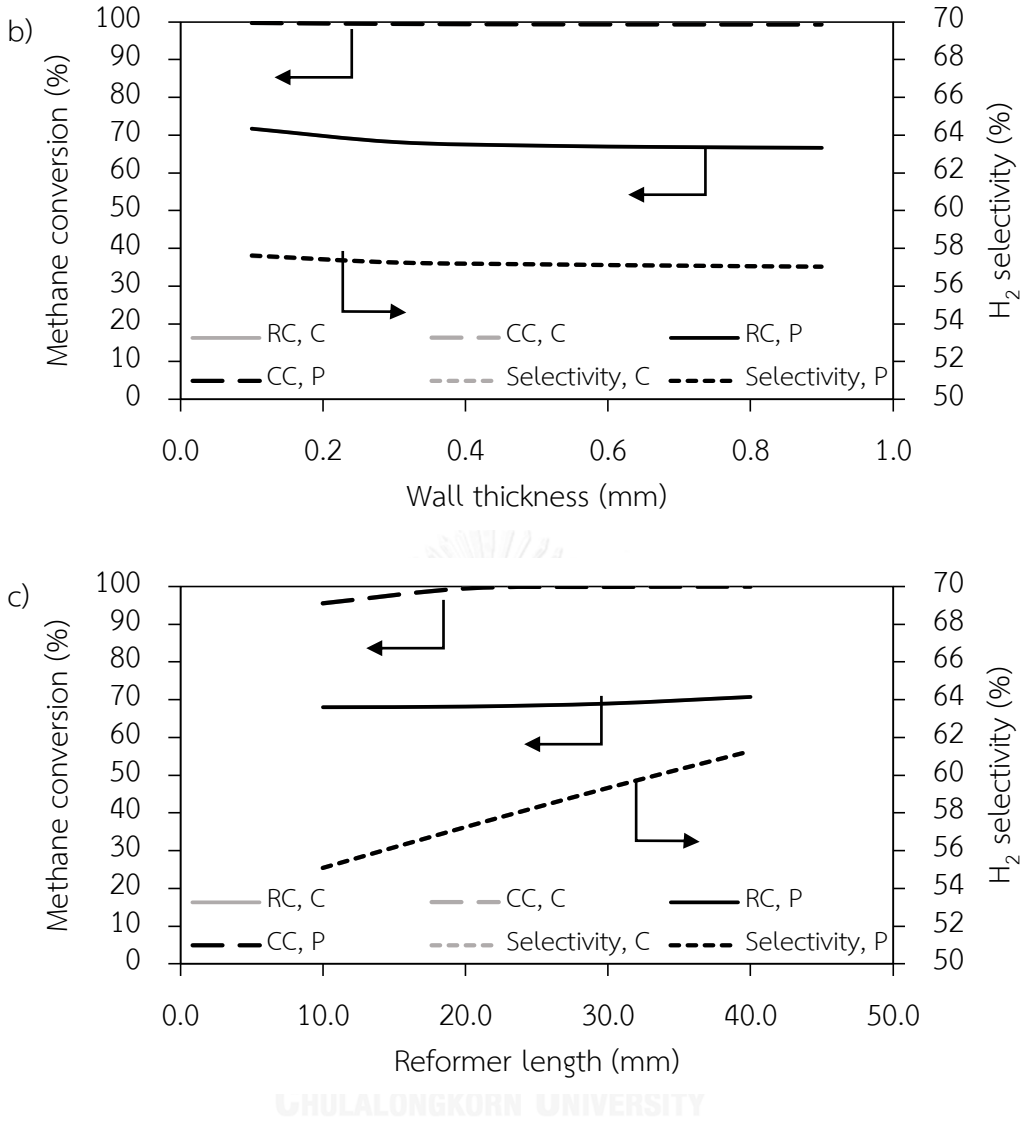

Figure 4.10 Reactor performances of both arrangements at varied design parameters: a) channel width, b) wall thickness, and c) reformer length

The wall thickness and reformer length show the unnoticeable results for both arrangements in the simulation ranges. As shown in Figure 4.10b and Figure 4.10c, the variation of wall thickness and reformer length present the complete overlap of black and gray lines. On the other hand, the variation of channel width (Figure 4.10a) provided the difference between the parallel arrangement and the checked

arrangement. When the channel width is larger than 5 mm, black lines is higher than the gray lines. In this larger channel width, the parallel arrangement presents the slightly higher methane conversion in both RC and CC but the cold and hot spots apparently occur in the reformer.

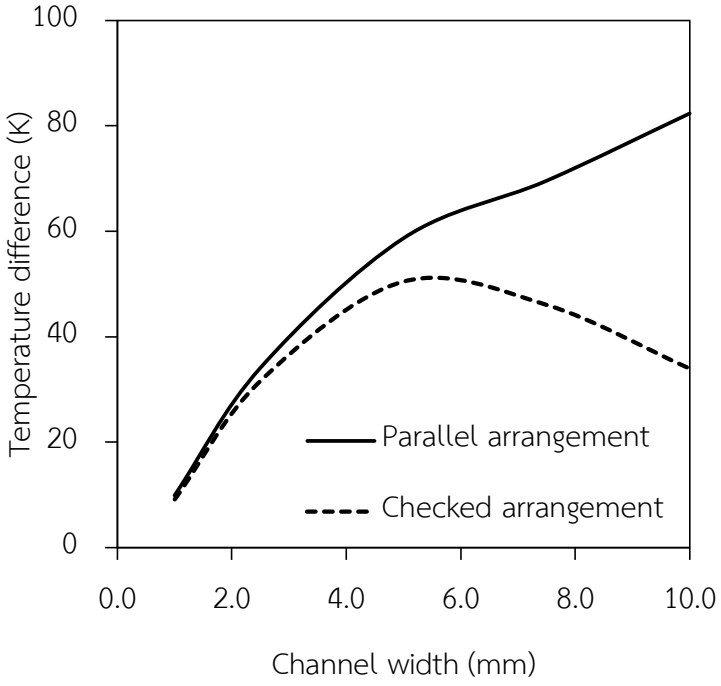

Figure 4.11 The differences between the maximum and minimum temperatures in the parallel arrangement and the checked arrangement

As shown in Figure 4.11, the difference between the maximum and minimum temperatures in the parallel arrangement is greatly more than that in the checked arrangement at the large channel width. As presence of the hot spot in the parallel arrangement, the higher reformer temperature promotes the methane conversion, but

the large temperature difference between cold and hot spots could cause structure fracture and uncontrolled reaction. Thus, in these conditions, the parallel arrangement is recommended for small channel width (< 5 mm) reformer, and the checked arrangement is suitable for large channel width (> 5 mm) reformer.

The influences of the design parameters on the reactor performance are similar for both arrangements. As shown in Figure 4.10a, with small channel width (< 5 mm), increasing channel width results in higher conversion which is the effect of increased flow rate at the fixed GHSV. Heat source is increased due to increasing flow rate in CC. Therefore, the temperature and methane conversion are enhanced in RC. However, in the larger channel width (> 5 mm), the effect of mass and heat transfers becomes important, and therefore methane conversion is reduced. As shown in Figure 4.10b, increasing the wall thickness leads to lower methane steam reforming conversion and outlet temperature. Methane conversion is decreased by increasing thermal resistance when the wall is thickened. For reformer length, the methane conversion increases when the length is increasing. The reactions in both RC and CC have more residence times in the longer reformer, so the methane conversion is enhanced.

CHAPTER V
EFFECT OF FLOW ARRANGEMENT ON MICRO MEMBRANE REFORMING FOR H_2 PRODUCTION FROM METHANE

For micro membrane reformer (MMR), the effects of the parallel arrangement and the checked arrangement on reformer efficiency were investigated via three dimensional computational fluid dynamics simulation. Reactor performance and the advantage of the checked arrangement are revealed in this chapter.

5.1 Micro structure configuration

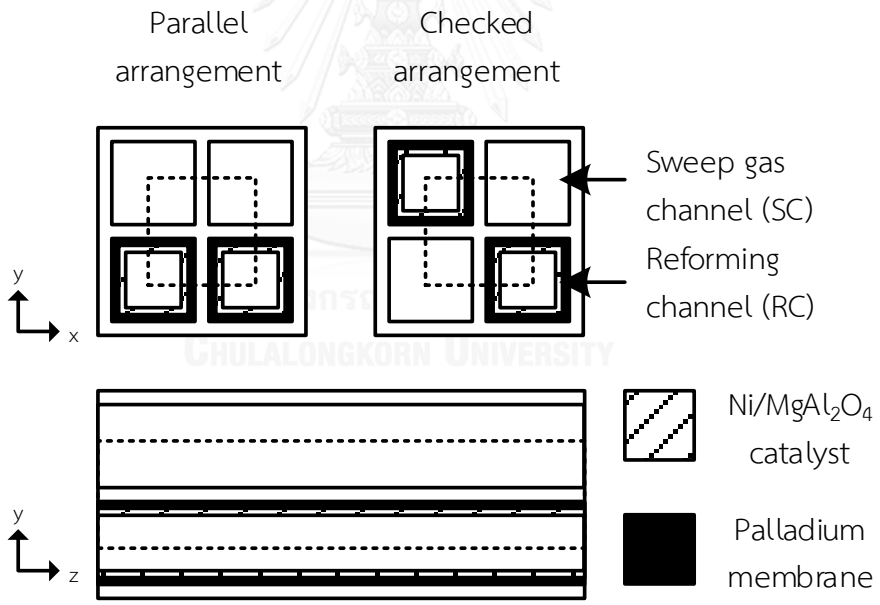

Figure 5.1 Micro reformer configuration of TMR in the parallel arrangement and the checked arrangement

In this study, square channel monoliths are employed (Figure 5.1). The reformer contains two channel types which are reforming channel (RC) and sweep gas channel (SC). Reactions and separation occur specifically in RC, thus only the wall inside of RC is coated with a catalyst and a membrane. The palladium film is deposited on the inner wall as a hydrogen selective membrane, and Ni-$MgAl_2O_4$ is applied over the membrane layer as the catalyst. For SC, nitrogen sweep gas is flowed through SC as carrier gas. The arrangement of both channels is shown in Figure 5.1 is the parallel arrangement and the checked arrangement. In Table 5.1, the dimensions of a monolith reactor use for the base case study are presented.

Table 5.1 Monolith reactor dimensions for base case study

Parameter	Value (unit)
Channel width	1 (mm)
Reformer length	20 (mm)
Catalyst loading in RC	0.04 (kg m^{-2})
Wall thickness	0.1 (mm)
Gas hourly space velocity in RC	6000 (hr^{-1})
Gas hourly space velocity in SC	16000 (hr^{-1})
Outlet pressure	1 (atm)
Inlet temperature	773 (K)
Steam to carbon ratio in RC	1.5

The center volume of the 2x2 unit channel is selected as the study domain due to the symmetry condition as indicated by the dotted lines in Figure 5.1. The

thickness of the membrane reported from Kim et al. (2009) was extremely thin at 8 μm, so the thickness is neglected in the calculations. In the case of the catalyst, Irani et al. (2011) suggested that simulation that excluded the thickness of the catalyst provided result which was close to the experimental data. Therefore, the catalyst and membrane thickness in Figure 5.1 are neglected in the calculation with the configurations and the reaction is considered as a surface reaction.

5.2 Modeling description

5.2.1 Governing equations

Three dimensional computational fluid dynamic simulation of the system is conducted with the steady state governing equations, i.e., mass, momentum and chemical species conservation equations, which can be written as Eqs. 5.1 – 5.3, respectively. As an isothermal study, the temperature is assumed to be constant along the length of the reactor so the energy conservation equation is excluded in this study.

$$\rho\left(\nabla \cdot \vec{v}\right) = 0 \tag{5.1}$$

$$\rho\left(\vec{v} \cdot \nabla\vec{v}\right) = -\nabla p + \nabla \cdot \left[\mu\left(\nabla\vec{v} + \nabla\vec{v}^{T}\right)\right] + \rho\vec{g} \tag{5.2}$$

$$\rho\nabla \cdot \left(\vec{v}\omega_i\right) = \rho\nabla \cdot \left(D_{i,eff}\nabla\omega_i\right) + Q \tag{5.3}$$

The gravity term in Eq. 5.2 is neglected. The last term in Eq. 5.3 which is a source term (Q) appears on the inner surface in RC. The source term of this equation is calculated

from the hydrogen flux and the surface reaction rate. The hydrogen flux (Eq. 5.4) adopted from Gallucci et al. (2004a) is employed. The mechanisms and kinetic models of methane steam reforming reaction were reported by Xuan et al. (2012).

$$H_2\,flux = \frac{1.12e^{-5}\left(mol/m\cdot s\cdot Pa^{0.5}\right)}{\text{Membrane thickness}}\cdot e^{\frac{-29.16\left(kJ/\ mol\right)}{Rg\cdot T}}\cdot\left(P^{0.5}_{H_2,retentate}-P^{0.5}_{H_2,permeate}\right) \tag{5.4}$$

The gas mixture density is a function of gas composition, temperature and pressure at each point along the reformer according to the ideal gas law. Data of Perry's Chemical Engineers' Handbook (Green and Perry (2008)) is employed to compute the gas viscosity. Diffusivity in the gas phase is calculated by Fuller correlation and the diffusivity of gas mixtures ($D_{i,mix}$) is computed using Stefan and Maxwell theory. In the solid phase, the effective diffusion is calculated by:

$$D_{i,eff} = \frac{\varepsilon}{\tau}\left(\frac{1}{D_{i,mix}}+\frac{1}{D_{i,KA}}\right)^{-1} \tag{5.5}$$

where ε and τ are the porosity and the tortuosity, respectively, of the solid phase. The porosity is fixed at 0.4, and the tortuosity is specified at 4.0., The Knudsen diffusion coefficient, $D_{i,KA}$, is computed by:

$$D_{i,KA} = 4850 d_p\sqrt{\frac{T}{MW_i}} \tag{5.6}$$

where d_p, the pore diameter of the solid phase, is fixed at 1×10^{-3} cm (10 μm) (Welty et al. (2007)).

Methane conversion and hydrogen separation factor are used as the indicators of the reactor performance. The methane conversion is computed using Eq. 5.7, and the hydrogen separation factor is calculated by Eq. 5.8:

$$\text{Conversion}_{CH_4} = \left(\frac{F_{CH_4,\text{inlet}} - F_{CH_4,\text{outlet}}}{F_{CH_4,\text{inlet}}} \right) \times 100 \qquad (5.7)$$

$$\text{Hydrogen separation factor} = \left(\frac{F_{H_2,\text{SC outlet}}}{F_{H_2,\text{SC outlet}} + F_{H_2,\text{RC outlet}}} \right) \times 100 \qquad (5.8)$$

5.2.2 Boundary conditions

As shown in Figure 5.1, the symmetry condition is applied for all lateral boundaries inside the area within the dashed lines. The velocities and the mass fractions are specified at the inlet, while atmospheric pressure is specified at the outlet. The no-slip condition is assumed at the walls of the insides of both RC and SC. In RC, the surface reactions and the hydrogen flux are applied at the inner surfaces of the walls of the reformer, which are coated with the membrane and the catalyst. The boundary conditions are described in Table 5.2

Table 5.2 Boundary conditions of MMR

Boundary	Conditions
Inlet	Composition: $\omega_i = \omega_{i,0}$ Velocity: $\vec{v} = \vec{v}_0$
Outlet	Zero flux: $\frac{\partial \omega_i}{\partial z} = \frac{\partial \vec{v}}{\partial z} = 0$ Pressure: $P = P_{atm}$
Lateral	Symmetry: $\frac{\partial \omega_i}{\partial x} = \frac{\partial \vec{v}}{\partial x} = 0$ $\frac{\partial \omega_i}{\partial y} = \frac{\partial \vec{v}}{\partial y} = 0$
Inner surface wall of RC	No-slip wall condition: $\vec{v} = 0$ Source term: $Q_i = \sum_j \left(r_j MW\right)_i$ $Q_{H_2} = \sum_j \left(r_j MW\right)_{H_2} - H_2 flux$
Inner surface wall of SC	No-slip wall condition: $\vec{v} = 0$

5.2.3 Simulation method

COMSOL Multiphysics® version 4.4 was employed to solve numerical simulation by the finite element method. The simulation step are described in Figure 4.2. Tetrahedral mesh was fixed at 2.56×10^6 elements, which were specifically finer at the inner wall surfaces to accommodate the surface reactions and the hydrogen flux. The validation of the methane steam reforming simulation was mentioned in

chapter IV. The computed conversions are acceptably close to the experimental data of Shu et al. (1994); thus the model accuracy is ensured.

5.3 Results and discussion

5.3.1 Base case study of MMR

In this section, the parallel arrangement and the checked arrangement were studied by using the base case parameters tabulated in Table 5.2.

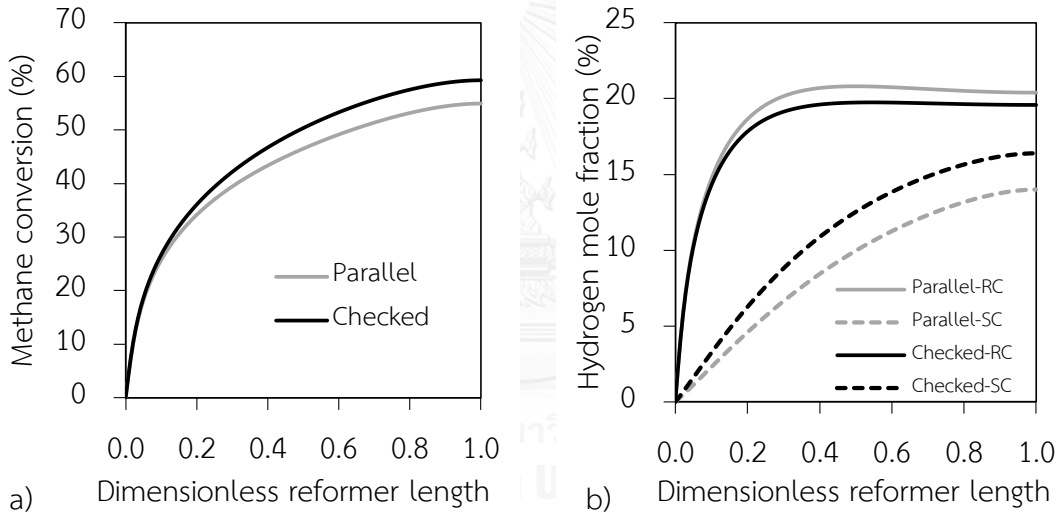

Figure 5.2 Methane conversion (a) and hydrogen mole fraction (b) of the parallel arrangement and the checked arrangement (in percentage)

The methane conversions and hydrogen mole fractions obtained from this simulation are shown in Figure 5.2. In Figure 5.2a, the gray and black lines are the methane conversions for the parallel arrangement and the checked arrangement, respectively. The methane conversions of both arrangements are increased along the

reactor length. At the outlet, the methane conversions are 54.93% for the parallel arrangement and 59.28% for the checked arrangement. Under this condition, the methane conversion in the checked arrangement is about 4% higher than that of the parallel arrangement. The hydrogen mole fractions for both arrangements in SC and RC are shown in Figure 5.2b. The hydrogen mole fractions of the checked arrangement is higher in SC but it is lower in RC when comparing with those from the parallel arrangement. Therefore, hydrogen transfer is better in the checked arrangement. Moreover, the hydrogen separation factor of the checked arrangement is 77.75%. This is 5% higher than that of the parallel arrangement (72.83%). It can be seen that the larger contact area of the checked arrangement results in the increase in hydrogen separation, which consequently enhances methane conversion by equilibrium shift forward given in the step-wise mechanism (Eqs. 2.8 – 2.10).

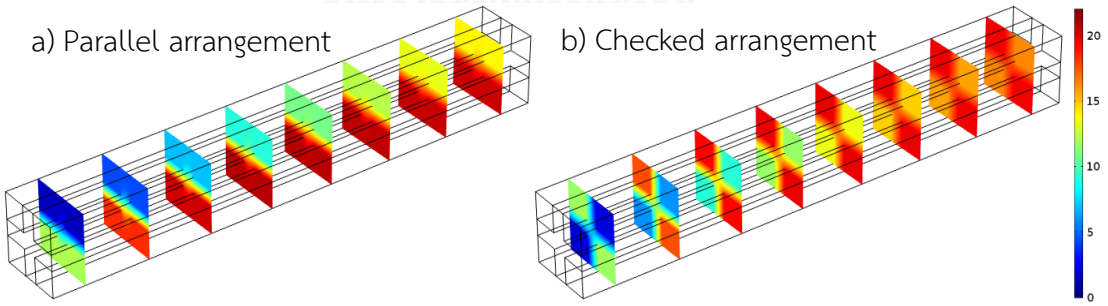

Figure 5.3 Hydrogen mole fraction profile (in percentage) in base case MMR study for a) the parallel arrangement and b) the checked arrangement

In Figure 5.3, the hydrogen mole fractions for both arrangements are reported as sliced profiles in three dimensional configuration. In the case of the parallel

arrangement (Figure 5.3a), the accumulation of hydrogen appears inside the reformer walls between RC. On the other hand, hydrogen is transferred smoothly in the checked arrangement (Figure 5.3b) and accumulation is not present.

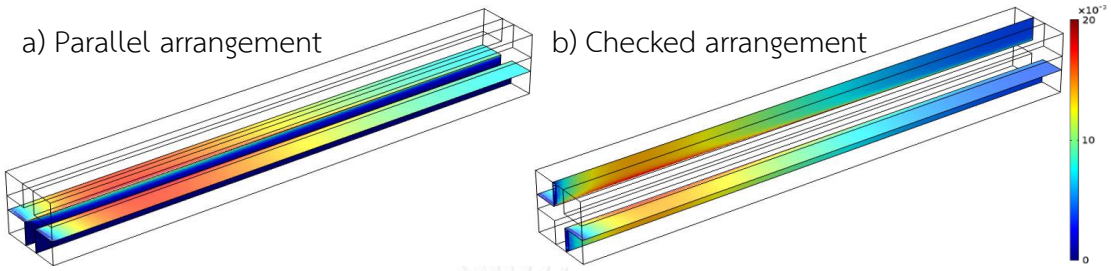

Figure 5.4 Hydrogen flux (in mole m^{-2} s^{-1}) in base case MMR study for a) the parallel arrangement and b) the checked arrangement

As shown in Figure 5.4, hydrogen flux appears only on the surface between RC and SC in the parallel arrangement (Figure 5.4a). Thus, the effective area for hydrogen transferred to SC is only a half of the membrane area; hence hydrogen accumulation occurs. In the case of checked arrangement (Figure 5.4b), the hydrogen flux is present in the entire contact area so the entire membrane area is utilized for hydrogen separation. Hydrogen flux along the reactor is average at 3.69 and 4.65 mmol m^{-2} s^{-1} for the parallel arrangement and the checked arrangement, respectively. As a result, the hydrogen production rate and the hydrogen permeation rate in the checked arrangement are 6.49×10^{-4} and 5.05×10^{-4} mol h^{-1}. On the other hand, lower hydrogen production rate and the hydrogen permeation rate are reported at 5.76×10^{-4} and 4.20×10^{-4} mol h^{-1} in the parallel arrangement.

Based on these results, the checked arrangement in the base case study provides a higher methane conversion and hydrogen separation factor in a monolithic membrane reformer. All areas in contact with the membrane are effectively used for separation, and the hydrogen accumulation in the reformer wall, which causes cracking by hydrogen embrittlement, is not present in the checked arrangement.

5.3.2 Operating parameter study

In this section, the temperature and the GHSV of both channels were studied to find the influence of the parallel arrangement and the checked arrangement on the performance of the monolithic membrane reactor. As an isothermal study, temperature is specified at a constant value between 673 and 823 K. GHSV in both channels are fixed within the same range of 6000-16000 h^{-1}.

5.3.2.1 Effects of reaction temperature

In Figure 5.5, the effect of varying the temperature on the methane conversion and hydrogen separation factor at the predetermined range are presented as straight and dashed lines, respectively. Increasing the temperature increases the rate of reactions and hydrogen flux is promoted. Thus, the methane conversions and hydrogen separation factors are enhanced for both arrangements. The methane conversions from the checked arrangement are higher than those from the parallel arrangement at all temperatures and the differences are over 4% beyond 773 K. With

increased hydrogen flux and reaction rates, hydrogen separation factors of both arrangements also increases as the temperature increases. The checked arrangement provides 4% higher hydrogen separation factors due to the larger separation area. The effects of the arrangement are more apparent at high temperature because the separation is significantly promoted.

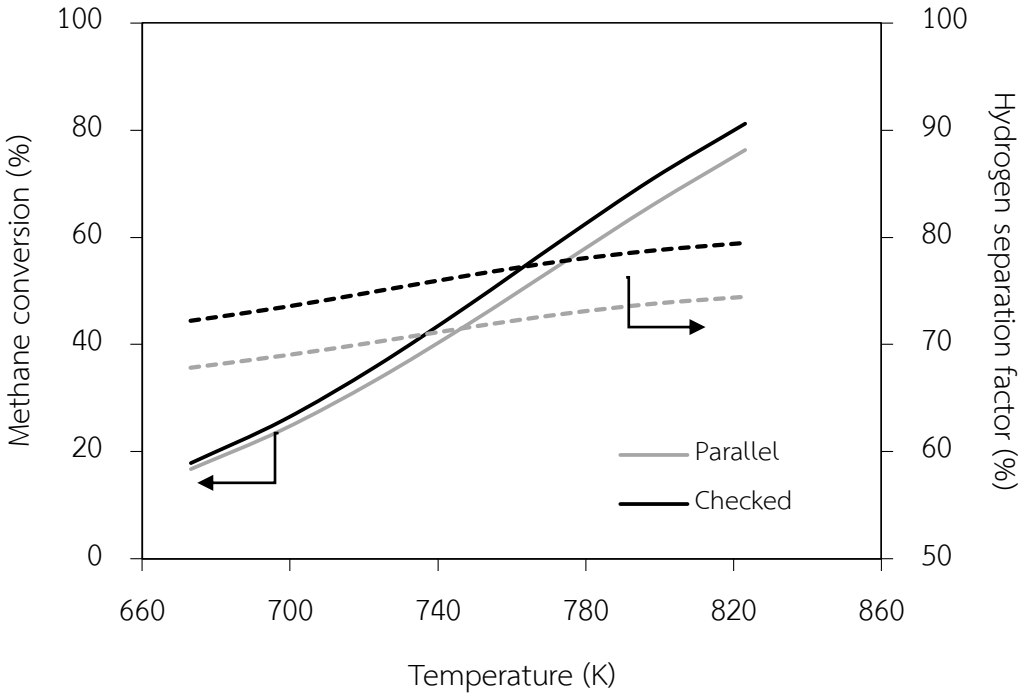

Figure 5.5 Effect of temperature on methane conversion and hydrogen separation factor (in percentage)

5.3.2.2 Effects of reactant gas feed rate in RC

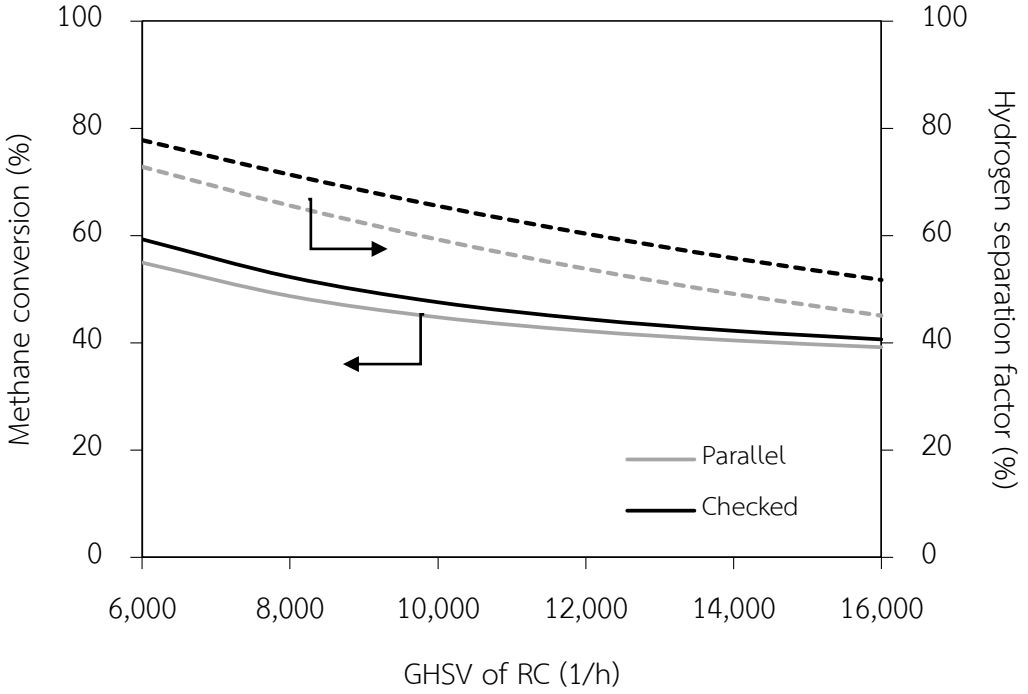

Figure 5.6 Effect of GHSV in RC on methane conversion and hydrogen separation factor (in percentage)

Increasing GHSV increases the gas flow rate and the gas velocity, all of which affects the performance of the reactor. Figure 5.6 shows the effects of GHSV on the performance of the reactor. Increasing the flow rate of the reactants in RC leads to the decrease of the methane conversions and hydrogen separation factors in both arrangements. The reactant flow rate, which is raised by increasing GHSV, dilutes hydrogen in RC. Thus, the driving force for the separation (Eq. 5.4) is weakened and results in a lower hydrogen flux. The methane conversions and hydrogen separation

factors are higher in the checked arrangement because of its better hydrogen transfer. Hydrogen separation of both arrangements is decreased significantly at high GHSV in RC. Therefore, the effect of the arrangement becomes less significant when GHSV in RC is increased.

5.3.2.3 Effects of reactant gas feed rate in SC

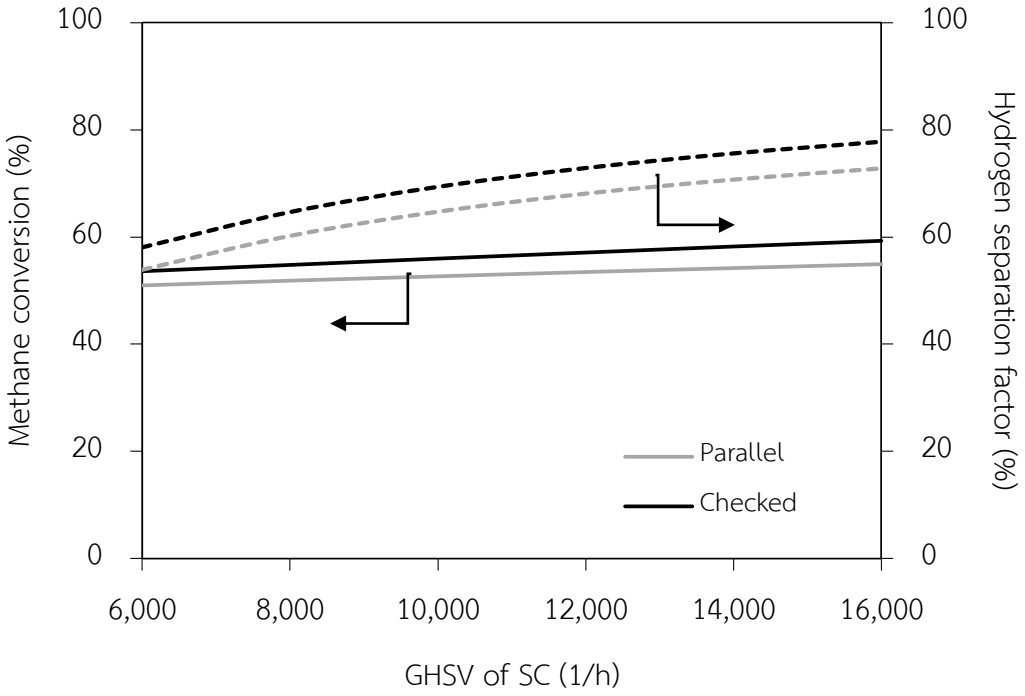

Figure 5.7 Effect of GHSV in SC on methane conversion and hydrogen separation factor (in percentage)

The effects of GHSV in SC on the performance of the reactor are shown in Figure 5.7. The methane conversions and hydrogen separation factors decrease with decreased GHSV in SC. A lower sweep gas flow rate leads to an increased hydrogen

concentration in SC. The hydrogen flux drops with a decrease in the driving force (Eq. 5.4). Thus, the reactor performance of both arrangements is lower. The checked arrangement with a higher exchange ability provides higher methane conversions and hydrogen separation factors. The effects of the checked arrangement and the parallel arrangement are weakened by a lower hydrogen flux when GHSV in SC is decreased.

In section 5.3.2, the effects of the operating parameters, i.e., temperature and GHSV, were also compared. The checked arrangement provides higher methane conversions and hydrogen separation factors in a monolithic membrane reactor at various operating parameters. The hydrogen separation is 4% greater from the checked arrangement within the studied operating parameters. Thus, the larger contact area in the checked arrangement is important since it significantly improves the performance of the membrane reactor. Moreover, the effects of the arrangement are enhanced with an increase in the temperature and GHSV of SC or a decrease in GHSV of RC.

5.3.3 Design parameter study

The design parameters including the reactor length and the channel width for both arrangements were investigated. Reactor lengths between 10 to 50 mm and channel widths between 0.5 and 1.25 mm are used in this study.

5.3.3.1 Effects of reactor length

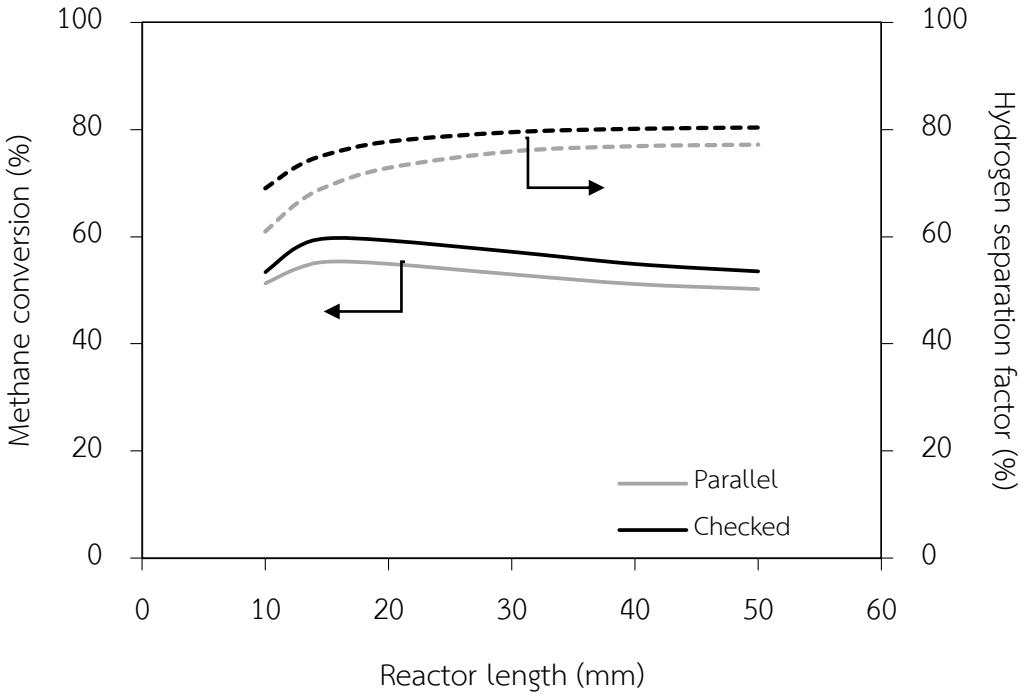

Figure 5.8 Effects of reactor length on methane conversion and hydrogen separation factor (in percentage)

In determining the effect of the reactor length, all other parameters are fixed as in the base case study. Increasing the length results in an increase in the flow rate of the reactants and the sweep gas in both channels as fixed GHSV. The methane

conversions and hydrogen separation factors at different reactor lengths are shown in Figure 5.8. Increasing the reactor length leads to enhanced hydrogen separation factors by increasing the surface area of the membrane. Furthermore, the hydrogen separation factors raise sharply with the increased reactor length up to 15 mm. A further increase in the reactor length results in only a slight increase in the hydrogen separation factors. This phenomenon is attributed to the changes in the hydrogen concentrations of both channels, which is the driving force for the separation. The hydrogen concentrations are largely constant at reactor lengths of 15 mm and beyond. Therefore, increases in the hydrogen separation factors and methane conversions only occur in a relatively short length. However, increasing the velocity in both channels results in decreases in the methane conversions after a length of 15 mm.

The checked arrangement provides higher reactor performance in terms of methane conversions and hydrogen separation factors as shown Figure 5.8. The increased contact areas between RC and SC promote the reactor performance. The effects of arrangement reported in terms of the differences in hydrogen separation factors between both arrangements are shown in Figure 5.9. The hydrogen separation factor differences decrease sharply at shorter lengths, i.e. 10 mm to 30 mm, and are almost constant at around 3% beyond 30 mm. At a longer length, the hydrogen separation factor increases slightly and reaches a constant value in both arrangements. Thus, the effects of arrangement is suppressed as the reactor length is increased.

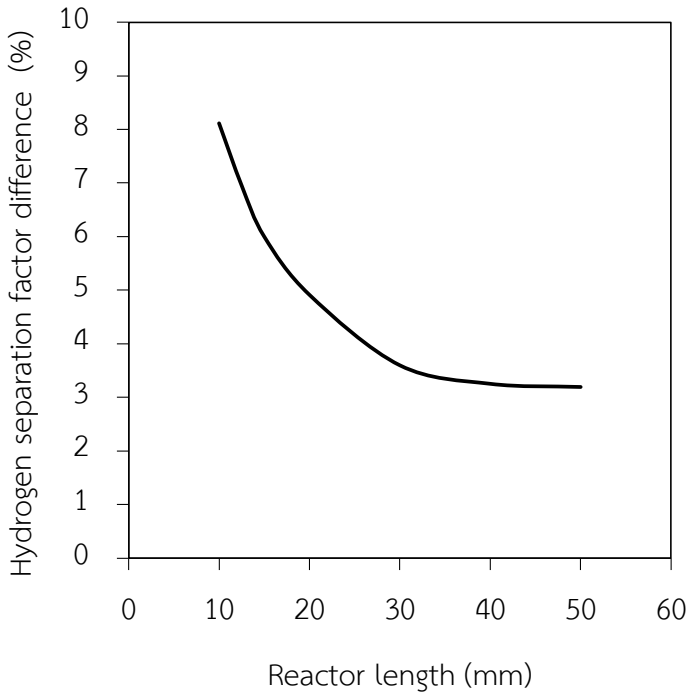

Figure 5.9 Differences in hydrogen separation factor between the parallel arrangement and the checked arrangements

5.3.3.2 Effects of channel width

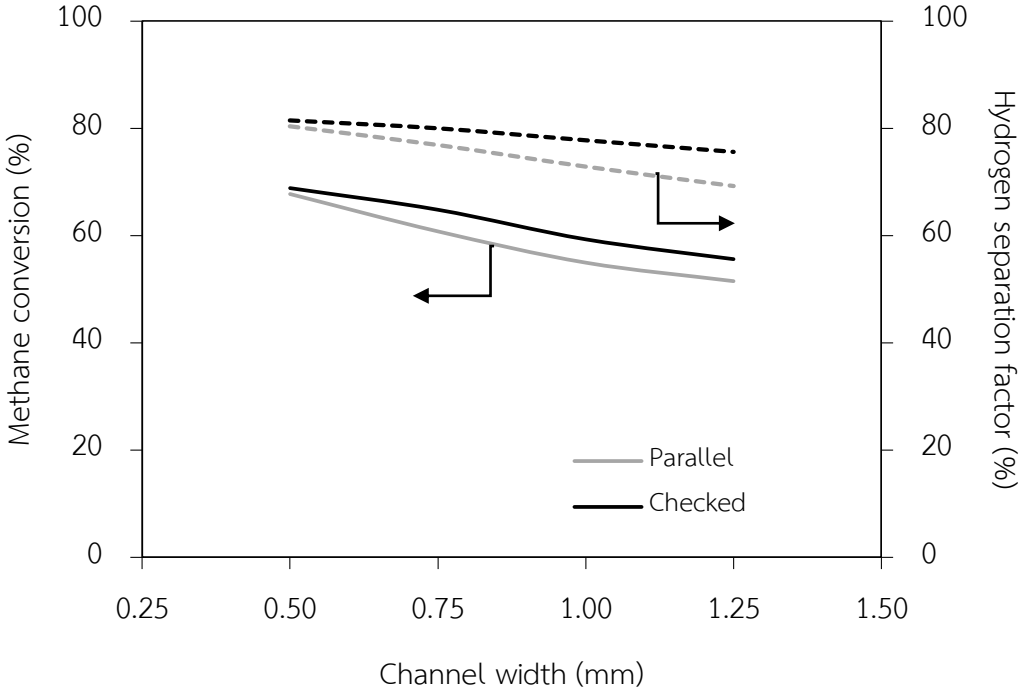

Figure 5.10 Effects of channel width on methane conversion and hydrogen separation factor (in percentage)

The effects of channel widths on the reactor performance of both arrangements are reported in Figure 5.10. The methane conversions and hydrogen separation factors are both decreased with the increase of channel width for both arrangements. Increasing the channel width leads to an increase in the reactant flow rate at a fixed GHSV and increases the mass transfer resistance inside both channels. When the methane conversions drop, the hydrogen concentrations are also decreased and dilute by the reactants. Consequently, the hydrogen separation factors are

reduced by dilution. The parallel arrangement and the checked arrangement provides nearly identical methane conversions and hydrogen separation factors at a small channel width (0.5 mm), but the checked arrangement offers slightly higher reactor performance. As the channel width is further increased, the methane conversions and hydrogen separation factors become significantly higher in the checked arrangement because of the larger surface area. The arrangement effects are stronger when the channel width is larger than 0.5 mm. As the channel width is increased, the hydrogen separation factor drops sharply in the parallel arrangement. Thus, the checked arrangement increases hydrogen separation and suppresses the effects from increasing the channel width.

The performance of the reactor is affected by the length and width of the channels. The hydrogen separation is promoted at short channel lengths and reaches a nearly constant value after 15 mm. On the other hand, increasing the channel width results in a sharp decrease in the reactor performance. The checked arrangement provides higher methane conversions and hydrogen separation factors in this micro membrane reactor. In conclusion, increased contact areas of the checked arrangement significantly promotes hydrogen transfer, which is affected by the reactor length and the channel width.

CHAPTER VI
MODELING OF THERMALLY COUPLED MONOLITHIC MEMBRANE REFORMER FOR HYDROGEN PRODUCTION IN VEHICULAR APPLICATION

Thermally coupled monolithic membrane reformer (TMMR) is a monolith reactor which integrates three processes of hydrogen production, combustor, reformer and separator, within a single unit. The simulation of TMMR using Aspen Plus is described. The results including preliminary study, thermodynamic based study, TMMR design and the flow arrangement effect are reported. These results lead to the final design of TMMR and the recommendation is in this chapter.

6.1 TMMR design using Aspen Plus

Hydrogen production using TMMR in vehicle is studied by simulation. After production, H_2 product is converted to electricity by PEMFC. Residues from PEMFC and reformer in TMMR are recovered and fed to combustor in TMMR as shown in Figure 6.1. The PEMFC is specified efficiency at 50%; hence, half mole of H_2 product is consumed in PEMFC (Ersoz et al. (2006), Yun and Ted Oyama (2011)).

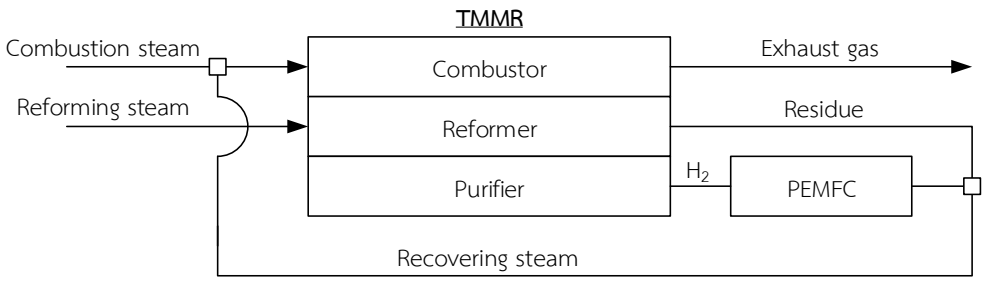

Figure 6.1 Hydrogen utilization system in vehicle

As in Figure 6.1, the TMMR model is simplified into three units which are combustor, reformer and purifier. In combustor, the reactants, input fuel, recovering steam and air were fed excessively at 3 mol/s. Combustion is approximately complete conversion at inlet according to fast reaction rate of catalytic combustion (Deutschmann et al. (2000), Hayes et al. (1996), Karagiannidis et al. (2007)). The hot combusted gas supplies heat to reformer of the TMMR. Overall heat transfer coefficient between both sections is specified at 132.6 W m^{-2} K^{-1}. In the reformer, fuel and water are heated and reacted based on the thermodynamic equilibrium and the kinetic model. After reforming, H_2 in product is separated through Pd membrane to the purifier. H_2 permeation rate is expressed by Eq. 4.5. Membrane thickness is fixed at 8 μm according to the experiment of Kim et al. (2009). Pressure in purifier is kept at atmospheric pressure atm. Hydrogen permeates specifically from the reformer to the purifier without reversing.

Square channel monolith structure is used as reactor model. Surface areas of the structure depending on the design and the flow arrangement are calculated for exchanging heat, separating hydrogen and calculation of the catalyst weight within the reformer. The parallel arrangement and the checked arrangement are employed as shown in Figure 6.2. The area ratio between reformer, heat exchanger and separator is 0.5:0.125:0.125 and 0.5:0.25:0.25 for the parallel arrangement and the checked arrangement, respectively. According to higher surface area, the checked arrangement

provides advantages over the parallel arrangement as reported in previous chapters. As a consequence, the checked arrangement is selected as the base arrangement of this study.

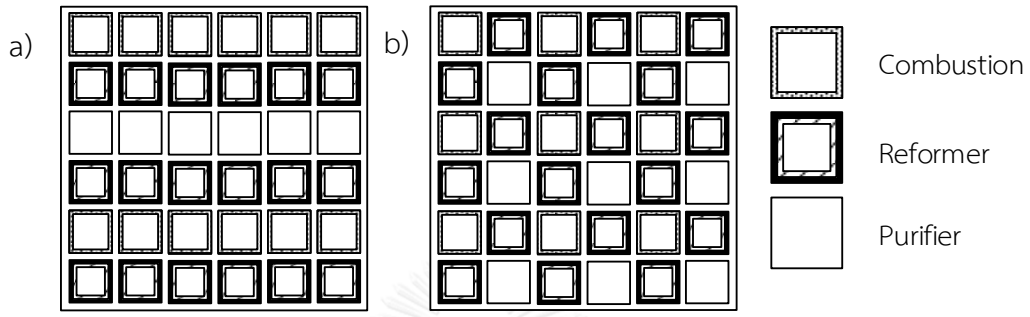

Figure 6.2 Flow arrangements of the TMMR when a) The parallel arrangement and b) The checked arrangement

6.2 Aspen simulation

Aspen Plus is a commercial program generally used in process simulation. In the simulation, Peng–Robinson equation is conducted as the equation of state and TMMR is set as adiabatic and isobaric. Since the model of the TMMR do not exist in the program, a sequential modular approach is employed to simulate the TMMR process. This method has been conducted in several Aspen Plus simulations (Jin et al. (2010), Ye et al. (2009)). As illustrated in Figure 6.3, TMMR is divided into sub-combustors, sub-reformers and sub-purifiers. Sub-combustors perform as heat exchanger units and supply heat from the combusted gas to the reforming stream. The reforming stream is reacted in sub-reformer and then product stream is separated

hydrogen in sub-purifier. The hydrogen permeation is calculated based on Eq. 5.4 by FORTRAN code in calculator section of the program.

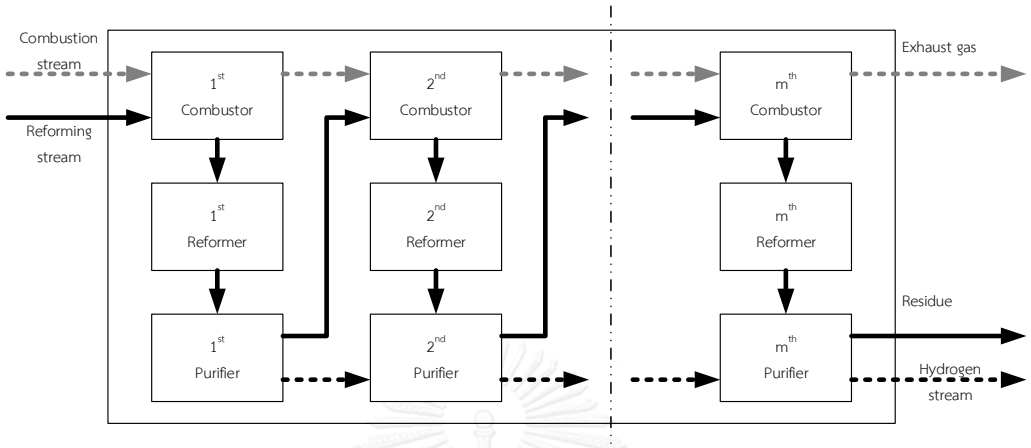

Figure 6.3 Sequential modular simulation diagram of the TMMR

In the simulation, hydrogen energy and energy efficiency are considered as indicators of the TMMR performance. Hydrogen energy is computed from hydrogen consumption as defined in Eq. 6.1, and energy efficiency is calculated followed Eq. 6.2.

$$\text{Hydrogen energy (kW)} = F_{H_2} \cdot \Delta\hat{H}^0_{c,H_2} \tag{6.1}$$

$$\text{Energy efficiency (\%)} = \frac{F_{H_2} \cdot \Delta\hat{H}^0_{c,H_2}}{F_{fuel} \cdot \Delta\hat{H}^0_{c,fuel}} \times 100 \tag{6.2}$$

The simulation consists of two studies which are thermodynamic based study and the TMMR design. Both simulations are described in the following sections.

6.2.1 Thermodynamic based study

This study is a preliminary investigation for designing TMMR based on the thermodynamic equilibrium. At each sub-reformer, the Gibbs reactor model in Aspen Plus is employed and free energy minimization is calculated to determine the equilibrium products at operating conditions. The total Gibbs function for the system is expressed by Eq 6.3.

$$FG = \Sigma\left(F_i G_i^0\right) + RT\Sigma\left(F_i \ln \frac{y_i p\hat{\varphi}}{f_i^0}\right) \quad (6.3)$$

Methane, methanol and ethanol which are considered as green fuels were examined to operate in the TMMR. The possible products of these fuels steam reforming are specified in the Gibbs reactor. From the experimental study, by-products such as formaldehyde, dimethyl ether, acetaldehyde, ethylene and acetone were produced by methanol steam reforming and ethanol steam reforming. However, these by-products are not thermodynamically stable; hence they are excluded in the simulation (Faungnawakij et al. (2006), Lima da Silva et al. (2009), Lwin et al. (2000), Rabenstein and Hacker (2008)). Therefore, only CH_3OH, C_2H_5OH, CH_4, H_2O, H_2, CO and CO_2 are the possible products in this model.

In this study, the monolith design has 100 mm of diameter, 200 mm of length and 300 cell per square inch (cpsi) of cell density. Green fuel and operating condition are selected to use in the design section. Operating conditions including reforming

pressure (3 - 5 atm) and molar flow rate of reforming (0.1 – 0.5 mol/s) and combustion (0.01 – 0.05 mol/s) are investigated. Steam to carbon ratio is specified at 2.0 for methane, 1.0 for methanol and 3.0 for ethanol according to their stoichiometry.

6.2.2 The TMMR design

In this section, plug flow model is used for the reformer. Catalyst weight is fixed at 0.04 kg/m^2. The surface area is calculated from monolith structure. The selected green fuel and proper operating condition are adopted from the thermodynamic based study. Methane which provides the highest efficiency is chosen as the fuel and used for designing the TMMR based on the kinetic model of methane steam reforming as reported in section 2.3.1.

The TMMR is designed by using a commercial monolith structure. Corning Incorporated presents material attributes of monolith, and the configuration is reported in Table 6.1. Therefore, cell density of monolith is specific at 200, 300 and 400 cpsi. Monolith diameter and reformer length are varied between 100 and 200 mm.

Table 6.1 Material attributes of monolith

Property (uncatalyzed)	Standard			Thin-wall	
	200/12	300/8	400/7	400/4	300/5
Cell density					
(cpsi)	200	300	400	400	300
($cpcm^2$)	31	47	62	62	47
Cell shape	Square	Square	Square	Square	Square
Wall thickness					
(in)	0.0120	0.0080	0.0070	0.0040	0.0055
(mm)	0.3	0.2	0.12	0.1	0.14
Open frontal area (OFA)					
(%)	69	74	74	83	82
Geometric surface area (GSA)					
(in^2/in^3)	47	60	69	73	63
(m^2/l)	1.85	2.36	2.72	2.87	2.47
Hydraulic diameter					
(in)	0.059	0.050	0.043	0.046	0.052
(mm)	1.50	1.27	1.09	1.17	1.32
Porosity					
(%)	35	35	35	35	35

6.3 Results and discussion

6.3.1 Model validation via Aspen Plus

The thermodynamic and kinetic based models were validated with experimental results from literatures. The experiments of methane steam reforming which were extensively studied with membrane reactor were employed in the validation. The number of sub-units (*m*) is varied from 1 to 40. Methane conversion is used as an indicator to determine the reasonable value of *m*.

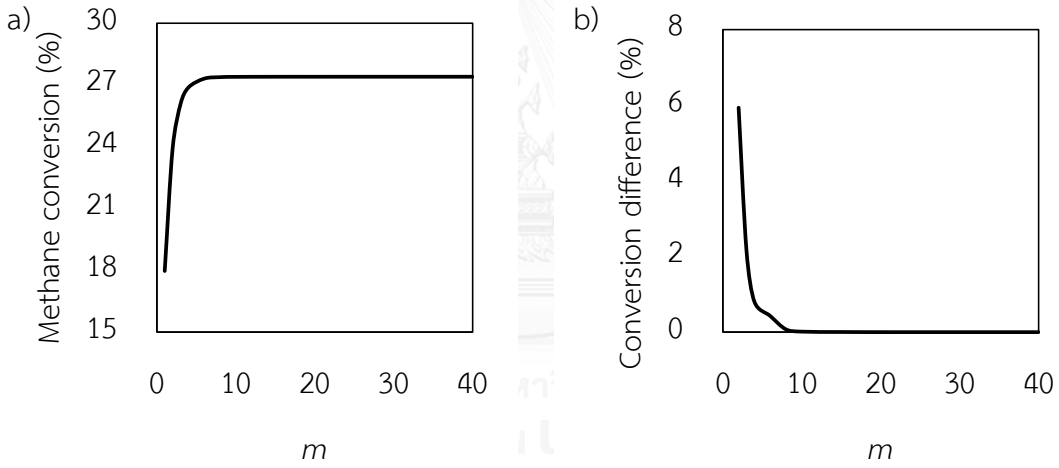

Figure 6.4 Effect of number of sub-units (*m*), a) methane conversion and b) methane conversion difference

The increment of *m* leads to the constant value of methane conversion as shown in Figure 6.4, as the model could represent the reformer. When *m* is equal to 40 in both models, the system offers the low variation of methane conversion within 0.0005 %. Therefore, the value of *m* of 40 is employed in both model studies.

The simulation results were compared the experimental data including traditional reactor (TR) and membrane reactor (MR) is adopted from the experimental of Shu et al. (1994) and Gallucci et al. (2004b). In the thermodynamic equilibrium model, comparison between the simulation and the data of Shu et al. (1994) are shown in Figure 6.5a. The kinetic model results and the experimental data of Gallucci et al. (2004b) are reported in Figure 6.5b. The simulation results of TR and MR could well represent the experimental data and therefore, the models are employed for further studies.

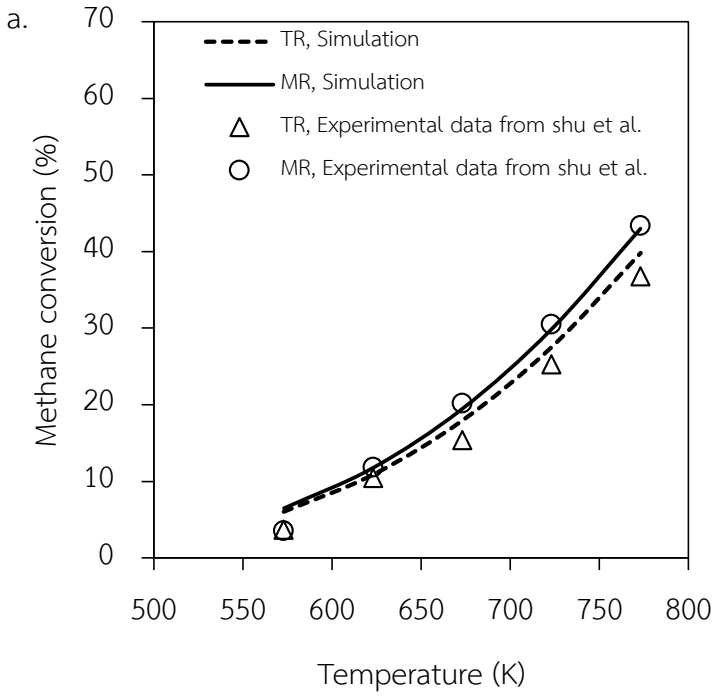

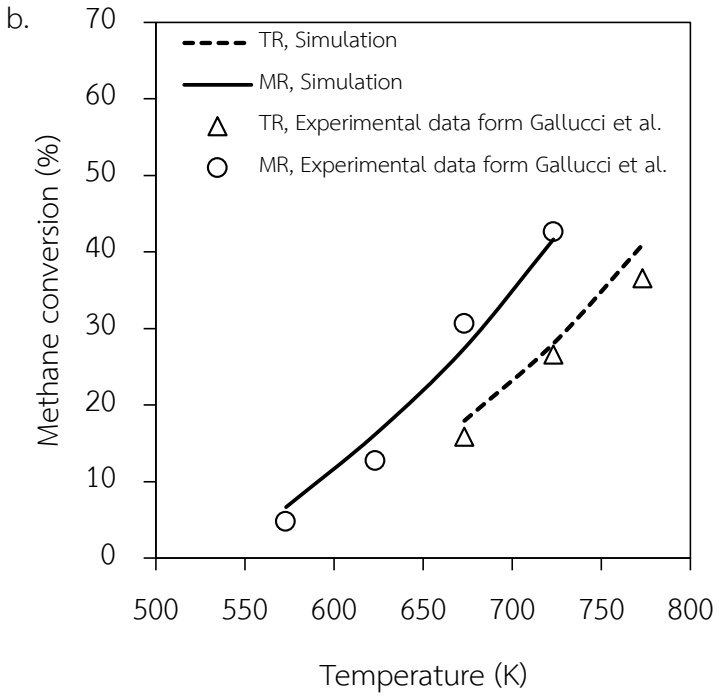

Figure 6.5 Experimental data and results of a) thermodynamic simulation and b) kinetic model for traditional reactor (TR) and membrane reactor (MR)

6.3.2 Preliminary study of TMMR

In this preliminary study, TMMR using nitrogen as sweep gas is evaluated the reactor performance indicated by energy efficiency and methane conversion. The TMMR configuration is adopted from the thermodynamic study. At the base conditions, the system is operated at 1 atm with 0.6 mol N_2/s, and 0.03 and 0.20 mol CH_4/s for the combustor and reformer, respectively. The TMMR is compared with a conventional monolith reformer with external membrane separation as shown in Figure 6.6 at the same specific volume.

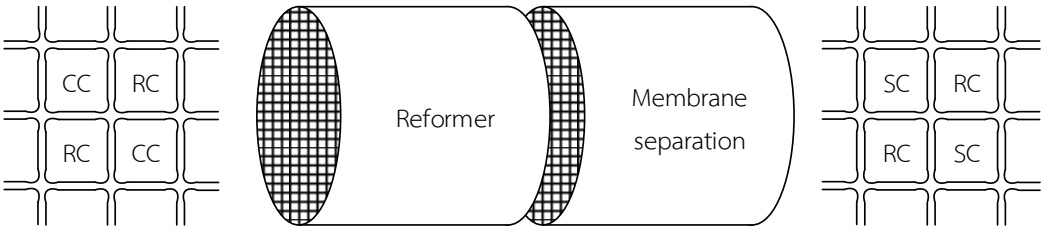

Figure 6.6 Conventional monolith reformer with external membrane separation

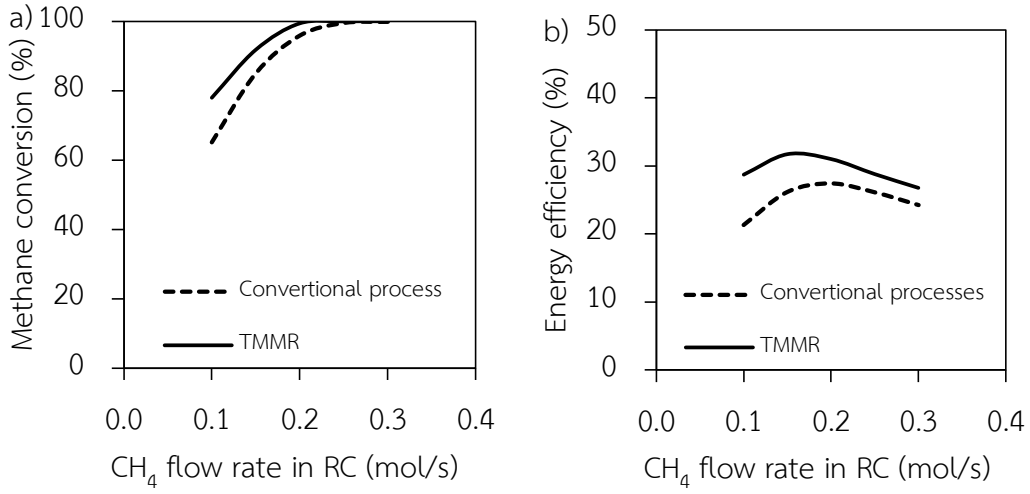

Figure 6.7 Comparison between the conventional process and TMMR: a) Methane conversion and b) Energy efficiency

In Figure 6.7, TMMR achieves higher methane conversion and efficiency about 4% higher in average. Membrane integration in TMMR shifts reaction equilibrium forward and enhances the performance. Therefore, TMMR improves the conventional process of monolith reformer. Furthermore, TMMR was investigated to determine the influence of operating parameters. The ranges of variation are summarized in Table 6.2.

Table 6.2 Operation condition of preliminary TMMR study

Parameters	Combustor	Reformer	Separator
CH_4 (mol/s)	0.01-0.05	0.10-0.50	
H_2O (mol/s)[a]		0.20-1.00	
Air (mol/s)	3.00		
N_2 (mol/s)			0.20-0.20
Pressure (atm)	1.00	1.00-5.00	1.00

[a] S/C = 2

The variation results are shown in Figure 6.8. The increase of the fuel to the combustor and reformer results in higher reforming temperatures. As the temperature of the reformer increases, the efficiency decreases because of the reverse water gas shift reaction and energy from the exhaust gases. The highest efficiency can be achieved at 0.02 and 0.15 mol/s for the combustor and reformer, respectively. At the highest efficiency, the reforming temperature is obtained appropriately in the range of 823-973 K. When the sweep gas flow rate is increased, the H_2 permeation increases, leading to the increase of the efficiency. However, the excessive sweep gas flow rate (more than 1.6 mol/s) reduces reforming temperature and the efficiency as a result of low methane conversion at low reforming temperatures. To increase the driving force for separation, the operating pressure is increased. It was found that higher pressures cause significant enhancements in H_2 permeation and efficiency. The highest efficiency at 43.6% was obtained at 5 atm.

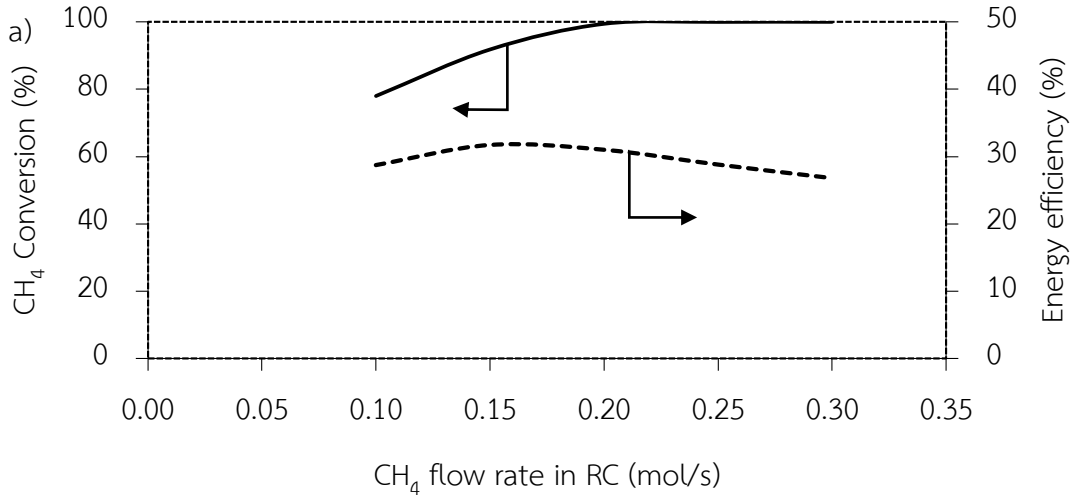
a)
CH4 Conversion (%)
Energy efficiency (%)
100
80
60
40
20
0
50
40
30
20
10
0
0.00
0.05
0.10
0.15
0.20
0.25
0.30
0.35
CH4 flow rate in RC (mol/s)

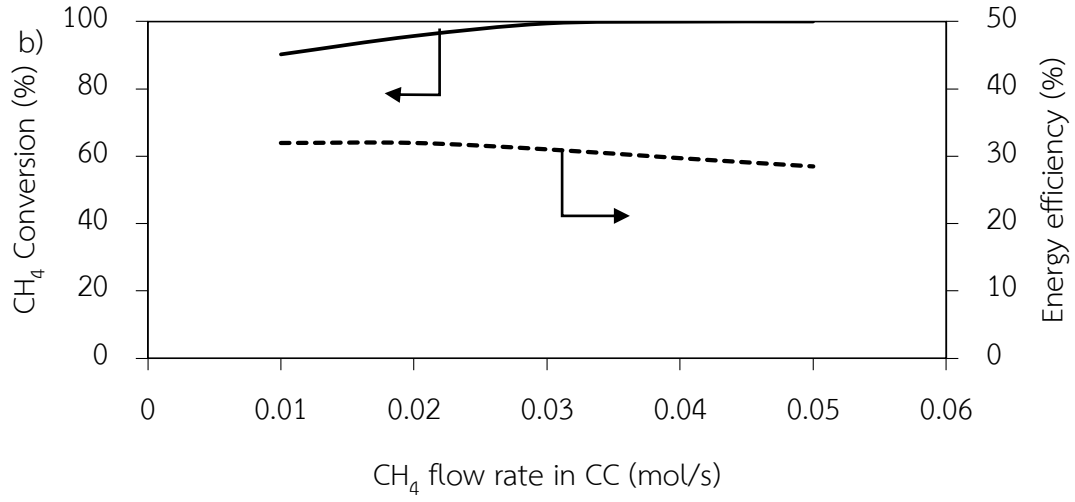
b)
CH4 Conversion (%)
Energy efficiency (%)
100
80
60
40
20
0
50
40
30
20
10
0
0
0.01
0.02
0.03
0.04
0.05
0.06
CH4 flow rate in CC (mol/s)

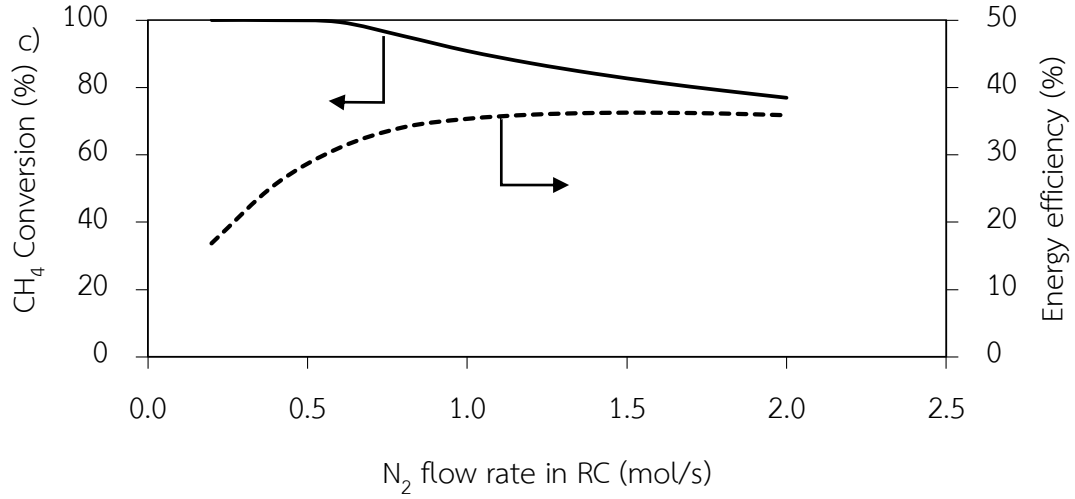
c)
CH4 Conversion (%)
Energy efficiency (%)
100
80
60
40
20
0
50
40
30
20
10
0
0.0
0.5
1.0
1.5
2.0
2.5
N2 flow rate in RC (mol/s)

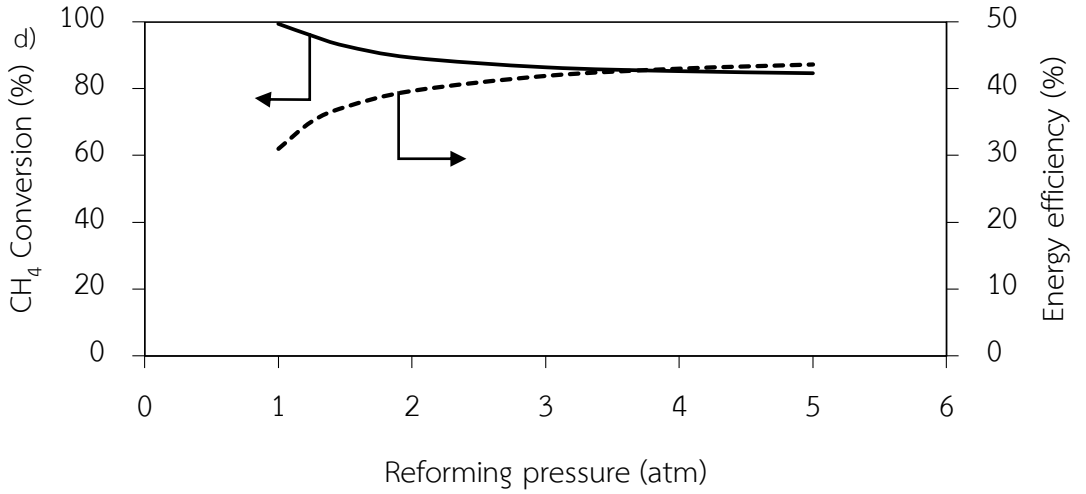

Figure 6.8 Operating parameter's influence in preliminary study of TMMR when a) methane flow rate in RC, b) methane flow rate in CC, c) sweep gas flow rate and d) reforming pressure

In this preliminary study, increasing nitrogen sweep gas and reforming pressure promotes driving force of H_2 separation, resulting in increasing energy efficiency. However, nitrogen sweep gas also suppresses the TMMR performance by decreasing reforming temperature, increasing energy loss in exhaust gases and reducing purity of H_2 gas product. Presence of sweep gas in H_2 stream also reduces performance of PEMFC. Consequently, nitrogen sweep gas is excluded in the further study of TMMR.

6.3.3 Thermodynamic based TMMR study

In this study, the suitable operating condition was investigated at a specific configuration of monolith. Methane, methanol and ethanol were examined with the feed flow rate for reforming and combustion. The range of fuel flow rate is

0.01- 0.05 mol/s for combustion. In the case of reforming, methane and methanol are fed at the same range from 0.10 - 0.50 mol/s. Due to higher hydrogen content of ethanol, the flow rate of ethanol is from 0.10 to 0.30 mol/s. Reforming pressure is between 3 and 5 atm.

6.3.3.1 Effects of feed flow rate of green fuels

The reforming pressure is specified at 4 atm in this case study. The steam reforming of ethanol and methanol reaches nearly 100% conversion in 1st sub-reformer due to their thermodynamic properties at equilibrium state (Lwin et al. (2000), Faungnawakij et al. (2006), Lima da Silva et al. (2009), Rabenstein and Hacker (2008)). Energy efficiency of green fuels which is limited at 50% by the efficiency of PEMFC is reported in Figure 6.9. When increasing flow rate in reforming and combustion, the temperature profile of the TMMR is raised; hence, the reaction rate and the hydrogen separation are enhanced. The conversion of fuel and hydrocarbon by-products is increased, leading to higher energy efficiency. After complete conversion, further increase of the flow rate promotes reverse water gas shift reaction. Hydrogen product is reduced in the reforming side; consequently, the energy efficiency is decreased. Therefore, the TMMR effectively performs when operates at high temperature with less presence of reverse water gas shift reaction.

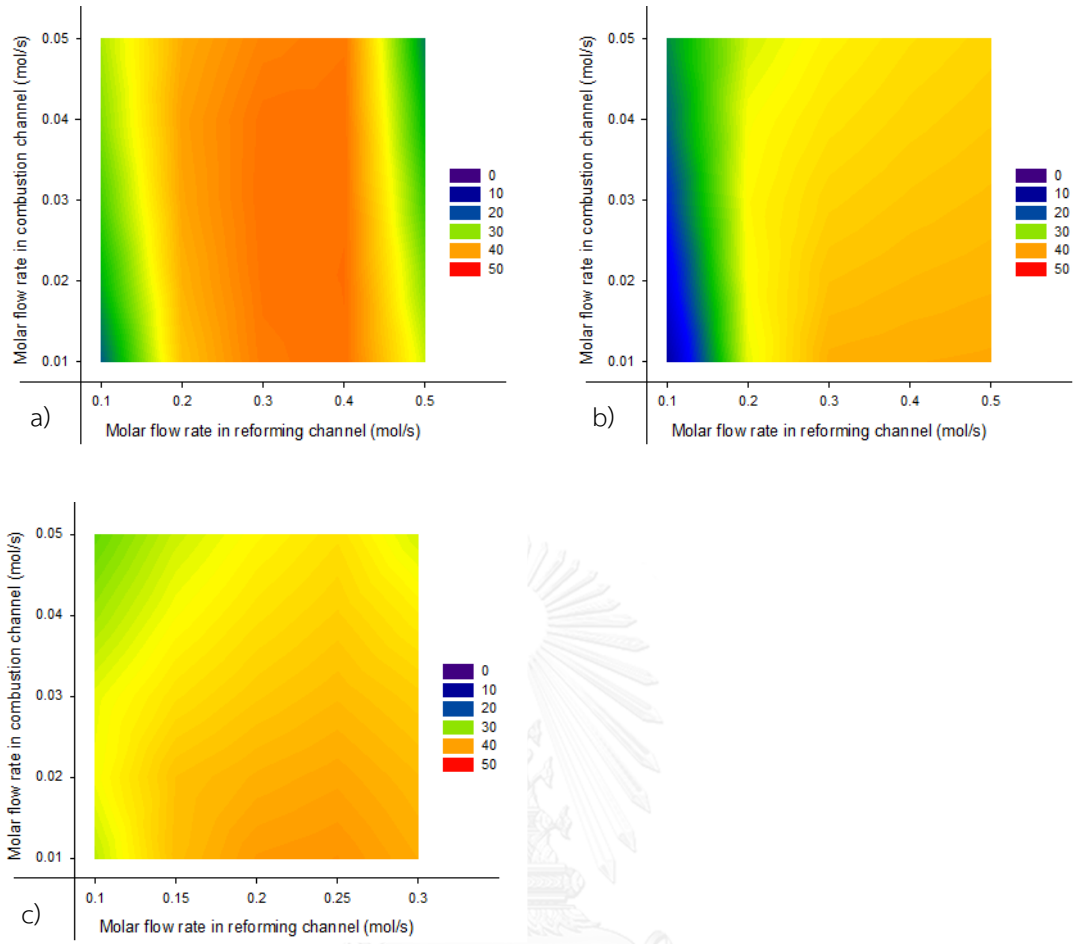

Figure 6.9 Energy efficiency of green fuel when reforming at 4 atm at various molar flow rate of a) Methane, b) Methanol and c) Ethanol

When comparing the efficiency between green fuels, the highest energy efficiency is provided from methane (Figure 6.9a) followed by ethanol (Figure 6.9b) and methanol (Figure 6.9c). Since conversion is complete at inlet, methanol and ethanol mainly convert to methane and hydrogen. When reforming temperature increases along the reactor, methane steam reforming and reverse water gas shift reaction occur. After complete methane conversion, the reverse water gas shift reaction strongly presents, resulting in lower energy efficiency. Therefore, methanol and ethanol which

are sensitive at high temperature are not suitable for large surface of the TMMR. Methane is proposed to be the green fuel for the TMMR.

6.3.3.2 Effect of reforming pressure

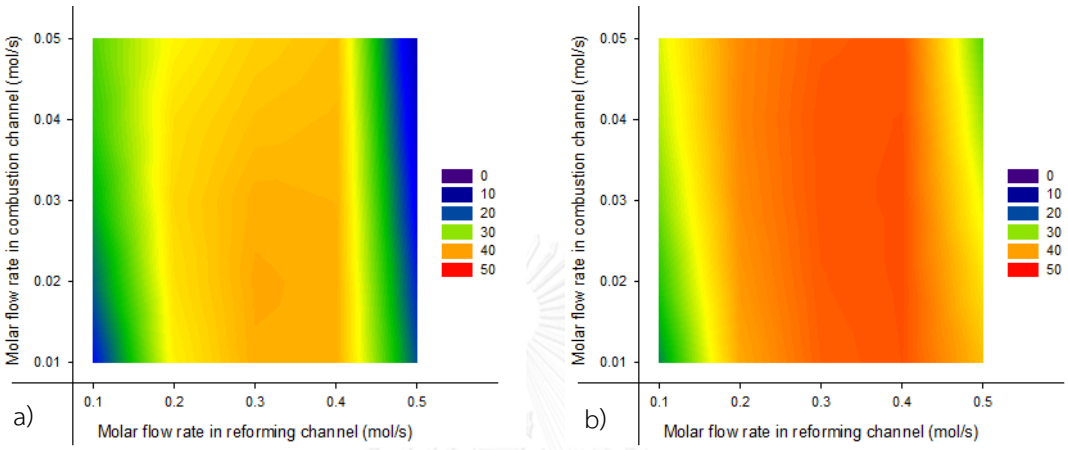

Figure 6.10 Energy efficiency at various flow rate of methane when reforming at a) 3 atm and b) 5 atm

As shown in Eq. 5.4, increasing reforming pressure enhances the driving force of hydrogen separation. Energy efficiency of the TMMR when operates at reforming pressure of 3, 4 and 5 atm is shown in Figure 6.10a, Figure 6.9a and Figure 6.10b, respectively. At each reforming pressure, the highest efficiency is 39.1% for 3 atm, 43.0% for 4 atm and 45.1% for 5 atm operation. When operates over 4 atm of reforming pressure, the increase of efficiency is insignificant. Thus, reforming pressure is selected at 4 atm.

When reforming at 4 atm, hydrogen energy produced from the TMMR system is reported in Figure 6.11. Hydrogen energy is higher than the target (100 kW) after the flow rate is beyond 0.30 mol/s for reforming and 0.01 mol/s for combustion. The highest efficiency at 43.0% provides excessive hydrogen energy at 160.9 kW when using 0.40 mol/s for reforming and 0.02 for combustion. The lower condition which is close to the objective is performed at 0.30 and 0.03 mol/s for reforming and combustion, respectively. This appropriate condition provides 126.1 kW with 42.9% of energy efficiency.

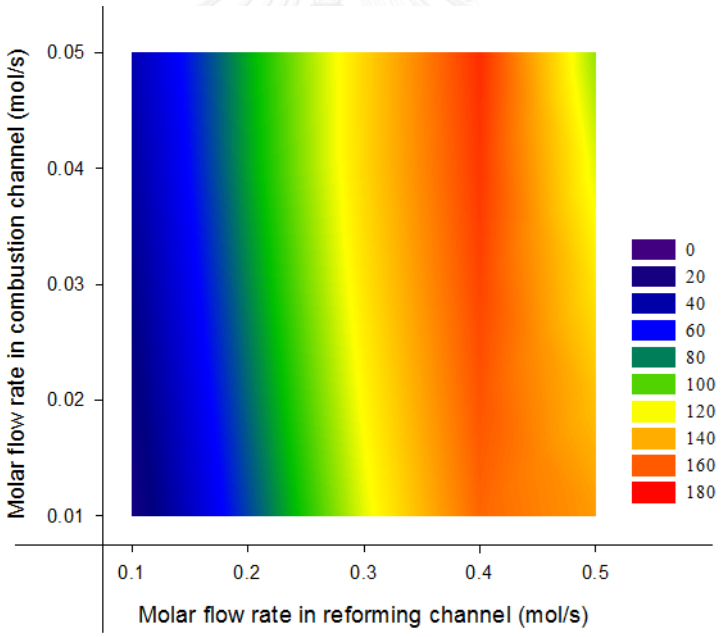

Figure 6.11 Hydrogen energy of methane steam reforming at 4 atm

In thermodynamic study, methanol and ethanol reforming strongly presents reverse water gas shift reaction, leading to decreasing hydrogen production after complete conversion. Therefore, methane which provides higher energy efficiency is

the suitable green fuel for the TMMR. The increase of feed flow rate of fuel results in increasing operating temperature of the TMMR. The energy efficiency is increased with the temperature, but increasing temperature after complete conversion decreases the efficiency by the presence of reverse water gas shift reaction. Moreover, the efficiency increases with the reforming pressure. As a result, the operating condition using methane fuel is suitable at 4 atm for reforming and the feed flow rate is reasonable at 0.30 mol/s for reforming and 0.03 mol/s for combustion.

6.3.4 TMMR design

To design the TMMR, the selected operating condition from the thermodynamic based study is employed. The configuration of monolith is specified as follows. The values of cell density are 200, 300, 400 cpsi and the diameter and length are between 100 and 200 mm. The checked arrangement is chosen and the area ratio is 0.25:0.25:0.50 for exchange heat, hydrogen separation and reaction, respectively.

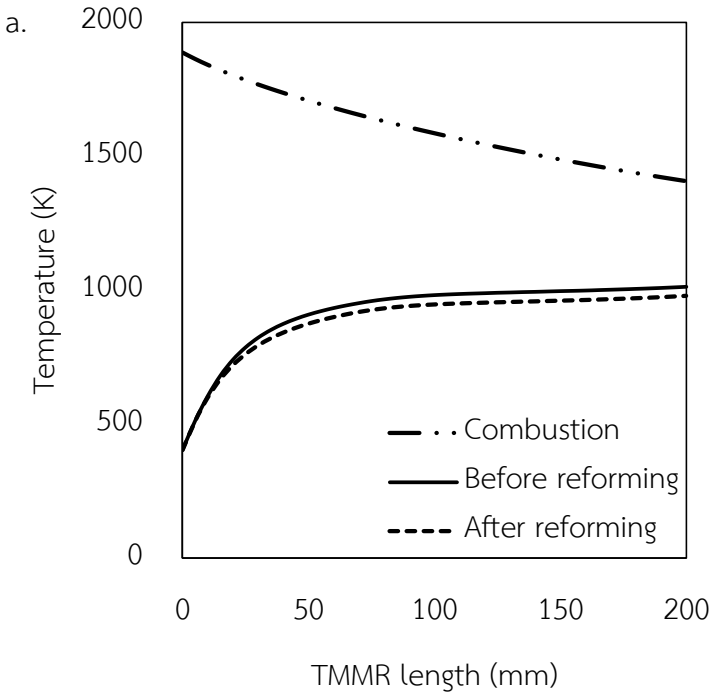

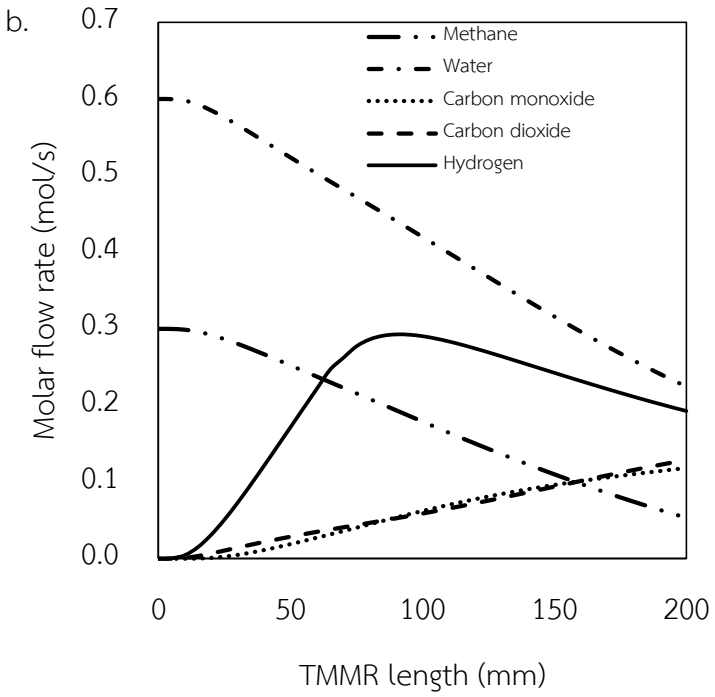

Figure 6.12 Temperature profiles (a) and molar flow rate (b) in reforming of small surface area monolith (100 mm diameter, 200 mm long, and 200 cpsi)

At small surface area monolith, the temperature profiles and the molar flow rate of reforming product are shown in Figure 6.12a and Figure 6.12b respectively. The small surface area monolith (100 mm diameter, 200 mm long, and 200 cpsi) provides low heat transfer, leading to losing energy in exhaust gas at the outlet. Reforming temperature slowly increases along the reformer length. Due to the low temperature at inlet, the reaction dilatorily occurs, leading to low hydrogen content and absence of hydrogen separation. When hydrogen partial pressure is higher than 1 atm at 65 mm of the reformer length, hydrogen separation appears and the reaction rate shifts forward. Consequently, methane conversion is about 82% at the outlet of the TMMR. The incomplete conversion and low hydrogen separation lead to the low energy efficiency at 32.8%.

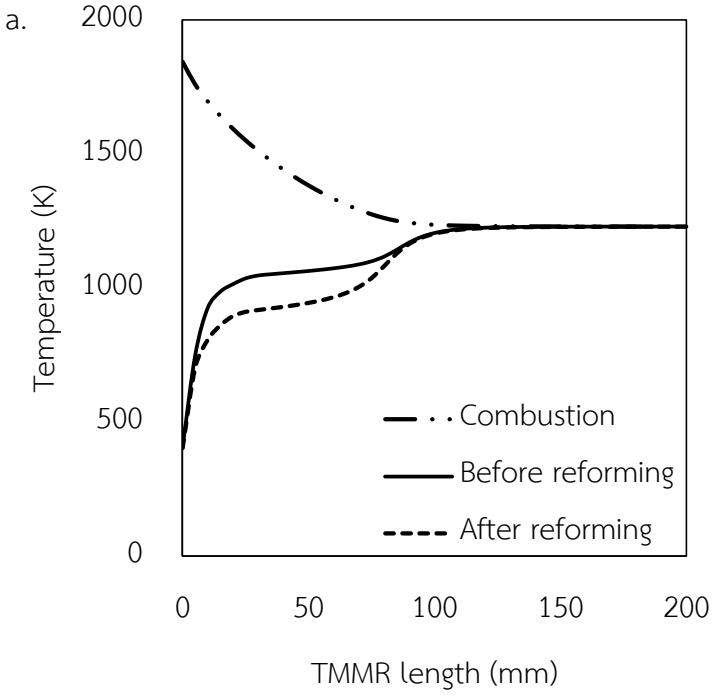

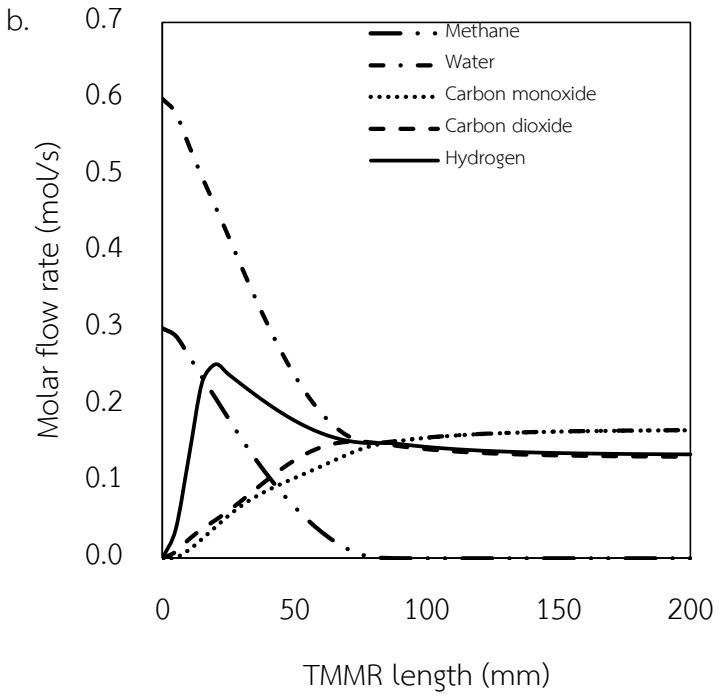

Figure 6.13 Temperature profiles (a) and molar flow rate (b) in reforming of high surface area monolith (200 mm diameter, 200 mm long, and 200 cpsi)

Monolith with high surface area, the temperature profile and the molar flow rate of reforming product are shown in Figure 6.13a and Figure 6.13b respectively. The high surface area monolith (200 mm diameter, 200 mm long, and 200 cpsi) is employed. In Figure 6.13a, the combustion gas temperature sharply decreases; hence heat is efficiently transferred to the reforming gas. The reforming temperature rapidly increases and approaches the combustion gas temperature when the reactor length is beyond 100 mm. According to the increasing reforming temperature, the reaction rate increases and the methane conversion is complete after 85 mm of the reformer length. Hydrogen separation starts at 15 mm long. After complete conversion, the reverse

water gas shift reaction strongly occurs at the high temperature, leading to lower hydrogen partial pressure which limits the separation. As a consequence, the energy efficiency of this design is moderately high at 43.6%.

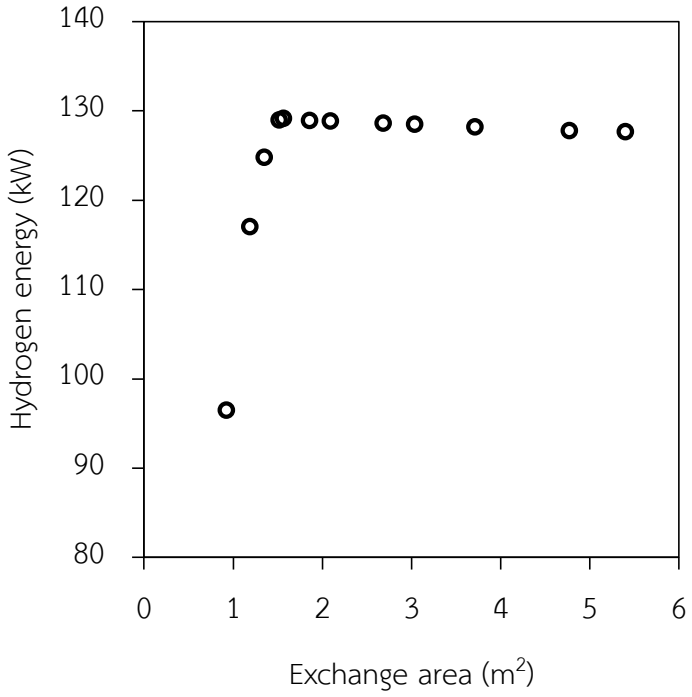

Figure 6.14 Energy efficiency versus exchange area of monolith

The design of the TMMR apparently depends on the monolith exchange area. The efficiency versus the exchange area is shown in Figure 6.14. The energy efficiency is increased sharply and reaches the highest at 1.5 m^2 of exchange area. However, further increase of the exchange area leads to slight decrease of energy efficiency by the influence of reverse water gas reaction from the excessive heat for reforming. At the best condition, 200 cpsi monolith with 150 mm of diameter and length is

performed and produces 129.0 kW of hydrogen energy with 44.0% efficiency. Therefore, this monolith design is the most appropriate design of TMMR in this study and the design requires small space which is only 2.65 liters of volume.

6.3.5 Effect of the flow arrangement on the TMMR

Table 6.3 Energy efficiency and hydrogen energy production of the parallel arrangement and the checked arrangement

Flow arrangement	Methane conversion (%)	Hydrogen production (kW)	Energy efficiency (%)
Parallel arrangement	77.1	88.19	30.01
Checked arrangement	99.7	129.16	43.96

The effect of flow arrangement at the specific configuration of the TMMR and the suggested operating condition is investigated. The exchange area in the parallel arrangement is lower than that in the checked arrangement. Energy efficiency and hydrogen energy production rate of both arrangements are reported in Table 6.3. The parallel arrangement provides energy efficiency at 30.0% and 88.0 kW of hydrogen energy. Thus, the parallel arrangement apparently decreases the reactor performance.

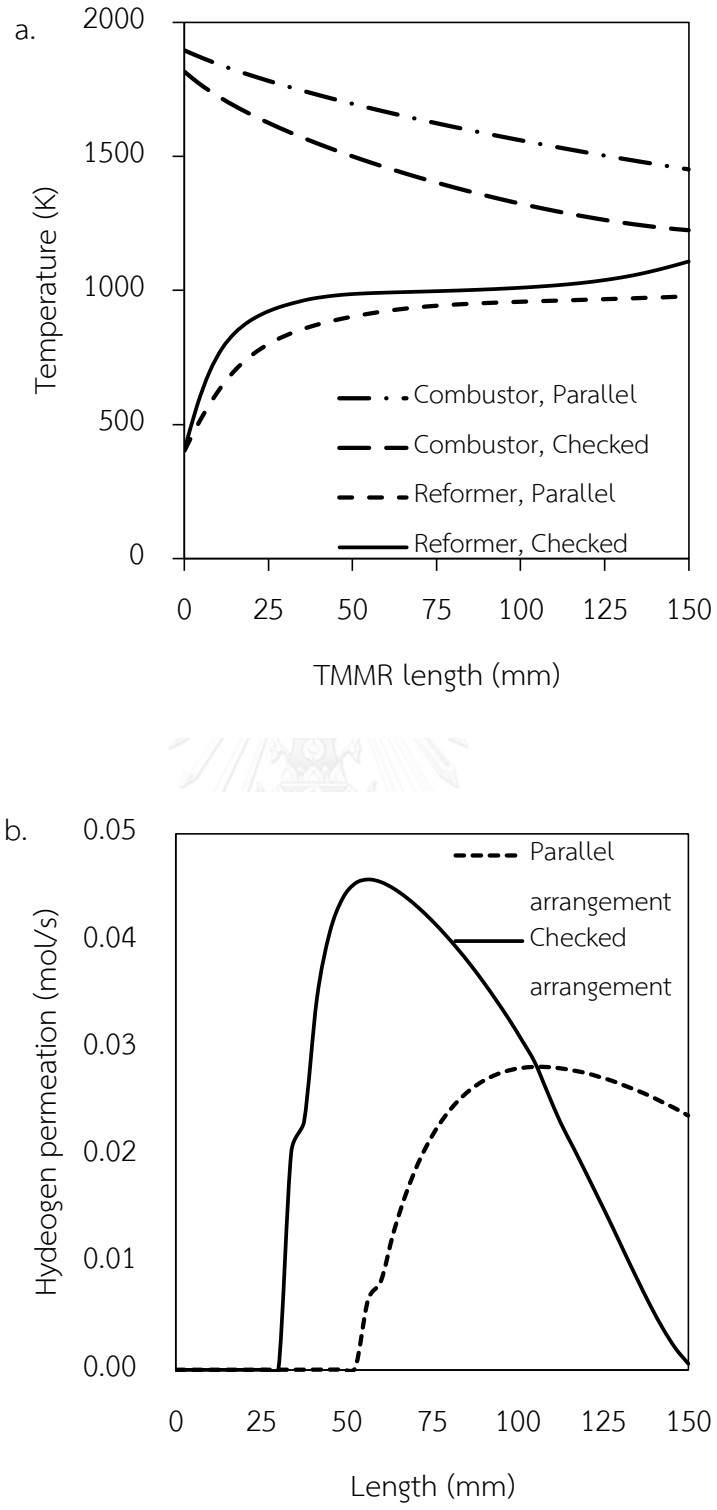

Figure 6.15 TMMR temperature profiles (a) and hydrogen permeation (b) of the parallel arrangement and the checked arrangement

The TMMR temperature profile and hydrogen permeation of both arrangements are shown in Figure 6.15. As shown in Figure 6.15a, heat transfer in the parallel arrangement is poor, leading to lower reforming temperature and higher combustion temperature. Moreover, hydrogen separation rate is slow and the reforming stream still contains high hydrogen content as shown in Figure 6.15b. More area is required to complete the separation. The hydrogen permeation in the parallel arrangement is 0.62 mol/s which is 0.28 mol/s lower than that in the checked arrangement. Low heat transfer and slow separation rate lead to the decrease of the shift of equilibrium. Hence, methane conversion is reduced to 77%.

Since the checked arrangement provides more efficient heat transfer and higher hydrogen separation than those of the parallel arrangement, and produces 40 kW higher hydrogen energy with 14% higher the energy efficiency. Thus, the check arrangement is preferable for the TMMR.

CHAPTER VII
CONCLUSIONS AND RECOMMENDATIONS

7.1 Conclusions

In this thesis, commercial multi micro-channel structure monolith which has been used typically in vehicle as a catalytic converter has been developed to be a compact reformer. The monolith is designed as heat and membrane integrated reformer.

Hydrogen production units are integrated within a monolith structure. Two feed flow configurations of the parallel arrangement and the checked arrangement are considered. Both arrangements are examined for their reaction performance of thermally coupled reformer (TMR) and micro membrane reformer (MMR). The results of the TMR (1 - 5) and the MMR (6 - 9) can be concluded as follows:

1) In the base case study, cold spot appears at the inlet of the parallel arrangement. Meanwhile the checked arrangement which has higher exchange area offers smooth temperature profile along the reformer.
2) For both arrangements, the co-current flow provides slightly higher reactor performance than the counter current flow due to higher temperature range in the co-current flow.

3) According to high heat transfer ability of micro-channel reactor, both arrangements shows unnoticeable results when varying Inlet temperature, steam to carbon ratio, methane composition for combustion, gas hourly space velocity in reforming channel and combustion channel, wall thickness and reactor length.
4) Channel width is only the major parameter that influences the effect of flow arrangement in TMR. When increasing channel width, the temperature difference between hot and cold spots increases because heat and mass transfer resistance became dominant at larger channel width.
5) The parallel arrangement which has lower contact area between channels appears high temperature difference between cold and hot spots at channel width larger than 5 mm. Consequently, the checked arrangement is recommended for large channel width reformer to avoid the cold and hot spot problems.
6) The checked arrangement apparently presents 4% higher methane conversion and 5% better hydrogen separation in the base case study of MMR.
7) Total membrane area in the checked arrangement is fully utilized, leading to higher hydrogen flux and significantly lower hydrogen accumulation in the reformer wall.
8) In the operating and design parameters variation, the MMR performance of checked arrangement is greater than that of the parallel arrangement.

9) The effect of the arrangement is increased with the increase of temperature, gas hourly space velocity of sweep gas channel and channel width. Meanwhile, increasing gas hourly space velocity of reforming channel and reactor length weaken the effect of the arrangement in MMR.

According to the better performance of checked arrangement in the study of TMR and MMR, the thermally coupled monolithic reactor (TMMR) is designed using the checked arrangement. The conclusion is as follows:

10) Methane is selected as the appropriate fuel for TMMR, since methanol and ethanol fuels usage apparently presents the reverse water gas shift reaction lowering the hydrogen production.
11) The reasonable flow rate of methane is 0.30 and 0.03 mol/s for steam reforming and combustion, respectively. The reactor performance achieves over 40% energy efficiency when performed steam reforming reaction at 4 atm.
12) For designing TMMR, it was found that the performance of TMMR depends on the exchange area of monolith. The highest energy efficiency is given by monolith with 1.5 m^2 of exchange area.
13) The design is 200 cpsi monolith with 150 mm of diameter and length and it requires only 2.65 liters of volume. This final design of TMMR can efficient produce 129 kW of hydrogen energy with 43.96% efficiency and it is applicable for vehicular system.

14) In TMMR, the checked arrangement offers 13.96% higher energy efficiency than the parallel arrangement.

7.2 Recommendations

1) This thermally coupled monolithic membrane reactor is an ideal design based on a monolith structure. Feed flow distributer at the inlet and product collector at the outlet are required and they should be designed to combine with the TMMR for application in a vehicle.
2) The study of TMR, MMR and TMMR was explored via modeling simulation. They should be constructed and investigated by experiments to verify with the simulation results in the future work.
3) For hydrogen energy production using TMMR and PEMFC, the recycling line also needs to recover hydrogen and syngas residues achieving the high performance. Therefore, TMMR, PEMFC and recycling line must be designed for vehicles.
4) For vehicle application, dynamic control of feed in the TMMR should be studied. Moreover, battery must be applied for storing excessive electrical energy from PEMFC.
5) Operation of the TMMR including start and stop steps must be concerned. For example, coke can be formed at low temperature operation which may occur in start step. In stop step, gases inside the TMMR should be released because condensation of water might deactivate the catalyst.

6) Combustion and reforming catalysts and membrane present inside the TMMR. Coating technic of these catalyst and membrane layers must be considered.
7) The TMMR performance using ethanol fuel must be studied, since ethanol fuel which is easily available will become the main green fuel on near future.
8) Metallic monolith is proposed as a ready-made catalyst for vehicular application. Preliminary study revealed that the steam reforming activity appeared over Hastelloy after oxidation at 1273 K for 2 hours in APPENDIX C. However, this structural catalyst should be improved. This study will be investigated in future.

REFERENCES

Al Seadi, T., D. Rutz, H. Prassl, M. Köttner, T. Finsterwalder, S. Volk and R. Janssen (2008). Biogas Handbook.–University of Southern Denmark Esbjerg, ISBN 978-87-992962-0-0.

Anzola, A. M., Y. M. Bruschi, E. López, N. S. Schbib, M. N. Pedernera and D. O. Borio (2010). "Heat Supply and Hydrogen Yield in an Ethanol Microreformer." Industrial & Engineering Chemistry Research **50**(5): 2698-2705.

Babita, K., S. Sridhar and K. V. Raghavan (2011). "Membrane reactors for fuel cell quality hydrogen through WGSR – Review of their status, challenges and opportunities." International Journal of Hydrogen Energy **36**(11): 6671-6688.

Baker, R. (1982). "The relationship between particle motion on a graphite surface and Tammann temperature." Journal of Catalysis **78**(2): 473-476.

Bampenrat, A., V. Meeyoo, B. Kitiyanan, P. Rangsunvigit and T. Rirksomboon (2010). "Naphthalene steam reforming over Mn-doped CeO_2–ZrO_2 supported nickel catalysts." Applied Catalysis A: General **373**(1): 154-159.

Bravo, J., A. Karim, T. Conant, G. P. Lopez and A. Datye (2004). "Wall coating of a CuO/ZnO/Al2O3 methanol steam reforming catalyst for micro-channel reformers." Chemical Engineering Journal **101**(1-3): 113-121.

Casanovas, A., M. Roig, C. De Leitenburg, A. Trovarelli and J. Llorca (2010). "Ethanol steam reforming and water gas shift over Co/ZnO catalytic honeycombs doped with Fe, Ni, Cu, Cr and Na." International Journal of Hydrogen Energy **35**(15): 7690-7698.

Centi, G. and S. Perathoner (2009). "Opportunities and prospects in the chemical recycling of carbon dioxide to fuels." Catalysis Today **148**(3-4): 191-205.

Cheng, W. H. (1995). "Reaction and XRD studies on Cu based methanol decomposition catalysts: role of constituents and development of high-activity multicomponent catalysts." Applied Catalysis A: General **130**(1): 13-30.

Cheng, W. H., I. Chen, J. Liou and S. S. Lin (2003). "Supported Cu catalysts with yttria-doped ceria for steam reforming of methanol." Topics in Catalysis **22**(3-4): 225-233.

Demirbas, A. (2007). "The influence of temperature on the yields of compounds existing in bio-oils obtained from biomass samples via pyrolysis." Fuel Processing Technology **88**(6): 591-597.

Deutschmann, O., L. Maier, U. Riedel, A. Stroemman and R. Dibble (2000). "Hydrogen assisted catalytic combustion of methane on platinum." Catalysis Today **59**(1): 141-150.

Ersoz, A., H. Olgun and S. Ozdogan (2006). "Reforming options for hydrogen production from fossil fuels for PEM fuel cells." Journal of Power Sources **154**(1): 67-73.

Faungnawakij, K., R. Kikuchi and K. Eguchi (2006). "Thermodynamic evaluation of methanol steam reforming for hydrogen production." Journal of Power Sources **161**(1): 87-94.

Faungnawakij, K., N. Shimoda, T. Fukunaga, R. Kikuchi and K. Eguchi (2008). "Cu-based spinel catalysts CuB_2O_4 (B= Fe, Mn, Cr, Ga, Al, $Fe_{0.75}$ $Mn_{0.25}$) for steam reforming of dimethyl ether." Applied Catalysis A: General **341**(1): 139-145.

Felder, R. M. and R. W. Rousseau (2005). Elementary principles of chemical process, John Wiley & Sons, Inc.

Fischer, C., V. Karius, P. G. Weidler and A. Lüttge (2008). "Relationship between Micrometer to Submicrometer Surface Roughness and Topography Variations of Natural Iron Oxides and Trace Element Concentrations." Langmuir **24**(7): 3250-3266.

Frauhammer, J., G. Eigenberger, L. v. Hippel and D. Arntz (1999). "A new reactor concept for endothermic high-temperature reactions." Chemical Engineering Science **54**(15–16): 3661-3670.

Fukuhara, C. and A. Igarashi (2005). "Performance simulation of a wall-type reactor in which exothermic and endothermic reactions proceed simultaneously, comparing with that of a fixed-bed reactor." Chemical Engineering Science **60**(24): 6824-6834.

Galbe, M. and G. Zacchi (2002). "A review of the production of ethanol from softwood." Applied microbiology and biotechnology **59**(6): 618-628.

Gallucci, F., M. De Falco, S. Tosti, L. Marrelli and A. Basile (2008). "Ethanol steam reforming in a dense Pd–Ag membrane reactor: A modelling work. Comparison with the traditional system." International Journal of Hydrogen Energy **33**(2): 644-651.

Gallucci, F., L. Paturzo and A. Basile (2004a). "Hydrogen recovery from methanol steam reforming in a dense membrane reactor: simulation study." Industrial and engineering chemistry research **43**(10): 2420-2432.

Gallucci, F., L. Paturzo and A. Basile (2004b). "A simulation study of the steam reforming of methane in a dense tubular membrane reactor." International Journal of Hydrogen Energy **29**(6): 611-617.

Garcia, L., R. French, S. Czernik and E. Chornet (2000). "Catalytic steam reforming of bio-oils for the production of hydrogen: effects of catalyst composition." Applied Catalysis A: General **201**(2): 225-239.

Green, D. W. and R. H. Perry (2008). Physical and Chemical Data. Perry's chemical engineers' handbook. B. E. Poling, G. H. Thomson, D. G. Friend, R. L. Rowley and W. V. Wilding, McGraw-Hill 421-444.

Grote, M., M. Maximini, Z. Yang, P. Engelhardt, H. Köhne, K. Lucka and M. Brenner (2011). "Experimental and computational investigations of a compact steam reformer for fuel oil and diesel fuel." Journal of Power Sources **196**(21): 9027-9035.

Hayes, R. E., S. T. Kolaczkowski, W. J. Thomas and J. Titiloye (1996). "Transient experiments and modeling of the catalytic combustion of methane in a monolith reactor." Industrial & Engineering Chemistry Research **35**(2): 406-414.

Holladay, J. D., J. Hu, D. L. King and Y. Wang (2009). "An overview of hydrogen production technologies." Catalysis Today **139**(4): 244-260.

Holladay, J. D., Y. Wang and E. Jones (2004). "Review of developments in portable hydrogen production using microreactor technology." Chemical Reviews **104**(10): 4767-4790.

Hong Mei, Chengyue Li, Shengfu Ji and Hui Liu (2007). "Modeling of a metal monolith catalytic reactor for methane steam reforming–combustion coupling." Chemical Engineering Science **62**(16): 4294-4303.

Hotza, D. and J. D. da Costa (2008). "Fuel cells development and hydrogen production from renewable resources in Brazil." International Journal of Hydrogen Energy **33**(19): 4915-4935.

Irani, M., A. Alizadehdakhel, A. N. Pour, N. Hoseini and M. Adinehnia (2011). "CFD modeling of hydrogen production using steam reforming of methane in monolith reactors: Surface or volume-base reaction model?" International Journal of Hydrogen Energy **36**(24): 15602-15610.

Jin, Y., Z. Rui, Y. Tian, Y. Lin and Y. Li (2010). "Sequential simulation of dense oxygen permeation membrane reactor for hydrogen production from oxidative steam reforming of ethanol with ASPEN PLUS." International Journal of Hydrogen Energy **35**(13): 6691-6698.

Karagiannidis, S., J. Mantzaras, G. Jackson and K. Boulouchos (2007). "Hetero-/homogeneous combustion and stability maps in methane-fueled catalytic microreactors." Proceedings of the Combustion Institute **31**(2): 3309-3317.

Karakaya, M. and A. K. Avci (2011). "Microchannel reactor modeling for combustion driven reforming of iso-octane." International Journal of Hydrogen Energy **36**(11): 6569-6577.

Katayama, Y. and Y. Tamaura (2005). "Development of new green-fuel production technology by combination of fossil fuel and renewable energy." Energy **30**(11-12): 2179-2185.

Katiyar, N., S. Kumar and S. Kumar (2013). "Polymer electrolyte membrane fuel cell grade hydrogen production by methanol steam reforming: A comparative multiple reactor modeling study." Journal of Power Sources **243**: 381-391.

Kim, D., D. Donohue, B. Kuncharam, C. Duval and B. A. Wilhite (2010). "Toward an integrated ceramic micro-membrane network: effect of ethanol reformate on palladium membranes." Industrial & Engineering Chemistry Research **49**(21): 10254-10261.

Kim, D., A. Kellogg, E. Livaich and B. A. Wilhite (2009). "Towards an integrated ceramic micro-membrane network: Electroless-plated palladium membranes in cordierite supports." Journal of Membrane Science **340**(1–2): 109-116.

Kolb, G. (2013). "Review: Microstructured reactors for distributed and renewable production of fuels and electrical energy." Chemical Engineering and Processing: Process Intensification **65**: 1-44.

Korotkikh, O. and R. Farrauto (2000). "Selective catalytic oxidation of CO in H2: fuel cell applications." Catalysis Today **62**(2–3): 249-254.

Lima da Silva, A., C. d. F. Malfatti and I. L. Müller (2009). "Thermodynamic analysis of ethanol steam reforming using Gibbs energy minimization method: A detailed study of the conditions of carbon deposition." International Journal of Hydrogen Energy **34**(10): 4321-4330.

Lindström, B., L. J. Pettersson and P. G. Menon (2002). "Activity and characterization of Cu/Zn, Cu/Cr and Cu/Zr on **γ**-alumina for methanol reforming for fuel cell vehicles." Applied Catalysis A: General **234**(1): 111-125.

Liu, K., C. Song and V. Subramani (2010). Hydrogen and syngas production and purification technologies, Wiley Online Library.

Lukyanov, B. N., D. V. Andreev and V. N. Parmon (2009). "Catalytic reactors with hydrogen membrane separation." Chemical Engineering Journal **154**(1-3): 258-266.

Lwin, Y., W. R. W. Daud, A. B. Mohamad and Z. Yaakob (2000). "Hydrogen production from steam–methanol reforming: thermodynamic analysis." International Journal of Hydrogen Energy **25**(1): 47-53.

Michelsen, F. A., Ø. Wilhelmsen, L. Zhao and K. I. Åsen (2013). "A distributed dynamic model of a monolith hydrogen membrane reactor." Energy Conversion and Management **67**(0): 160-170.

Mills, G. A. and F. W. Steffgen (1974). "Catalytic methanation." Catalysis Reviews **8**(1): 159-210.

Montané, D., E. Bolshak and S. Abelló (2011). "Thermodynamic analysis of fuel processors based on catalytic-wall reactors and membrane systems for ethanol steam reforming." Chemical Engineering Journal **175**(0): 519-533.

Moreno, A. M., S. Damodharan and B. Wilhite (2010). "Influence of Two-Dimensional Distribution Schemes upon Reactor Performance in a Ceramic Microchannel Network for Autothermal Methanol Reforming." Industrial & Engineering Chemistry Research **49**(21): 10956-10964.

Moreno, A. M. and B. A. Wilhite (2010). "Autothermal hydrogen generation from methanol in a ceramic microchannel network." Journal of Power Sources **195**(7): 1964-1970.

Ni, M., D. Y. Leung and M. K. Leung (2007). "A review on reforming bio-ethanol for hydrogen production." International Journal of Hydrogen Energy **32**(15): 3238-3247.

Obert, R. and B. C. Dave (1999). "Enzymatic conversion of carbon dioxide to methanol: enhanced methanol production in silica sol-gel matrices." Journal of the American Chemical Society **121**(51): 12192-12193.

Olah, G. A., A. Goeppert and G. S. Prakash (2008). "Chemical recycling of carbon dioxide to methanol and dimethyl ether: from greenhouse gas to renewable, environmentally carbon neutral fuels and synthetic hydrocarbons." The Journal of organic chemistry **74**(2): 487-498.

Paglieri, S. and J. Way (2002). "Innovations in palladium membrane research." Separation & Purification Reviews **31**(1): 1-169.

Palo, D. R., R. A. Dagle and J. D. Holladay (2007). "Methanol Steam Reforming for Hydrogen Production." Journal Name: Chemical Reviews, 107(10):3992-4021; Journal Volume: 107; Journal Issue: 10: Medium: X.

Patel, K. S. and A. K. Sunol (2007). "Modeling and simulation of methane steam reforming in a thermally coupled membrane reactor." International Journal of Hydrogen Energy **32**(13): 2344-2358.

Peppley, B. A., J. C. Amphlett, L. M. Kearns and R. F. Mann (1999a). "Methanol–steam reforming on Cu/ZnO/Al 2 O 3 catalysts. Part 2. A comprehensive kinetic model." Applied Catalysis A: General **179**(1): 31-49.

Peppley, B. A., J. C. Amphlett, L. M. Kearns and R. F. Mann (1999b). "Methanol–steam reforming on Cu/ZnO/Al 2 O 3. Part 1: the reaction network." Applied Catalysis A: General **179**(1): 21-29.

Rabenstein, G. and V. Hacker (2008). "Hydrogen for fuel cells from ethanol by steam-reforming, partial-oxidation and combined auto-thermal reforming: A thermodynamic analysis." Journal of Power Sources **185**(2): 1293-1304.

Rioche, C., S. Kulkarni, F. C. Meunier, J. P. Breen and R. Burch (2005). "Steam reforming of model compounds and fast pyrolysis bio-oil on supported noble metal catalysts." Applied Catalysis B: Environmental **61**(1): 130-139.

Sá, S., H. Silva, L. Brandão, J. M. Sousa and A. Mendes (2010). "Catalysts for methanol steam reforming—A review." Applied Catalysis B: Environmental **99**(1–2): 43-57.

Sahoo, D. R., S. Vajpai, S. Patel and K. K. Pant (2007). "Kinetic modeling of steam reforming of ethanol for the production of hydrogen over Co/Al2O3 catalyst." Chemical Engineering Journal **125**(3): 139-147.

Sanz, O., F. J. Echave, F. Romero-Sarria, J. A. Odriozola and M. Montes (2013). Chapter 9 - Advances in Structured and Microstructured Catalytic Reactors for Hydrogen Production. Renewable Hydrogen Technologies. L. M. Gandía, G. Arzamendi and P. M. Diéguez. Amsterdam, Elsevier**:** 201-224.

Sekizawa, K., S. Yano, K. Eguchi and H. Arai (1998). "Selective removal of CO in methanol reformed gas over Cu-supported mixed metal oxides." Applied Catalysis A: General **169**(2): 291-297.

Shu, J., B. P. A. Grandjean and S. Kaliaguine (1994). "Methane steam reforming in asymmetric Pd- and Pd-Ag/porous SS membrane reactors." Applied Catalysis A: General **119**(2): 305-325.

Sun, Y. and J. Cheng (2002). "Hydrolysis of lignocellulosic materials for ethanol production: a review." Bioresource technology **83**(1): 1-11.

Sutton, D., B. Kelleher and J. R. H. Ross (2001). "Review of literature on catalysts for biomass gasification." Fuel Processing Technology **73**(3): 155-173.

Tadbir, M. A. and M. H. Akbari (2011). "Methanol steam reforming in a planar wash coated microreactor integrated with a micro-combustor." International Journal of Hydrogen Energy **36**(20): 12822-12832.

Tadbir, M. A. and M. H. Akbari (2012). "Integrated methanol reforming and oxidation in wash-coated microreactors: A three-dimensional simulation." International Journal of Hydrogen Energy **37**(3): 2287-2297.

Tagawa, T., S. R. de la Rama, S. Kawai and H. Yamada (2013). "Partial Oxidation Catalysts Derived from Ni Containing Alloys for Biomass Gasification Process." Chemical Engineering Transaction **32**: 6.

Tanaka, Y., T. Utaka, R. Kikuchi, K. Sasaki and K. Eguchi (2003). "Water gas shift reaction over Cu-based mixed oxides for CO removal from the reformed fuels." Applied Catalysis A: General **242**(2): 287-295.

Versteeg, H. K. and W. Malalasekera (2007). An introduction to computational fluid dynamics: the finite volume method, Pearson Education.

Von Hippel, L., D. Arntz, J. Frauhammer, G. Eigenberger and G. Friedrich (1999). Reactor head for a monolithic co-current or countercurrent reactor, Google Patents.

Wang, D., S. Czernik and E. Chornet (1998). "Production of hydrogen from biomass by catalytic steam reforming of fast pyrolysis oils." Energy & Fuels **12**(1): 19-24.

Welty, J. R., C. E. Wicks, R. E. Wilson and G. L. Rorrer (2007). Fundamentals of Momentum, Heat, and Mass Transfer, Wiley.

Xu, J. and G. F. Froment (1989). "Methane steam reforming, methanation and water-gas shift: I. Intrinsic kinetics." AIChE Journal **35**(1): 88-96.

Xuan, J., D. Y. C. Leung, M. K. H. Leung, M. Ni and H. Wang (2012). "Chemical and transport behaviors in a microfluidic reformer with catalytic-support membrane for efficient hydrogen production and purification." International Journal of Hydrogen Energy **37**(3): 2614-2622.

Yan, X., Y. Liu, B. Zhao, Z. Wang, Y. Wang and C.-j. Liu (2013). "Methanation over Ni/SiO 2: effect of the catalyst preparation methodologies." International Journal of Hydrogen Energy **38**(5): 2283-2291.

Ye, G., D. Xie, W. Qiao, J. R. Grace and C. J. Lim (2009). "Modeling of fluidized bed membrane reactors for hydrogen production from steam methane reforming with Aspen Plus." International Journal of Hydrogen Energy **34**(11): 4755-4762.

Yun, S. and S. Ted Oyama (2011). "Correlations in palladium membranes for hydrogen separation: A review." Journal of Membrane Science **375**(1–2): 28-45.

Zanfir, M. and A. Gavriilidis (2003). "Catalytic combustion assisted methane steam reforming in a catalytic plate reactor." Chemical Engineering Science **58**(17): 3947-3960.

Zhou, X., M. Meng, Z. Sun, Q. Li and Z. Jiang (2011). "Prominent enhancement of Mn or Co addition on the performance of Cu-Ce-O catalyst used for H_2 production via dimethyl ether steam reforming." Chemical Engineering Journal **174**(1): 400-407.

APPENDIX

APPENDIX A

KINETIC MODEL OF METHANE STEAM REFORMING

Methane steam reforming was considered in this thesis. Kinetic model was adopted from Xu and Froment (1989). Mechanism of this reaction was steam reforming and water gas shift as shown in Eqs. 2.8 – 2.10 and the reaction rate expressions are shown in Eqs. A1-A3, respectively.

$$r_{A1} = \frac{\frac{k_{A1}}{p_{H_2}^{2.5}}\left(p_{CH_4}p_{H_2O} - \frac{p_{H_2}^3 p_{CO}}{K_{eqA1}}\right)}{\left(1 + K_{CO}p_{CO} + K_{H_2}p_{H_2} + K_{CH_4}p_{CH_4} + \frac{K_{H_2O}p_{H_2O}}{p_{H_2}}\right)^2} \quad \text{(A1)}$$

$$r_{A2} = \frac{\frac{k_{A2}}{p_{H_2}}\left(p_{CO}p_{H_2O} - \frac{p_{H_2}p_{CO_2}}{K_{eqA2}}\right)}{\left(1 + K_{CO}p_{CO} + K_{H_2}p_{H_2} + K_{CH_4}p_{CH_4} + \frac{K_{H_2O}p_{H_2O}}{p_{H_2}}\right)^2} \quad \text{(A2)}$$

$$r_{A3} = \frac{\frac{k_{A3}}{p_{H_2}^{3.5}}\left(p_{CH_4}p_{H_2O}^2 - \frac{p_{H_2}^4 p_{CO_2}}{K_{eqA3}}\right)}{\left(1 + K_{CO}p_{CO} + K_{H_2}p_{H_2} + K_{CH_4}p_{CH_4} + \frac{K_{H_2O}p_{H_2O}}{p_{H_2}}\right)^2} \quad \text{(A3)}$$

where K_{eq} are the equilibrium constants of reactions in Eqs 2.8 - 2.10. The reaction rate constants are expressed in Eqs. 2.6 and 2.7 and the kinetic parameters are reported in Table A.1.

Table A.1 Kinetic parameters of methane steam reforming reactions (Xu and Froment (1989))

Parameters	Pre-exponential factors (A)	E_a (kJ/mol)	ΔH (kJ/mol)
k_{A1}	4.225×10^{15}	240.10	-
k_{A2}	1.955×10^{6}	67.13	-
k_{A3}	1.020×10^{15}	243.90	-
K_{CO}	8.23×10^{-5}	-	-70.65
K_{H_2}	6.12×10^{-9}	-	-82.90
K_{CH_4}	6.65×10^{-4}	-	-38.28
K_{H_2O}	1.77×10^{5}	-	88.68

APPENDIX B

EXCHANGE AREA OF MONOLITH CONFIGURATION

Table B.1 Exchange area of monolith configuration for TMMR design

Monolith configuration			Exchange area (m^2)	
Cell density (cpsi)	Diameter (mm)	Length (mm)	Parallel arrangement	Checked arrangement
200	100	100	0.2325	0.4650
200	100	150	0.3488	0.6975
200	100	200	0.4650	0.9300
200	150	100	0.5231	1.0463
200	150	150	0.7847	1.5694
200	150	200	1.0463	2.0925
200	200	100	0.9300	1.8600
200	200	150	1.3950	2.7900
200	200	200	1.8600	3.7200
300	100	100	0.2985	0.5969
300	100	150	0.4477	0.8954
300	100	200	0.5969	1.1938
300	150	100	0.6715	1.3430
300	150	150	1.0073	2.0145
300	150	200	1.3430	2.6861
300	200	100	1.1938	2.3876
300	200	150	1.7907	3.5814
300	200	200	2.3876	4.7752
400	100	100	0.3379	0.6758
400	100	150	0.5069	1.0137
400	100	200	0.6758	1.3516
400	150	100	0.7603	1.5206
400	150	150	1.1404	2.2808

Monolith configuration			Exchange area (m^2)	
Cell density (cpsi)	Diameter (mm)	Length (mm)	Parallel arrangement	Checked arrangement
400	150	200	1.5206	3.0411
400	200	100	1.3516	2.7032
400	200	150	2.0274	4.0548
400	200	200	2.7032	5.4064

APPENDIX C

OXIDATION PRETREATED HASTELLOY

For Hastelloy, oxidation pretreatment condition was optimal at 1273 K for 2 hour. This condition was used to evaluate the catalytic activity of methanol steam reforming. The results are showed as follows.

C.1 Catalytic activity of Hastelloy

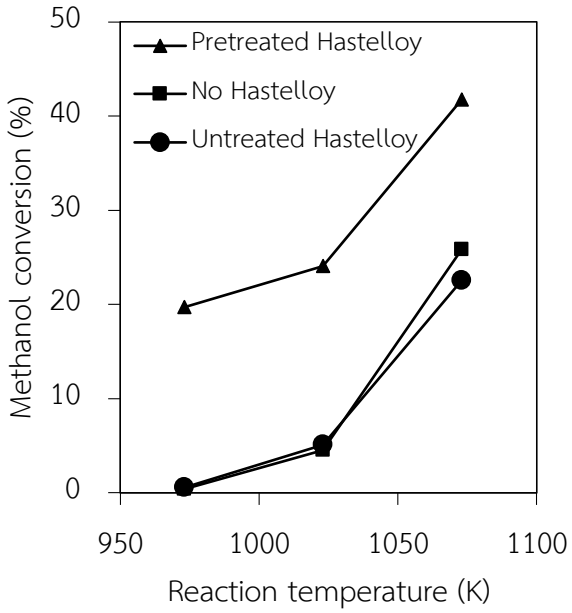

Figure C.1 Methanol conversion after one hour reaction for different systems

As shown in Figure C.1, the untreated Hastelloy and the thermal decomposition without Hastelloy in the system provided similar results respectively at low methanol conversion. Meanwhile, higher methanol conversion was apparently achieved with the oxidation pretreated Hastelloy at 1273 K for two hours. Thus, the oxidation pretreatment potentially improved the catalytic activity of Hastelloy.

Table C.1 Gas products from reaction at 1023 K for no Hastelloy, untreated Hastelloy and pretreated Hastelloy after an hour reaction

	Rate of gas production (μmol/s)			
	H_2	CH_4	CO_2	CO
No Hastelloy	5.19	0.02	0.00	1.27
Untreated Hastelloy	4.34	0.26	0.00	1.19
Pretreated Hastelloy	16.18	0.10	1.81	4.95

To evaluate the reaction performance, the gas production rates from the reaction at 1023 K for one hour is reported in Table C.1. In the study of thermal decomposition, H_2 and CO were mainly produced in the product stream with low methane production (0.02 μmol/s of CH_4). However, the large amount of CH_4 (0.26 μmol/s) appeared in the outlet product stream for the untreated Hastelloy. The untreated Hastelloy was obviously active for the methanation, converting syngas to methane. The H_2 and CO production rates slightly decreased. On the other hand, the oxidation pretreated Hastelloy produced much higher H_2 and CO production rates with higher CO_2 and lower CH_4 selectivity. According to Eq. 2.11, the presence of CO_2 showed that the steam reforming activity occurred, and the H_2 was highly produced. Consequently, the methanol steam reforming only occurred over the oxidation pretreated Hastelloy, while the untreated Hastelloy is active for the methanation.

The oxidation pretreatment apparently activated Hastelloy as the catalyst for the methanol steam reforming reaction. After oxidation pretreatment, the methanation reaction which was active in the untreated Hastelloy was suppressed, while the methanol steam reforming activity of Hastelloy was significantly promoted. Therefore, the Hastelloy with oxidation pretreatment at 1273 K can be potentially used for methanol steam reforming.

C.2 Morphology of the oxidation pretreated Hastelloy

Figure C.2 shows SEM photographs of the untreated Hastelloy and oxidation pretreated Hastelloy for a magnification level of 1,200 times. The appearance of the untreated surface was clearly smooth as shown in Figure C.2a. However, scratches also appeared, probably during its production and compression steps. After oxidation pretreatment, the small scales were formed over the surface as shown in Figure C.2b-d, leading to the increase of the roughness on the surface. A linear correlation between roughness and surface area is generally assumed (Fischer et al. (2008)). Thus, the oxidation pretreatment relatively increased the surface area of Hastelloy, resulting in catalytic activity improvement.

The elements on the surface were analyzed by EDS and the results were reported in Table C.2. The metal compositions of the untreated Hastelloy were 57.1% of Ni, 11.9% of Cr and 17.0% of Mo, similar to the bulk composition of the commercial Hastelloy. After oxidation pretreatment at 1273 K for two hours, Ni which is the main

active component was reduced to 11.4%, while Cr and Mn increased up to 60.1 and 19.9%, respectively.

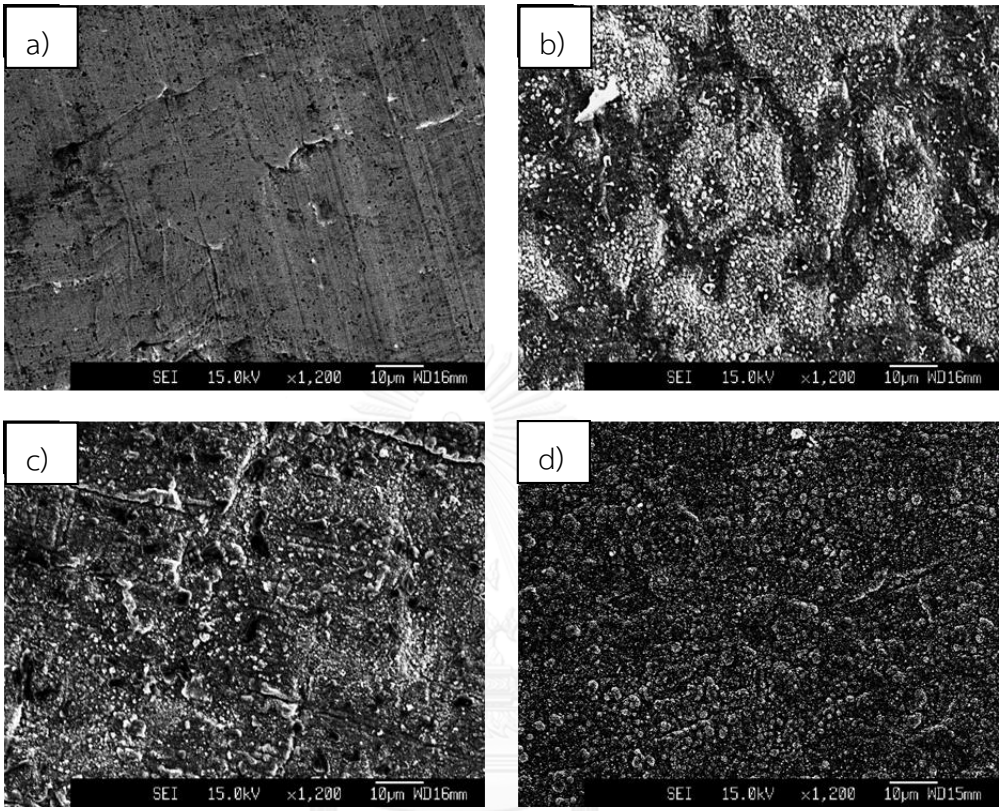

Figure C.2 Scanning electron micrographs for a) Hastelloy and the oxidation pretreated Hastelloy for two hours at b) 1073 K, c) 1173 K and d) 1273 K

At this oxidation temperature, most of metals except Mo were reactive and movable according to Tamman temperature which was approximately 0.51 of melting point (Baker (1982)). Cr and Mn strongly moved to the surface, so the main metals of Hastelloy surface after oxidation pretreatment were Ni, Cr and Mn. In several studies, Cr and Mn are usually promoters of steam reforming and water gas shift catalysts which provide several advantages. The addition of Cr increased dispersion of the active site,

resulting in the improvement of the stability and activity of catalysts (Casanovas et al. (2010), Cheng (1995), Cheng et al. (2003), Faungnawakij et al. (2008), Lindström et al. (2002), Sekizawa et al. (1998)). Moreover, Mn promoted the catalytic activity and the oxygen vacancy of catalysts which reduced the coke formation and increased the selectivity of CO_2 (Bampenrat et al. (2010), Cheng (1995), Faungnawakij et al. (2008), Sekizawa et al. (1998), Tanaka et al. (2003), Zhou et al. (2011)). Therefore, the presence of Cr and Mn on the surface of Hastelloy improved the activity of steam reforming and water gas shift.

Table C.2 EDS analysis of untreated Hastelloy and the oxidation pretreated Hastelloy (1273 K, 2 hours)

Metal	Weight (%)	
	Untreated Hastelloy	Pretreated Hastelloy
Cr	16.99	60.11
Mn	1.44	19.87
Fe	6.68	5.42
Ni	57.12	11.38
Mo	11.95	1.27
C, Al, Zr, Sn	5.82	1.95

Figure C.3 presents the XRD patterns of the untreated Hastelloy and the pretreated Hastelloy. Ni metal which is active for methanation reaction (Mills and Steffgen (1974), Yan et al. (2013)) was the main peak of the untreated Hastelloy.

Therefore, methanation followed by non-catalytic thermal decomposition strongly occurred when using the untreated Hastelloy. After oxidation, the Ni peak was smaller, and the several unknown peaks appeared at 2θ between 55 and 70 degree. Thus, the unknown peaks were possibly the peaks of Ni alloys which controlled the oxidation state of Ni. Tagawa et al. suggested that Ni formed with other metal oxides such as NiMoO, NiMoSiO and NiMoFeO from lower angle diffraction pattern (Tagawa et al. (2013)). The formation of these Ni species should result in the increase of steam reforming activity and the decrease of methanation.

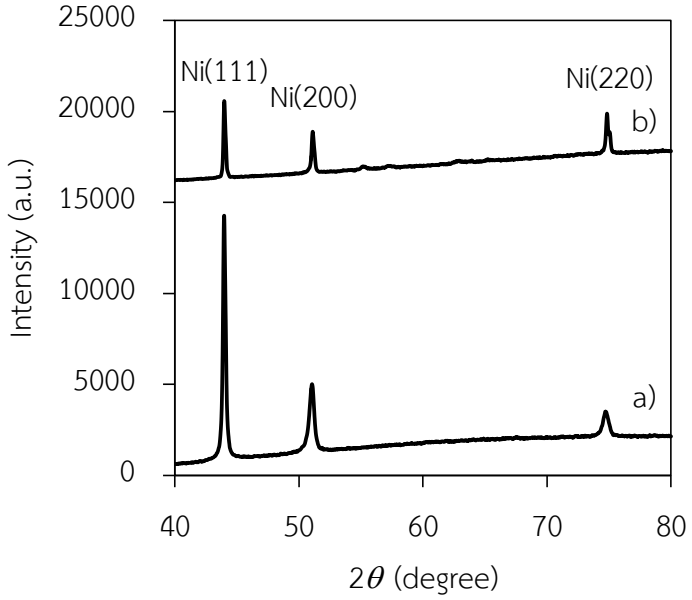

Figure C.3 XRD spectra of a) the untreated Hastelloy and b) the oxidation pretreated Hastelloy (1273 K, 2 hours)

APPENDIX D
LIST OF PUBLICATION

D.1 International publications

- Jiwanuruk, T., Putivisutisak, S., Ponpesh, P., Bumroongsakulsawat, P., Tagawa, T., Yamada, H, Assabumrungrat, S. (2015). "Comparison between parallel and checked arrangements of micro reformer for H 2 production from methane." Chemical Engineering Journal 268: 135-143. (*Impact factor: 4.32 (2015)*)
- Jiwanuruk, T., Putivisutisak, S., Ponpesh, P., Kositanont, C., Tagawa, T., Yamada, H, Fukuhara, C., Assabumrungrat, S. (2016). "Effect of flow arrangement on micro membrane reforming for H2 production from methane." Chemical Engineering Journal 293: 319-326. (*Impact factor: 4.32 (2015)*)

D.2 International conference

- Tara Jiwanuruk, Pimporn Ponpesh, Sompong Putivisutisak, Tomohiko Tagawa, Choji Fukuhara, Suttichai Assabumrungrat: Influence of Flow Pattern on Monolithic Reactor for Methanol Steam Reforming Reaction Coupled with Methane Combustion. ISCRE23&APCRE7; 09/2014
- Tara Jiwanuruk, Tomohiko Tagawa, Hiroshi Yamada, Sompong Putivisutisak, Pimporn Ponpesh, Suttichai Assabumrungrat: Methanol Steam Reforming over The Oxidation Pretreated Hastelloy for Biorefinery Applications. The 5th International Conference of the Thai Institute of Chemical Engineering and Applied Chemistry (ITIChE2015), Pattaya, Thailand; 11/2015
- Tara Jiwanuruk, Sompong Putivisutisak, Palang Bumroongsakulsawat, Tomohiko Tagawa, Hiroshi Yamada, Suttichai Assabumrungrat: Design of Thermally Coupled Monolithic Membrane Reformer as Portable Hydrogen Production System. CHEMREACTOR-22, London, United Kingdom; 09/2016

VITA

Mr. Tara Jiwanuruk was born on January 2, 1990 in Bangkok, Thailand. He finished elementary school and high school from Assumption College Thonburi, Bangkok in 2008. He received the Bachelor's Degree of Engineering in Chemical Engineering from King Mongkut's University of Technology Thonburi in April 2012. Afterward, he entered the Doctoral degree of Engineering program in Chemical engineering at Chulalongkorn University since June 2012. During his Doctoral degree, he received the Royal Golden Jubilee scholarship from the Thailand Research Fund and Chulalongkorn University. In September, 2015, he participated Nagoya University Program for Academic Exchange in Japan. He was research student in Chemical Reaction Engineering laboratory for 1 year.